COMPUTATIONAL STUDIES OF STRUCTURE-REACTIVITY RELATIONSHIPS IN THE REACTION OF HYDROXYL RADICAL WITH ARENES.

A DISSERTATION

SUBMITTED TO THE GRADUATE SCHOOL

IN PARTIAL FULFILLMENT OF THE REQUIREMENTS

FOR THE DEGREE

DOCTOR OF PHILOSOPHY

BY

DEVINDER KAUR

ADVISOR: DR. JAMES S. POOLE

BALL STATE UNIVERSITY

MUNCIE, INDIANA

DECEMBER 2016

COMPUTATIONAL STUDIES OF STRUCTURE-REACTIVITY RELATIONSHIPS IN THE REACTION OF HYDROXYL RADICAL WITH ARENES.

A DISSERTATION

SUBMITTED TO THE GRADUATE SCHOOL

IN PARTIAL FULFILLMENT OF THE REQUIREMENTS

FOR THE DEGREE

DOCTOR OF PHILOSOPHY

BY

DEVINDER KAUR

ADVISOR: DR. JAMES S. POOLE

APPROVED BY:

_____	_____
Committee Chairperson	Date
_____	_____
Committee Member	Date
_____	_____
Committee Member	Date
_____	_____
Committee Member	Date
_____	_____
Committee Member	Date
_____	_____
Dean of Graduate School	Date

BALL STATE UNIVERSITY
MUNCIE, INDIANA
DECEMBER 2016

ABSTRACT

DISSERTATION: **Computational studies of structure-reactivity relationships in the reaction of hydroxyl radical with arenes.**

STUDENT: Devinder Kaur

DEGREE: Doctor of Philosophy

COLLEGE: Science and Humanities

DATE: December 2016

PAGES: 162

The primary steps of the decomposition of the aromatic pollutants in the environment involve their reactions with hydroxyl radical (OH•). Structure-reactivity models capable of accurately predicting both the reactivity and selectivity of these reactions in gas and solvent phases are of interest to the environmental and biochemical communities. High accuracy computational methods (CBS-Q// BH&HLYP/6-31G(d,p)) were employed to explore the possible reaction pathways for reaction of OH• with a range of substituted aromatic compounds with functional groups ranging in activity from strongly electron donating (such as $-NH_2$, $-OCH_3$) to strongly electron withdrawing ($-NO_2$, $-CF_3$). It was determined that in the case of addition of hydroxyl radical to arenes, the reactivity was largely controlled by polar effects, demonstrated by linear relationships between the calculated rates of reaction and the ionization potentials and Hammett substituent parameters of the arenes. Addition at positions *ortho*- and *para*- to the substituent are the dominant modes of addition to arenes in general, but addition at the meta- position becomes more favored, and addition at *ortho*- less favored with rings bearing strongly electron withdrawing groups.

Inclusion of solvent effects in the form of a polarizable continuum (SMD) model indicates that these effects become more pronounced in polar solvents. Initial investigations indicate that such effects are less pronounced when considering hydrogen abstraction from side chains. Calculated rate coefficients support solution phase experimental studies that show that addition to the ring is dominant mode of reaction for hydroxyl radicals with alkylated arenes.

ACKNOWLEDGEMENTS

I would like to sincerely thank my Research Supervisor Dr. James S Poole, for his valuable time, advice, guidance, patience, and understanding throughout the processes of research work and writing.

I would like to extend my appreciation to my committee members, Dr. Mahamud Subir, Dr. Carolyn Dowling, Dr. Mahfuza Khatun, and Dr. Jill Coleman for their valuable time and constructive comments.

I would like to thank Spencer Davis, administrator for the College of Sciences and Humanities Beowulf Cluster at Ball State University for helpfulness and advice with respect to carrying out my calculations.

I also want to thank my parents Mr. Shamsher Singh and Mrs. Gurmeet Kaur who had been a big inspiration in my life and the support they had provided me emotionally and financially throughout my studies.

Finally, last but not least I would like to thank my husband Mr. Ranjit Singh and my daughter Akaljot Kaur and my son Pavneet S Saini for all the love and encouragement they had given me for completing this step of my life. Thank you very much for always being supportive.

TABLE OF CONTENTS

LIST OF SCHEMES

LIST OF FIGURES

LIST OF TABLES

CHAPTER 1- INTRODUCTION

Organic materials are present in the Earth's atmosphere and hydrosphere, and are known to arise from various sources. A large portion of these materials may be said to arise from natural sources: volatile organic chemicals (VOC) in the atmosphere [1], or humic substances in natural waters [2]. However, it is recognized that a significant fraction arise from anthropogenic sources [3], such as combustion of fossil fuels or large scale industrial processes [4]. These organic compounds are degraded in the environment by photolysis and/or reaction with reactive oxygen species (ROS) such as [5] :

- Superoxide ($^{\bullet}O_2^-$), nitrate and nitrite radicals,
- Peroxides ($^{\bullet}O_2^{-2}$) , Alkylperoxyl ($ROO^{\bullet}$) and peroxyl ($HOO^{\bullet}$) radicals,
- Hydroxyl ($OH^{\bullet}$) and alkoxyl ($RO^{\bullet}$) radicals,
- Singlet oxygen ($^1O_2$), and ozone (O_3)

Emission of organic compounds and products formed *in situ* in the environment can lead to number of adverse effects. For example [6, 7]:

- Formation of ozone, an air pollutant that is problematic in the lower troposphere and beneficial in the stratosphere, in the presence of nitrates

- Formation of secondary organic aerosol (smog) resulting in visibility degradation and risks to human health.

Therefore, it is essential to understand the reactions that are involved in the environmental degradation of organic compounds via processes mediated by reactive oxygen species (ROS). This includes an understanding of the fundamental chemistry of these organic compounds: their reaction mechanisms and identification of primary and secondary reaction products.

1.1 An Introduction to the Chemistry of Hydroxyl Radical

Degradation of organic compounds in environment often involves free radical intermediates: atoms or molecules that contain one unpaired electron that are consequently highly reactive towards other compounds, and therefore typically short-lived. Free radicals with an unpaired electron on oxygen are typically ROS. The relative importance of ROS depends on the discipline in which they are considered. For example, ozone is considered an important reactive oxygen species in environmental studies [8], whereas superoxide plays an important role in biological studies [9].

Of all of these reactive oxygen species, the hydroxyl radical is the one that garners the most interest because this particular reactive intermediate is involved in range of biological and environmental processes [10-12]. The Hydroxyl radical can be generated thermo-, electro- and photo-chemically, and reactions of many aromatic compounds such as polycyclic aromatic hydrocarbons (PAHs) with hydroxyl radical ($OH^{\bullet}$) are the primary steps in their degradation mechanisms. Therefore, it would be valuable to be able to accurately predict the thermodynamics and kinetics of hydroxyl

radical reactions with a view to understanding and modelling processes of environmental significance; for example, the uptake of hydroxyl radical at aqueous interfaces and its subsequent reactivity.

The hydroxyl radical can undergo different reactions with organic compounds, including hydrogen abstraction, addition to π-bonds and redox (electron-transfer) reactions (Scheme 1.1) [13, 14].

Scheme 1.1: Modes of Reactivity of Hydroxyl Radical

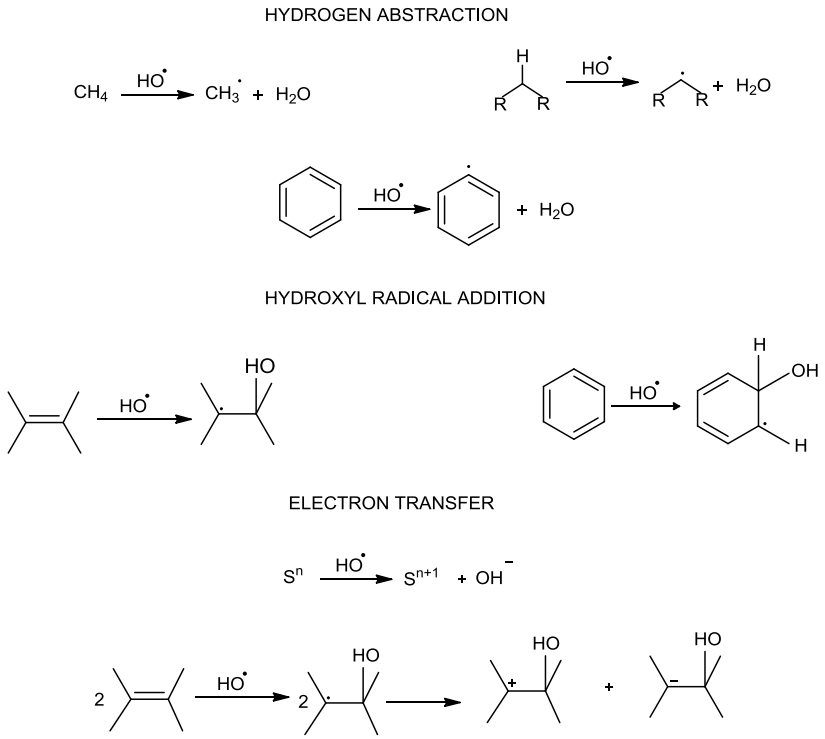

Hydrogen abstraction is the reaction between the hydroxyl radical and organic compounds which involves simultaneous cleavage of C-H bond and the formation of water and a carbon centered radical [15]. The carbon centered radical is typically more stable than hydroxyl due to the lower electronegativity of carbon. The hydroxyl radical is

generally held to be more reactive and less selective than hydrogen radical because the formation of H-OH bond is more thermodynamically favorable than the formation of H-H bond (an example of the so-called reactivity-selectivity principle) [16]. The product carbon centered radical can undergo additional reactions to form a stable product [17].

Addition involves reaction of the hydroxyl radical with π-electrons in aromatic systems or alkenes resulting in formation of an O-C bond [18] and in the case of arenes, the generation of cyclohexadienyl radical intermediates [19]. Cyclohexadienyl radicals are resonance stabilized (Scheme 1.2), but will typically seek to be re-oxidized to regain aromaticity via hydrogen abstraction.

Scheme 1.2. Resonance Stabilization of Cyclohexadienyl Radicals

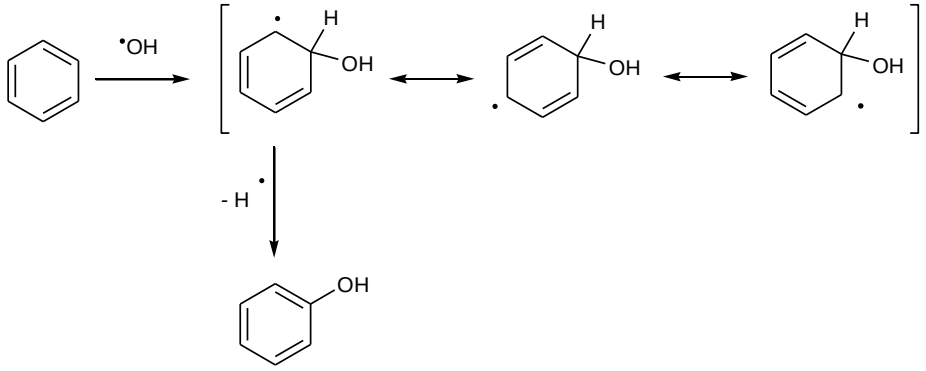

Electron transfer reactions between the hydroxyl radical and alkyl radicals formed by processes such as radical addition are known in some cases to generate carbocations [20], although these reactions are not typically dominant [21-23]. Theoretical calculations and experimentation have shown the hydroxyl radical is a powerful oxidant, and generally reacts as an electrophilic species. Thus, the extent of

electron transfer between a hydroxyl radical and an arene has been shown to be dependent on the ionization potential of the aromatic molecule [16, 20]. A hydroxyl radical is also capable of oxidizing molecules other than carbon centered radicals; for example it may also undergo redox reactions with thiocyanate, halide and nitrite anions [16] .

Thus, any given molecule (particularly those containing multiple functional groups) may undergo more than one reaction with hydroxyl radical. A relatively simple example involving an arene hydrocarbon, toluene, is shown in Scheme 1.3: one may envisage addition of the hydroxyl radical at positions *ortho*-, *meta*-, *para*- and *ipso*- to the methyl group. In the first three cases, oxidative re-aromatization would lead to the formation of isomeric cresols, in the latter case, the loss of a relatively unstable methyl radical will lead to re-aromatization: such reactions are more likely where the leaving radical is stable (for example, a halogen group).

Alternatively, one may postulate a sequence of hydrogen abstraction reactions from the phenyl ring at *ortho*-, *meta*- or *para*- from the methyl group. Such reactions are possible, but are unlikely to be thermodynamically favored as the resultant phenyl radicals from hydrogen abstraction have significant s-character, and are not resonance stabilized. Far more likely is the abstraction from the benzylic position of toluene to generate the resonance stabilized benzyl radical.

Thus, even for a simple molecule such as toluene, as many as eight competing reactions, each giving products with distinct chemical, physicochemical and biological properties, are in play to a greater or lesser extent. The reactivity and selectivity of reaction may vary depending on the functional groups present on the given molecule.

Scheme 1.3. Potential Hydroxyl Radical Reactions with Toluene

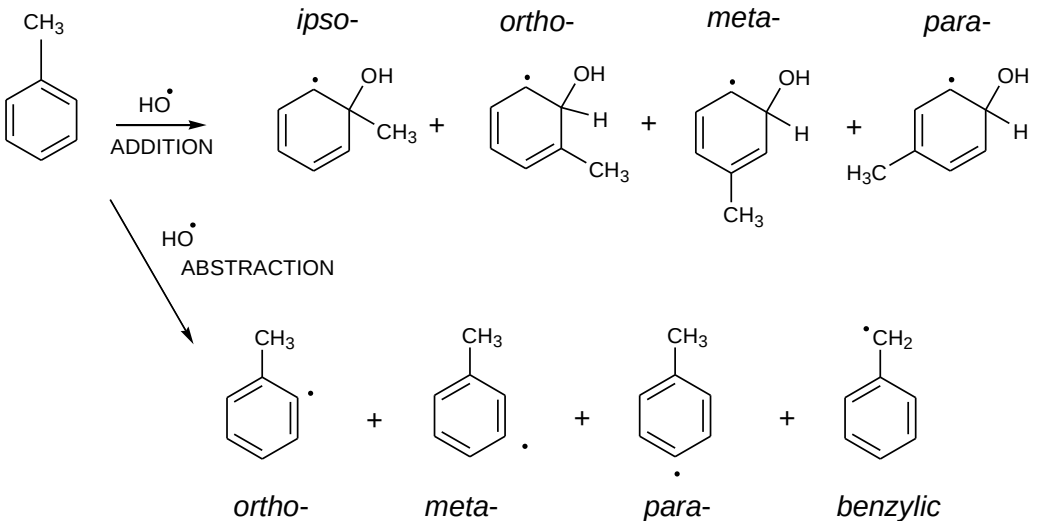

Much research has been performed regarding the rate constants and mechanisms of the initial reactions of hydroxyl radicals with organic compounds [24, 25]. However, due to limitations in synthetic availability, or in physicochemical properties, such as solubility, there remain organic compounds that have not yet been studied, which still need to be understood in terms of their reactivity towards hydroxyl radicals. Therefore, an ability to accurately measure, and ultimately predict, both the reactivity and selectivity of hydroxyl radicals is of utility to those who wish to model hydroxyl radical reactions of environmental and biological import.

1.2 Hydroxyl Radical Reactions – An Overview of Experimental Approach

1.2.1 Reactivity of Hydroxyl Radical - Kinetic Methods

Given the short lifetime (nanosecond or sub-nanosecond timescales) of hydroxyl radical under typical laboratory conditions, many of the methods used to study the kinetics of hydroxyl radical have features in common: hydroxyl radical is generated, often by photochemical means, and detected by their spectroscopic signatures. Direct detection of hydroxyl radical may be achieved in gas phase. In solution phase a "reporter species"; one formed by reaction of a precursor with hydroxyl, having a distinct and characteristic spectroscopic signature and known kinetics; is utilized. A competing substrate is introduced, and changes to the rate of reaction (or yield of reporter species) may be analyzed to find the rate of reaction of hydroxyl radical with substrate. Three examples of such an experiment are discussed below: laser induced fluorescence, laser flash photolysis and pulse radiolysis.

Laser Induced Fluorescence: Laser induced fluorescence methods are sensitive for observing free radical reactions in the gas phase. They have been used to study the reactivity of hydroxyl [25-29], nitrate [30, 31], methoxyl [32, 33] and other alkoxyl [34-38] radicals. In terms of hydroxyl radical chemistry, these fluorescence techniques rely on the fact that the electronically excited states of HO•, generated by radiation of an appropriate wavelength (282 or 308 nm) are short-lived and will fluoresce at 308 nm as they relax back to the ground state [39]. The fluorescence may be monitored in an axis perpendicular to the exciting radiation in order to separate the fluorescence signal from the excitation source [40, 41]. Hydroxyl radical is either generated directly from water vapor or may be generated as result of reactions of other

molecules (for example H• + NO_2 → OH• + NO). The exciting laser pulses (282 nm for so-called off-resonant fluorescence and 308 nm for resonant fluorescence, Figure 1.1) are focused onto a sample under high vacuum. The resultant fluorescence is measured and analyzed. Hydroxyl radical can be detected in both on resonant and off resonant fluorescence. The laser induced fluorescence technique for is typically applied in the off resonance mode [42, 43].

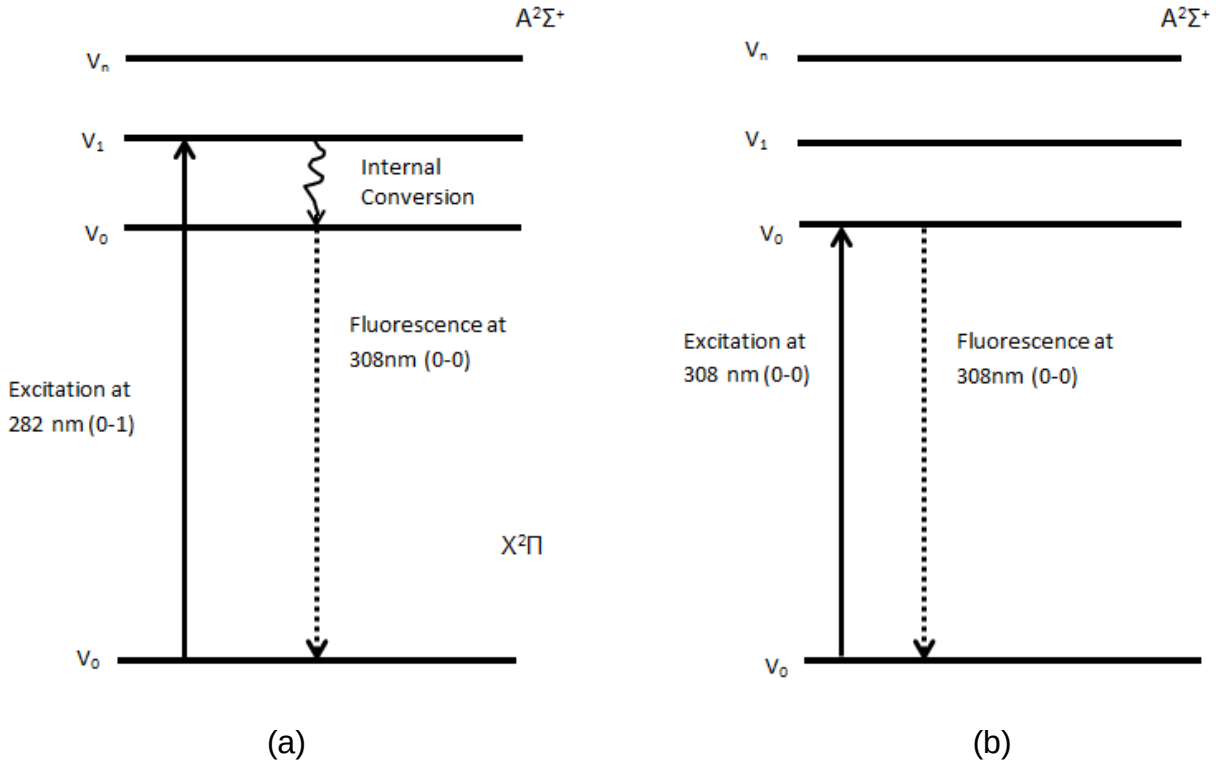

Figure 1.1: Simplified Jablonski diagrams for (a) off-resonant and (b) on resonant emission of hydroxyl radicals as they de-excite from the first electronically excited ($A^2\Sigma^+$) state to the ground ($X^2\Pi$) state.

One of the potential limitations of this method is that only reactions in the gas phase may be monitored in this fashion. In solution, non-radiative collisional deactivation is rapid and laser induced fluorescence cannot be used. Moreover, the hydroxyl radical does not have any practical direct spectroscopic handle in the solution

phase, and so experimental methods in solution must utilize reporter species.

Laser Flash Photolysis: Flash photolysis is a method used to probe the kinetics of reactive intermediates in solution, and has been used in hydroxyl radical reaction kinetics [44, 45]. In this technique, reactive intermediates are generated in solution by excitation of a precursor using a light pulse produced by a flash lamp or laser [44, 46, 47]. A broad spectrum monitoring beam (from a high intensity light source) is passed through the sample, usually perpendicular to the laser beam path, and dispersed by a diffraction grating in the detector. The change of absorbance in the sample at one or more wavelengths may be monitored either by fast photomultiplier tube, or using a CCD camera.

The hydroxyl radical does not have to have a useful UV-absorbance or fluorescence in solution to achieve detection, but there are a number of reporter species reported for hydroxyl. The thiocyanate anion (SCN^-) has been shown to be an effective reporter for hydroxyl radical reactions in water. This species undergoes an apparent electron transfer reaction to yield thiocyanatyl radical (possibly via an addition intermediate, $HOSCN^{\bullet-}$), which in turn reacts with a second equivalent of thiocyanate to generate the dithiocyanatyl radical anion, $(SCN)_2^{\bullet-}$, which has a strong absorbance at 475 nm in water [16, 48]. This species is rapidly formed (essentially at the diffusion limit) and readily detected, making it a useful proxy for hydroxyl radical.

Thiocyanate exhibits solubility in organic solvents, but it is limited and so alternative reporters must be found. In acetonitrile, *trans*-stilbene may be used as a reporter molecule (Scheme 1.4) [46].

Scheme 1.4. *Trans*-Stilbene as a Hydroxyl Radical Reporter for LFP

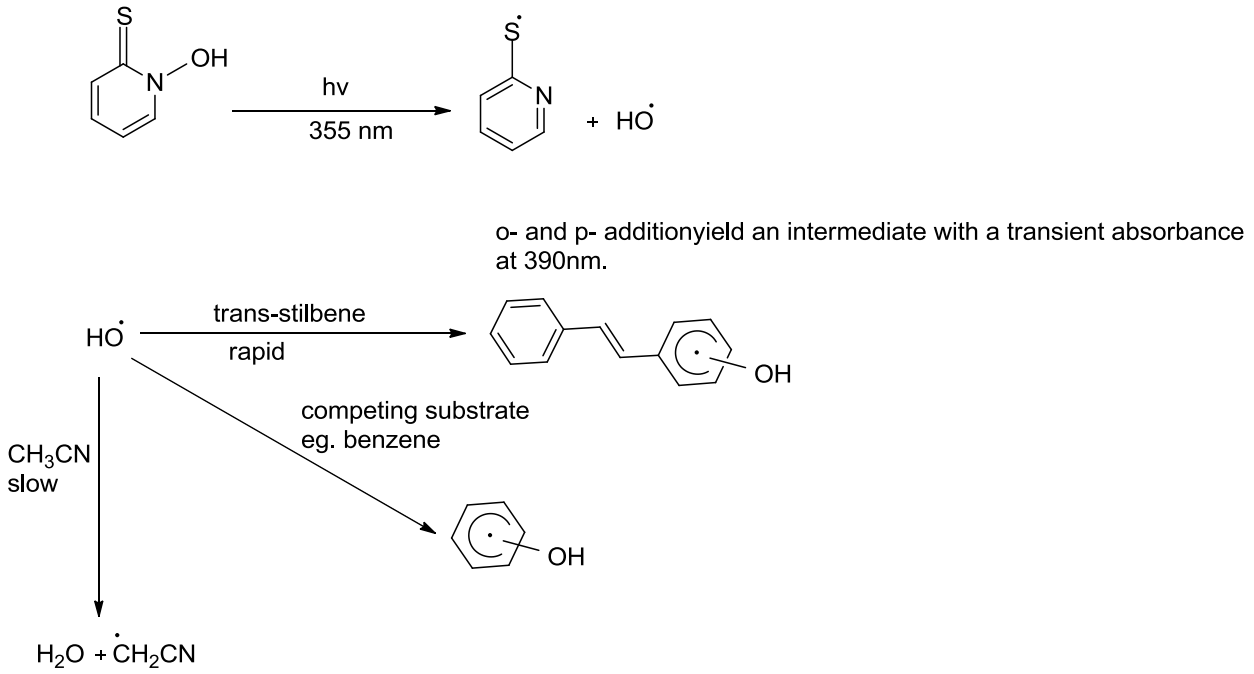

Hydroxyl radical, formed by photolysis of *N*-hydroxypyridine-2-thione at 355nm (or the pyridone analogue at 308nm) reacts with stilbene to form a transient species which has strong absorbance at 390 nm. Therefore the rate coefficient for hydroxyl radical reaction with stilbene ($k_{stilbene}$) can be observed and determined directly by monitoring absorbance at 390 nm.

Other rates are determined by constructing an experiment with a competing substrate, preferably one without any appreciable absorbance at 355-390 nm (either the substrate or its hydroxyl-derived products). Increasing amounts of competitor will decrease the amount of reaction with stilbene, and Stern-Volmer analysis of quenching (Equation.1.1) of the stilbene signal in the presence (A_{390}) and absence ($A_{0,390}$) of competing substrate yields a ratio of bimolecular rate coefficients, the value of one already established [44, 49, 50].

$$\frac{A_{0,390}}{A_{390}} = 1 + \frac{k_{\text{arene}}[\text{arene}]}{k_{\text{stilbene}}\,[\text{stilbene}]} \qquad (\text{Eq. } 1.1)$$

Pulse Radiolysis: Pulse radiolysis was developed for studying fast processes in solution about 20 years after flash photolysis [51], and has features in common with the earlier method. The major differences lie in the generation of hydroxyl radicals. Hydroxyl radicals are generated by highly energized gamma radiation, which is known to excite and rapidly fragment water [16, 52]. As such, pulse radiolysis is particularly useful for studying reactions in aqueous phases. Gamma radiolysis of water molecules produces hydroxyl radicals, solvated electron, H_2O_2 and H_2 [53] (Scheme 1.5). The generation of hydroxyl radicals is further enhanced by the presence of N_2O, which reacts with solvated electrons to generate more hydroxyl radicals.

Scheme 1.5 Generation of Hydroxyl by Radiolysis of Water

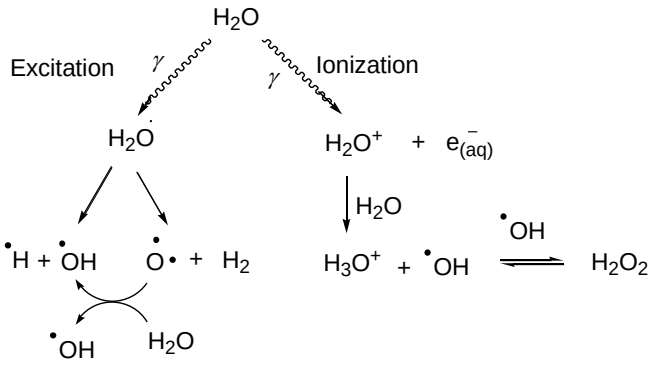

Given the lack of selectivity of gamma radiation, it is desirable that most of the energy absorbed in pulse radiolysis is absorbed by the solvent, and so dilute aqueous solutions of the species of interest are used. This method is therefore limited to

compounds that have measurable solubility in water, which many compounds (eg. larger PAH), do not exhibit. Consequently, sulfonate analogues are often used under such circumstances [54, 55]. Hydroxyl radicals are detected by absorbance of reporter molecules, in particular systems such as the dithiocyanatyl radical anion. This method is effective in measuring the kinetics of reactive species in very dilute solutions but will not work for other solvents or concentrated solutions [56, 57].

There are a number of other experiments of this general type, which are often termed ‘’direct’’ kinetic experiments, even though many of the rate coefficients determined are in fact obtained from ratios of rate coefficients. However, these methods do share a fundamental limitation that they provide information on *reactivity* (i.e. rate coefficients), but because the product radicals are often not directly detected, they provide only limited information regarding the *selectivity* (product distributions or relative rate coefficients). The observed rate coefficient, $k_{obs,}$

$$\frac{\mathrm{d[HO^{\cdot}]}}{\mathrm{dt}} = -k_{\mathrm{obs}}[\mathrm{HO^{\cdot}}][\mathrm{Substrate}] \qquad (\mathrm{Eq.}\,1.2)$$

is actually a sum of elementary rate coefficients. Since there are going to be addition and abstraction products from the reactions, we may write

$$\mathrm{k_{obs}} = \left(\sum_{\mathrm{i}} \mathrm{n_i}\, \mathrm{k_{add,i}} + \sum_{\mathrm{j}} \mathrm{n_j} \mathrm{k_{abstr,j}}\right) \Big/ \left(\sum_{\mathrm{i}} \mathrm{n_i} + \sum_{\mathrm{j}} \mathrm{n_j}\right) \qquad (\mathrm{Eq.}\,1.3)$$

where *i* and *j* represent each of the possible sites for addition and hydrogen abstraction, respectively. Some indications of selectivity may be gleaned by methods that involve the study of protonated and deuterated analogues of a given substrate, and determining the magnitude of kinetic isotope methods (KIE) in their measured rate coefficients. However, the magnitude of a given KIE is dependent on the mechanism: a hydrogen

abstraction reaction would be expected to exhibit a large primary KIE (4-8), whereas as addition reaction would be expected to exhibit a much more modest secondary effect [42, 58].

1.2.2 Selectivity of Hydroxyl Radical - Product Analysis

There have been number of experimental studies of hydroxyl radical selectivity with most of these involving the continuous generation of hydroxyl radicals in the presence of the substrate of interest. The system is permitted to react for a certain amount of time, and the product distribution analyzed by techniques such as liquid or gas chromatography (LC and GC respectively). The relative rate constant data estimated based on the relative importance of a product or family of products in the overall product distribution. Again, such experiments may be conducted in the solvent or gas phase.

Smog chambers are environments where gas phase reactions of radicals and substrates are investigated. They provide controlled environments to study the formation and the subsequent fates of specific compounds [59, 60]. In the gas phase, hydroxyl radical may be generated by the UV photolysis of nitrous acid in a sealed smog chamber symmetrically surrounded by fluorescent black lamps [61]. Hydroxyl radical generated can then react with the substrate in chamber. Excess NO is added to the chamber to avoid the formation of ozone [62-64]. The products formed are analyzed by gas chromatography with detection by mass spectrometry (GC/MS) and compounds are identified by their retention times and MS fragmentation patterns.

A similar approach may be used in the solution phase, although in these cases

there are a greater range of methods that one may use to generate hydroxyl radical, such as thermolysis or photolysis of hydroperoxides, or more simply, the reduction of hydrogen peroxide by metal salts or complexes, such as Fe^{II} salts (the Fenton reaction).

$$Fe^{2+} + H_2O_2 \longrightarrow Fe^{3+} + OH^- + \bullet OH$$

Fenton chemistry is very cost effective for remediation of low-volume, high-concentration of pesticide waste such as unused stocked commercial mixes. Fenton-mediated degradation of carbamate [65] and phosphorothiate [66] insecticides and chloroacetanilides [67] have been described. Once again, product analysis is usually performed via chromatographic techniques [67-69]. Application to arene systems involves the detection of isomeric phenolic derivatives (phenols or silyl ethers, depending on method used) by chromatographic methods (Scheme 1.6) [70-72].

Scheme 1.6 Product Analysis for Reaction of Arenes with Hydroxyl Radical

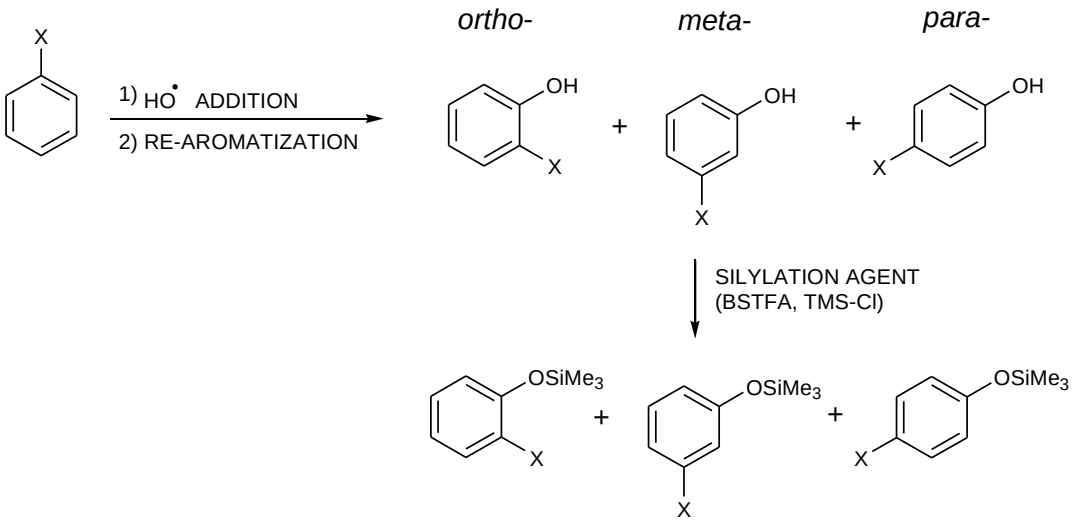

Product distribution (often termed “indirect”) methods have the advantage over direct methods, in that they provide information on selectivity of the reaction, based on

the relative importance of the products in the distribution generated under a given set of experimental conditions. However, the rate coefficients obtained are typically relative rate coefficients or rate coefficients ratios, and cannot, in and of themselves, provide absolute rate coefficients. Thus, product distribution studies must be complemented, where possible, with rate coefficient data from “direct” methods such as LIF or LFP.

Another drawback of product distribution studies is that they measure outcomes of complex multistep radical reactions. The products of the first reaction are susceptible to secondary reactions, and in fact, primary products may be more reactive toward hydroxyl radical than the starting material. In principle, this may lead to biases in the product distribution. Prolonged exposure to oxidative conditions will lead to exhaustive oxidation (often referred to as “mineralization”) of the organic compound. In addition, studies are limited to substrates that are readily available synthetically, exhibit physicochemical properties (such as solubility, volatility) that are amenable to the experimental conditions, and can be present and/or generated in readily quantifiable concentrations. Different functional groups on the reactant are going to have different effects on reactivity and selectivity of hydroxyl radical reactions on that reactant. What, then, shall we do if we encounter the oxidation product or metabolite of a new compound, which may be identified on the basis of high resolution analytical techniques (such as high resolution mass spectrometry), but is not available synthetically (due to limitations in synthetic methodology or prohibitive cost)?

Clearly, it would be advantageous to develop a model of chemical reactivity that allows us to predict the outcomes and rates of reactions based upon the structure and functionalization of a given reactant.

1.2.3 Structure-Reactivity Relationships-An Introduction

Qualitative structure-activity relationship models (QSAR) are mathematical models that can be used to relate the relationship between chemical properties (thermodynamic and kinetic) and chemical structure of known compounds, with a view to applying those models to compounds that are not readily available [73, 74]. QSAR models have broad applications in finding the potential impacts of chemicals, materials and nanomaterials on human health and ecological systems [75]. QSAR modelling typically involves regression analysis of experimental data. There have been a number of regression models available, of varying levels of complexity, which have been utilized to predict a range of physical properties including, but not limited to, acidity [76], solvent partition coefficients [77] and toxicity [78] . For the purposes of this introductory discussion, it is useful to consider one of the archetypal QSAR models: the Hammett equation for describing the reactions of arenes [79].

The Hammett equation describes a linear free energy relationship relating reaction rates or equilibrium constants for many arene reactions with two parameters: a substituent constant (σ) and a reaction constant (ρ) (Equation 1.4).

$$\log\frac{k_X}{k_H} = \sigma\rho \qquad \text{(Eq.1.4)}$$

In the case of the kinetic equation (Eq. 1.4), k_x is the rate constant observed for reaction of a substituted arene, and k_H is the rate constant observed for the unsubstituted analog. A similar equation exists for thermodynamics that involve equilibrium constants that may be denoted K_X and K_H for the substituted and unsubstituted species respectively. Since log K_H and log K_X is directly related to the standard free energy change of reaction ΔG° (Equation 1.5):

$$\Delta G° = -2.303RT \log K \qquad \text{(Eq.1.5)}$$

the substituent constant is actually a measure of the substituent effect expressed in terms of a free energy quantity.

The substituent constant (*σ*) of different functional groups on arenes is found from the measurement of the acid dissociation constant of substituted benzoic acids (an equilibrium constant). Experimental data [80] shows that the acidity of benzoic acid is enhanced by electron withdrawing groups and diminished by electron donating groups, thus a positive value of *σ* indicated the capacity of a substituent (a functional group) to withdraw electron density from the ring (for the rates of hydrolysis of benzoate esters , the value of *ρ* is set to unity). Electron donation or withdrawal may be achieved by a combination of resonance and inductive effects (Scheme 1.7):

Scheme 1.7: Resonance Contributors for Electron Donating and Electron Withdrawing Groups

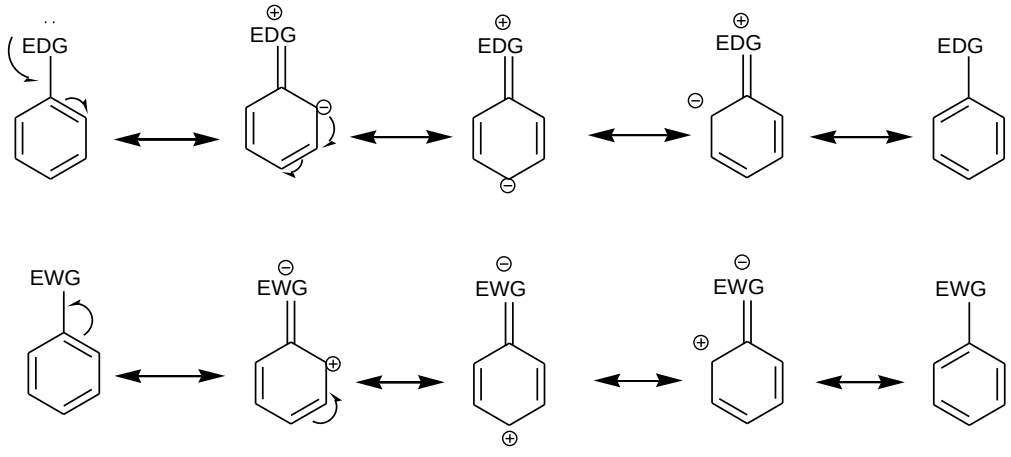

The relative importance of the two effects is dependent of their position on the aromatic ring: substituents on the *meta* position of aromatic ring (substituent parameter σ_m), exert an effect that is dominated by inductive effects. On the other hand, substituents on *para* position of the aromatic ring (substituent parameter σ_p), exert an effect that is primarily a resonance effect but also an inductive effect (although to a lesser degree) [81, 82].

It is possible to derive a different set of substituent parameters (σ_I and σ_R) that treat inductive and resonance effects as separable [83], but this lies outside the scope of discussion presented here. Data for *ortho* substituents is typically excluded as there is a steric component that also influences reactivity [84]. In the case of hydroxyl radical chemistry, there is the additional possibility that unusual stabilization of the *ortho* product may be observed due to favorable intramolecular hydrogen bonding interactions.

When the log of the ratio of rate constants is plotted with the corresponding σ the slope of the line (assuming the correlation is linear) is the reaction constant ρ. The value of ρ is indicative of the amount of negative charge build-up that is generated on the ring during a reaction, and the sensitivity of the reaction to the substituents. In cases where $\rho > 0$, the reaction is likely to involve negatively charged intermediates or negative charge character in transition state of the rate determining step, for example:

- Base-catalyzed benzoic ester hydrolysis [85] and
- Reaction of benzoic esters with amines [86]

In cases where $\rho < 0$ the reaction is likely to involve positively charged intermediates or positive charge character in transition state of the rate determining step, for example:

- Reaction of anilines with acyl chloride [87] and
- Epoxide cleavage with phenoxides [88]

In the latter case, the reaction correlation is not due to build-up of positive charge in the transition state, but the diminution of negative charge on the phenoxide moiety.

In addition to the sign of ρ, the magnitude also provides an indication of the sensitivity of a reaction towards charge effects. For example in a situation where $0 < \rho < 1$ the reaction will involve a certain degree of negative charge build-up in the rate determining step, but will probably not involve an anionic intermediate. A free-radical reaction involving neutral but polar species (for example, reaction of hydroxyl radical with alkenes or arenes), might be expected to exhibit a weak positive Hammett correlation. Neutral, non-polar reactions (for example those involving alkyl radicals or pericyclic reactions) will yield ρ values close to 0. There are reactions that exhibit non-linear Hammett correlations. Such correlations usually indicate a change in the reaction mechanism.

Hammett plots are a useful tool in probing the electronic effects which different substituents impose onto a system, and their linearity provides a predictive model for reactions that have yet to be probed experimentally. As described above, these models are based primarily on experimental data, and typically involve “clean” reactions that yield a single product from a synthetically available source. However, free radical reactions in general, and hydroxyl radical reactions in particular, are not necessary “clean”- even for a simple substrate such as toluene there are a number of possible reaction pathways. Deconvoluting a sufficient number of product distributions to obtain predictive models for individual processes (e.g. the QSAR for addition *o*-, *m*-, *p*- to a

given substituent) is difficult. How does one isolate and analyze each possible reaction pathway without interference from alternative reaction pathways? The answer lies in the usage of computational chemistry to calculate rate coefficients that may be used to construct QSAR correlations.

1.3 Previous Computational Studies of HO• Reactions

Due to its importance in atmospheric, combustion and biological chemistry,[24, 39, 89, 90] hydroxyl radical has been well studied by both experimental and computational methods. A number of computational studies have been performed, using a variety of methods, and so only a representative sample is included in this discussion. The methods used in these computational studies are described in greater detail in the following chapter.

The reaction of alkyl and hydroxyl radical with alkenes has been studied at high levels of theory due to the importance of such reactions in free-radical polymerization [91, 92]. Hydroxyl is an important initiator for free radical polymerization reactions, and so there have been various studies done to understand hydroxyl radical reactions with alkenes [93, 94]. The structure of reactants, pre-reactive complexes, products and transition states have been optimized using different methods including MP2/6-31G(d,p) (MP2 level of theory in conjunction with a 6-31G(d,p) basis set, see Chapter 2), QCISD/6-31G(d) and B3LYP/6-31G(d) [91]. In each case, the authors found that radical addition barriers were within the mean absolute deviation (MAD) for the methods used of experimental values in solution (1.2-1.5 kcal/mol for typical additions of hydroxyl radical to 1-butene). It should be noted that the MAD for some of the methods used are

quite large. At MP2/6-311G(d,p) and MP2/6-31G(d,p) levels, Farmer and Moore [95] found that the addition of hydroxyl radical to the vinyl group is a more favorable pathway than the abstraction of hydrogen atom from the vinyl group for styrene; they did not measure addition and abstraction on the ring.

Hydroxyl radicals can attack at α (head) and β (tail) positions of a given alkene to form a functionalized alkyl radical, with preferences dictated by the functional groups and their impact on the transition states for addition [95]. Transition states for addition exhibit a buildup of positive charge on the substituted ethylene species that can be stabilized by electron donating substituents and destabilized by electron withdrawing substituents. The results suggest that a polar effect is important as the reacting system evolves from reactants to transition state.

Scheme 1.8: Reaction of Alkenes with Hydroxyl Radical.

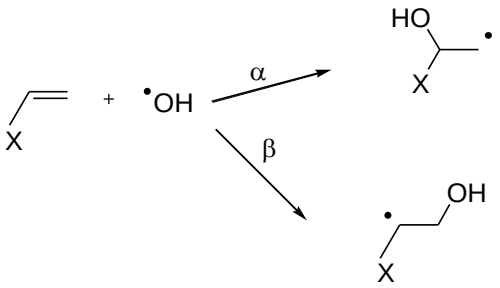

Uc and Tully have studied the reaction of Benzene and Toluene with hydroxyl radical using BH&HLYP/aug-cc-pVTZ, BH&HLYP/6-311++G(d,p)) and CCSD(T)/6-311++G(d,p) levels of theory. In the case of toluene, Uc and Tully found the following: (a) *ortho* products are the more favored outcomes for addition to the ring; (b) abstraction

from the side chain occurs through a complex mechanism which includes the reversible formation of a reactant complex, and (c) ring abstraction is non-negligible at high temperatures but remains relatively small about 11% at 1000K [42, 96]. In an earlier study at the MP2/6-311G(d,p) and B3LYP/6-311G(d,p) levels of theory, Uc *et al*. found that *ortho* and *ipso* are most favorable addition products but *ipso* is considered to be less abundant and may also result in different species [97].

Shiroudi *et al*. studied the oxidation mechanisms of naphthalene by hydroxyl radicals at the CBS-QB3 level of theory and found that the addition of hydroxyl radical to the ring yielded a 2:1 ratio of 1-naphthol: 2-naphthol. They also studied hydrogen abstraction to yield 1- and 2-napthyl radicals, and found that both products were derived from a common pre-reactive complex, with little selectivity [19, 98]. DeMatteo *et al*. [46] carried out a combined LFP and computational study on the kinetics of hydroxyl radical reactions with benzene and naphthalene in acetonitrile, and a comparison with reaction kinetics in aqueous solution. CBS-QB3 calculations indicated that there was a substantial degree of charge transfer character in the transition state for addition to benzene, consistent with the behavior exhibited upon addition to alkenes. The authors found that the solvent effect calculated by PCM methods had relatively little impact on kinetics, but that larger effects could be observed by adopting an explicit solvent model.

Investigation of the reaction of *p*-xylene (1,4-dimethylbenzene) with hydroxyl radicals was performed at the B3LYP6-31G(d,p) level of theory, and indicated that hydroxyl addition to the ring is dominated by attack at the *ortho* position (80%, 298K) and 20% at *ipso* position. Attack at the *ipso* positions yield epoxy and bicyclic peroxy radicals [99]. Hydroxyl radical attack on *ortho* (1,2-dimethylbenzene), *meta* (1,3-

dimethylbenzene) and *para* xylenes was investigated at the B3LYP/6-31G//MP2/6-31G (this notation indicates that geometry optimization was performed using MP2 method, and energies calculated using DFT). For *o*-xylene, product distributions were calculated as follows: 3:4-substitution 60: 40; for *m*–xylene, 2:4:5-substitution 53:47:0. Only 2-substitution was observed for *p*-xylene, and *ipso* addition was not considered [100]. It should be noted that the methods utilized are known not to yield chemical accuracy for reaction barriers or energies of reaction.

With respect to functionalized arenes, Wu *et al*. studied the reaction mechanism and kinetics for addition of hydroxyl radical to phenol at the B3LYP/6-311G(2dp,2df) and CBS-APNO levels of theory. Their study indicated that *ortho* addition pathways account for 97-100% of addition products in the gas phase at 210 to 360 K [18]. Kovacevic *et al*. studied kinetics of hydroxyl radical to fluorobenzene at G3/B3LYP, BH&HLYP (aug-cc-pvDZ), and CBS-QB3 methods. Their calculations predicted the distribution of fluorohydroxycyclohexadienyl radicals to be 31% *o*-, 23% *m*-, 38% *p*- and 8% *i*- [101]. Bryukov *et al*. studied gas phase kinetics of hydroxyl radical reactions with chlorobenzene using apulsed laser photolysis fluorescence technique over wide range of temperature and pressure and compared the results with computational data obtained at CBS-QB3 levels of theory. This study indicated that addition preferentially occurs at the *o*- and *p*- positions, and the authors also investigated the *ipso*- addition-elimination reaction that leads to the formation of phenol and chlorine free radicals [102].

DFT methods B3LYP/6-31G(d), and BH&HLYP/6-31+G (d,p) were used to calculate barriers and rate constants for reaction between adenine and the HO• radical.

Abstraction and addition reactions were found to contribute equally to the overall rate constant [103].

Chan *et al*. used the BH&HLYP/6-31+G(d,p) method to calculate energies and vibrational frequencies for α-hydrogen abstraction from amino acids which results in formation of a stable carbon radical which in turn results in peptide bond cleavage and induced changes in the structure of amino acids in the sequence [104-106]. Similar studies of hydrogen abstraction reactions have been carried out at high levels of theory. For example, G2, G2(MP2) and B3LYP6-31G(d) calculations have been used to investigate the reaction of hydroxyl radical with methane and halomethanes, primarily fluorinated and chlorinated species [107-109]. The motivations behind these studies were connected with the atmospheric oxidation of greenhouse and ozone depleting species. In a study of the oxidation of 2-butanol, multiple pathways were considered (Scheme 1.9) [110]:

Scheme 1.9: Reaction Pathways for Hydroxyl Radical and 2-Butanol

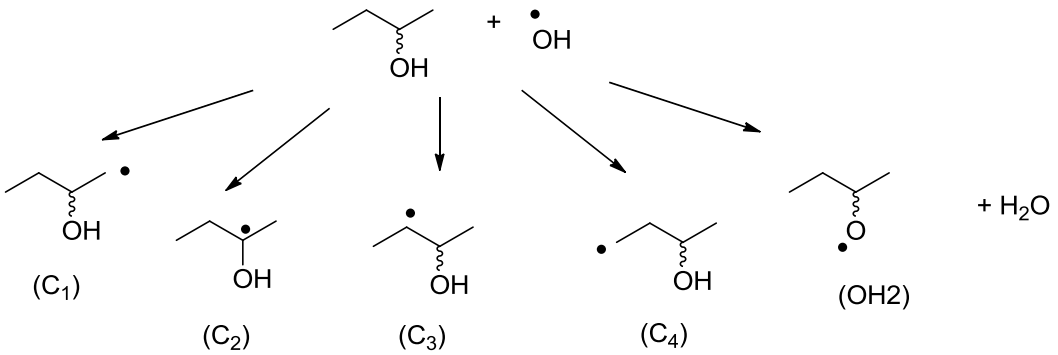

The reaction barrier heights for abstraction from various sites follow the order C2 < C3 < C4 < C1 < O (as might be expected based on the relative stabilities of the

product radicals), but the reactivities of the various sites do not precisely reflect the order of barrier heights (suggesting a significant entropic effect), and the major products in the distribution are strongly dependent on temperature.

There is possibility of hydrogen abstraction by hydroxyl radical from the ring which results in formation of phenyl radical or from the side chain which results in formation of benzyl radical. Hydrogen abstraction from the ring has been studied by Hollman *et al.* [111] in which the geometries were optimized at MP2/6-31G and the energies were obtained at CCSD(T) level of theory which gives the transition state energy at 4.2 kcal/mol which is in agreement with previous studies of hydrogen abstraction in benzene [112]. Hydrogen abstraction from both the side chain and ring has been studied by Uc *et al.* [96] at the range 275-1000K by CCSD(T)/6-311G(d,p) calculations using structures optimized at the BH&HLYP/6-311G(d,p) level of theory. They considered four different pathways: side chain abstraction and three possible ring hydrogen abstractions. This study shows that the ring H abstraction is negligible at low temperature and at high temperature it contributes 11% to the total abstraction products. It also shows that the transition state energy for the abstraction from the side chain is 3.5 kcal/mol, which is consistent with the experimental value of 3.5-5.0 kcal/mol. The ring hydrogen abstraction transition states occur much later than in the case of the side chain hydrogen abstraction. They also performed intrinsic reaction coordinate (IRC) calculations following the reaction and found that the ring abstraction channels do not involve pre-reactive complexes, which is consistent with the previous study carried out by Tokmakov and Lin [112] for hydrogen abstraction from benzene.

Much of the computational literature on hydroxyl radical reactions with arenes have emphasized the BTX (benzene, toluene, xylene) hydrocarbons, as well as halocarbon species and phenol (a common disinfectant) using a range of theoretical methods capable of greater or lesser degrees of thermochemical accuracy. There have been experimental studies for benzene and toluene in organic solutions but only benzene has been studied with the theoretical models. As far as can be determined, no group has presented a consistent study of a range of functionally diverse arenes with a view to identifying structure-reactivity relationships such as those alluded to in Section 1.2.3.

1.4 Project Description and Motivation

Given the importance of hydroxyl radicals, it is desirable to obtain an accurate picture of hydroxyl radical reactivity and selectivity with important classes of compounds, such as arenes. Structure-reactivity relationships and reactivity-selectivity relationships allow us to predict the rates and outcomes of hydroxyl radical reactions with substrates that for one reason or another are not accessible experimentally. Such relationships would also allow us to predict rates and outcomes for hydroxyl radical with novel or yet to be developed substrates. Finally, a useful relationship between structure and reactivity will provide us with predictive kinetic data which assist in (a) the understanding and accurate modeling of environmental processes and (b) assists in the development of effective remediation technologies.

Hydroxyl radical reactivity data is difficult to obtain experimentally as the hydroxyl radical is very reactive and rapidly generates complex mixtures due to successive

oxidative reactions, and it is difficult to isolate and study a single step within multiple-step processes. In addition, more than a single reaction pathway is an accessible as hydroxyl radicals react with aromatic compounds by abstracting hydrogen atoms from the alkyl group or by adding to the aromatic ring [99].

The hydroxyl radical is also short lived (typical solution lifetimes of the order of ns at 298K), reacts with most organic compounds including solvents, and in solution phase does not have a unique, usable spectroscopic signature. Nonetheless, some preliminary structure-reactivity relationships may be constructed via a combination of pulse radiolysis and laser flash photolysis techniques. Ultimately, however, these techniques inform us about the *reactivity* of hydroxyl radical with arenes, but provided only limited information regarding the *selectivity* of reaction: given different sites on a molecule, does hydroxyl radical chemistry show preferences for certain sites over others? A complementary approach is to study these mechanisms by computations methods. Most simple computational models consider a molecule in the gas phase (or more precisely, in isolation); computational models have only recently begun to incorporate effects of solvents.

There are two primary questions that this contribution aims to address and both are related to hydroxyl radical reactions with aromatic rings.

Question1: *What is the effect of substitution on the reactivity and selectivity of hydroxyl radical addition to the aromatic ring?*

(a) How fast are hydroxyl radical reactions with arenes?

(b) What is the effect of functional group on the reactivity of hydroxyl radical addition to the aromatic ring?

(c) What is the effect of functional group on the selectivity of hydroxyl radical addition to the aromatic ring?

It is well-established fact that the presence of functional groups on an aromatic ring can have a significant effect on the delocalized π- electron density in the ring. Previous experimental [89, 90] and computational studies [46, 68, 107] suggest that hydroxyl radical may be considered electrophilic. An electron-donating group attached to ring should enhance the reactivity of ring. In addition, it is known that electron-donating groups mostly favor *ortho* and *para* (1,2-and 1,4-disubstituted) products with ionic electrophiles (Lewis acids); and that electron-withdrawing groups heavily favor *meta* (1,3-disubstituted) products. Will the same hold true for a neutral free radical species such as hydroxyl radical and if so, does it hold to the same extent?

Experimental studies show that with respect to toluene, *ortho* products are considerably more favored than *para* and *meta* substituted products. In addition, previous computational studies on benzene indicate that the charge on hydroxyl radical becomes increasingly negative as the system progresses from reactant to transition state and at same time the charge on aromatic ring becomes increasingly positive, to the point where significant cation character is present in the transition state. The positive charge appears to accumulate at *ortho* and *para* positions (with respect to the carbon under attack) as expected from resonance theory.

On the other hand, radical centers, unlike carbocations, are stabilized by *both* electron donating and electron withdrawing groups. If radical stabilization and bond

strength factors are important, one should observe a situation where electron withdrawing groups may also enhance the reactivity of an arene, and lead to preferential formation of *ortho* and *para* products.

As a secondary issue, the potential for hydrogen abstraction from the side chain is also considered. Kinetic isotope effect studies for reaction of hydroxyl with toluene, with rates measured by LFP, suggest that abstraction from the benzylic position plays a relatively minor role, at least in acetonitrile.

The relative energies of reaction have been calculated for benzene rings bearing a range of substituents, in an effort to glean structure-reactivity and structure selectivity correlations based on ring substitution. In addition, where possible, hydrogen abstraction reactions have also been considered.

Question2: ***How do computed kinetic data (nominally computed in the gas phase or in vacuum) compare with experimental data?***

Previous experimental and computational data [16, 89, 90] suggest that the reactivity of the hydroxyl radical is enhanced in certain solvents certainly an order of magnitude difference in rate coefficient is observed from acetonitrile solvent to water. The data have been obtained in

- a non-complexing solvent (benzene),
- a polar, but non-protic solvent (acetonitrile),and
- a polar protic solvent (water)

There are a number of secondary issues that arise, the first of which is that if the comparisons are unfavorable, are they improved by implementing a polarizable

continuum model for solvent effects? A secondary issue to be determined is whether the selectivity is changed by the presence of a solvent.

In the following chapters, a computational study of hydroxyl radical reactions with arenes in the gas phase and in solution is described:

Chapter 2 provides an overview of the theoretical models of quantum chemistry that are used to describe molecular structures, and discusses how these models are implemented within quantum chemistry program suites. In addition, a discussion of the computation of molecular partition functions, and how these may be utilized to estimate the thermodynamics and kinetics of reacting systems, is presented.

Chapter 3 describes the results calculated for the addition of the hydroxyl radical to the aromatic ring in the gas phase. Optimized geometries, and calculated free energies and rate coefficients are presented, and the utility of various structure-reactivity relationships for describing these reactions is discussed. Chapter 4 considers the role of solvent on addition reactions, where the solvent is modelled as a structureless polarizable continuum.

Chapter 5 describes a preliminary study of hydrogen abstraction reactions from the side chains of the arene ring in the gas phase, and discusses the potential structure-reactivity relationships that could be constructed to describe these reactions. Finally, Chapter 6 summarizes the conclusions from the study, and discusses both the future work required to broaden the coverage of structure-reactivity relationships, and the broader impacts of this study with respect to the experimental and theoretical environmental sciences.

CHAPTER 2-THEORETICAL OVERVIEW AND COMPUTATIONAL METHODOLOGY

Computational chemistry may be defined as the application of mathematical and computing models to the solution of chemical problems [113]. There are a large number of computational models that are used to generate information regarding the properties of molecules or to simulate experimental results. Using commercial computational chemistry software such as GAUSSIAN (SPARTAN and MOLCAS are other widely used program suites) one may readily calculate the following:

- Molecular geometries, spin and charge distributions,
- Spectroscopic quantities (IR and Raman frequencies, rotational constants, chemical shifts, UV-visible absorption and florescence wavelengths amongst others), and their associated thermodynamic partition functions,
- Transition state structures, reaction barriers, reaction paths and potential energy surfaces (PES),
- Thermochemistry (enthalpies, entropies and free energies of activation and reaction), and hence kinetics and equilibrium constants.

These computational packages utilize numerical solutions of the Schrödinger Equation to calculate the above mentioned properties, as well as wide range of other molecular and bulk physical and chemical properties. There are number of advantages to the computational approach:

- Reaction mechanisms can be studied on a step-by-step basis, to look at specific reaction types without interfering side reactions,
- Substrates that for various reasons are not accessible experimentally can be considered, such as model compounds that may not be synthetically available.
- Structural and energetic information (particularly with respect to reaction transition states) that are not available by experimental observation may be computed with “chemical” accuracy in which thermochemical data are reliable within 1-2 kcal/mol of the experiment.

2.1 An Overview of Theoretical Models

There are a number of available approaches to calculating molecular properties, depending on the size of the system involved. Molecular mechanics (MM) is a relatively low-level methodology typically used in large systems such as proteins (often a subset of the structure, such as an active site, is treated using quantum mechanics (QM), leading to QM/MM hybrid methods). For small systems, such as the model systems considered in this study, quantum mechanical methods are more typically and widely utilized, and may be broadly classified them in terms of (a) a*b initio*, (b) density functional and (c) composite methods. Definitions of these terms are helpful in understanding the use of computational techniques for chemistry:

2.1.1 *Ab Initio* Methods

Ab initio refers to a group of methods in which molecular structures can be calculated using nothing but the time independent Schrödinger equation, the values of some fundamental constants and the atomic numbers of the atoms present. It is based directly on theoretical principles, with no inclusion of, or parametrization based on, experimental data beyond the values of the fundamental constants [114]. The time-independent Schrödinger equation is often written as follows:

$$\hat{H}\Psi(x,y,z) = E\Psi(x,y,z) \qquad (Eq.2.1)$$

where $\hat{H}$ is the Hamiltonian mathematical operator that yields the system's total energy *E* upon the solution of wave equation. The final component of the equation is the spatial wavefunction $\Psi(r)$, which will be discussed further below.

The classical Hamiltonian is made up of kinetic and potential energy terms [115, 116], and for a many-electron system, may be written in atomic units as follows:

$$\hat{H} = -\frac{h^2}{8\pi^2}\sum_{A}^{nuclei}\frac{1}{m_A}\nabla_A^2 - \frac{h^2}{8m_e\pi^2}\sum_{a}^{electrons}\nabla_a^2 - e^2\sum_{A}^{nuclei}\sum_{a}^{electrons}\frac{Z_A}{r_{Aa}} + e^2\sum_{A}^{nuclei}\sum_{>B}\frac{Z_A Z_B}{r_{AB}} + e^2\sum_{a}^{electrons}\sum_{>b}\frac{1}{r_{ab}} \qquad (Eq.2.2)$$

where *h* is Planck's constant, m_A is the mass of particle A, ∇_A the Laplacian operator (Eq. 2.3) for a given particle A, where capitalized particles correspond to atomic nuclei, and lower case to electrons.

$$\nabla = \left(\frac{\partial^2}{\partial x^2} + \frac{\partial^2}{\partial y^2} + \frac{\partial^2}{\partial z^2} \right) \qquad \text{(Eq. 2.3)}$$

The terms r_{AB} r_{ab} and r_{Aa} represents the separation between pairs of nuclei and electrons, and the separation between nucleus-electron pairs. The first two terms in equation 2.2 represent the kinetic energies of the nuclei, and electrons respectively. The remaining terms represent the potential energies (in the form of Coulombic interactions) between nuclei and electrons, between pairs of nuclei, and between pairs of electrons respectively. The Born-Oppenheimer approximation simplifies (Eq.2.2) further by separating the nuclear and electronic motions, taking into account the fact that mass of a typical nucleus is several thousand times greater than that of electron. The nuclei move very slowly with respect to electrons, so the nuclei look fixed to the electrons. The kinetic energy term for the nuclei is ignored [115, 117].

The simplified Hamiltonian is applied to an electronic wavefunction $\Psi(x,y,z)$, which describes the state of the system as a function of all the particle coordinates *x,y,z*, including the spatial distribution of electronic charge. The wavefunction construct is consistent with the notion that an electron is a quantum particle, and exhibits properties consistent with particle and wave mechanics, depending on the observation being made. As chemists, a more usable expression of the wavefunction is the product of the wavefunction and its complex conjugate, $\Psi\Psi^*$

$$\Psi(x,y,z)\,\Psi^*(x,y,z)\mathrm{d}x\mathrm{d}y\mathrm{d}z \qquad \text{(Eq.2.4)}$$

The Born interpretation of this product is that it represents the spatial electron probability density; that is the probability of finding an electron in an incremental volume of space defined by d*x*d*y*d*z* (often abbreviated dτ). This probability density (often referred to as the electron density) defines the charge distribution in a molecule, and its

chemical bonding patterns. Application of the Hamiltonian operator on Ψ yields the total energy of the system, other operators will yield different physical properties.

Most quantum chemistry programs (including those used in this study) are built upon the precepts of molecular orbital (MO) theory. The overall wavefunction of the system Ψ is a product of molecular orbitals ψ_i that describe the spatial distribution of the electrons, as well as components that describe the electrons' magnetic moments (electronic spin, often denoted by α or β) – the spin components are emplaced to ensure that the electrons obey Fermi-Dirac statistics (ie. that the system obeys the Pauli Principle – no two electrons in a system can have the same set of quantum numbers). Commonly, MOs are constructed from a linear combination of atomic orbitals (LCAO), where MOs can be expanded as:

$$\psi_i = \sum_{i,j} c_{ij}\, \varphi_j \qquad \text{(Eq. 2.5)}$$

where ψ_i is the molecular orbital, c_{ij} are the molecular orbital expansion coefficients (essentially weighting factors), and ϕ_j are the atomic orbitals. Since only hydrogen atoms have atomic orbitals that yield analytical integrals, it is necessary to approximate the functional forms of the orbitals of heavier atoms, based on the following:

- Heavy atom atomic orbitals are essentially hydrogenic (i.e. they are similar in form/topology to hydrogen s, p, d, f… orbitals).
- Both heavy atom and hydrogen orbitals may be estimated as of a sum of simple, appropriately scaled, continuous functions with analytical integrals (e.g. Gaussian functions).

The set of functions utilized to describe such orbitals is termed the basis set for a calculation.

2.1.2 Hartree-Fock Methods and Electron Correlation

The most common and fundamental type of *ab initio* method is the Hartree-Fock (HF) self-consistent field method. The HF method defines a system of one-electron, molecular orbital wavefunctions where the electron interacts with an average field generated by all the other electrons in the system. These wavefunctions are eigenvectors of the Fock equation

$$\mathrm{F}\psi_i = \varepsilon_i \psi_i \qquad (\mathrm{Eq.}\,2.6)$$

where ε_i is the individual orbital energy, and ψ_i represents the spatial and spin components of the i^{th} one-electron wavefunction. The operator F is known as the Fock operator. The orbital energies may be calculated as follows:

$$\varepsilon_i = H_i + \sum_j^n (2J_{ij} - K_{ij}) \qquad (\mathrm{Eq.}\,2.7)$$

In (Eq. 2.7), each of the terms corresponds to integrals evaluated over all space. H_i is core integral - the Hamiltonian operator for the one-electron system that includes the kinetic energy of the i^{th} electron, and its attraction to all the nuclei present in the system. J_{ij} is the Coulomb integral which takes into account the repulsion between electrons present in orbitals ψ_i and ψ_j, and K_{ij} is the exchange integral which includes the exchange of (indistinguishable) electrons of same spin between two orbitals ψ_i and ψ_j, ensuring that the wavefunction has the correct behavior with respect to an exchange operator, and that the electrons obey Fermi statistics (see Appendix I).

The Hartree-Fock method provides a reasonable model for wide range of problems and molecular systems, but suffers from the limitation that it does not completely account for effects due to electron correlation. HF theory models the potential experienced by a given electron this in averaged terms, but the potential experienced by an electron in an instant is dependent on the instantaneous location of the other electrons in the system – the motions are not independent (as they are assumed to be in the HF self-consistent field), but are correlated with one another. The exchange integral K_{ij} does capture correlation of electrons with parallel spins, but not those with antiparallel spins. Neglect of electron correlation can lead to large deviations from experimental data. Treatment of electron correlation may be achieved by a number of methods, which are commonly referred to as post-SCF methods.

Møller-Plesset (MP) perturbation theory treats the correlation as a perturbation of the Hamiltonian, such that

$$H = H_0 + \lambda H' \qquad \text{(Eq. 2.8)}$$

where H_0 is the Hartree-Fock Hamiltonian, H' is the Hamiltonian for the perturbation, and λ is a parameter applied to introduce the perturbation gradually to the system ($0 < \lambda < 1$). Both the energy of the system and the wavefunction will also be a function of λ, and the effect of the perturbation may be expressed as a Taylor series expansion (Equation 1.12).

$$\psi = \psi_{\lambda=0} + \lambda . \left(\frac{\partial \psi}{\partial \lambda}\right)_{\lambda=0} + \frac{\lambda^2}{2!} . \left(\frac{\partial^2 \psi}{\partial \lambda^2}\right)_{\lambda=0} + \ldots \qquad \text{(Eq. 2.9)}$$

The level of MP calculations is defined by where one chooses to truncate the series expansion. Thus, MP2 is a calculation that truncates the expansion at the second-order level, MP3 at the third, MP4 at the fourth, and so on. The number of

terms to be evaluated in the course of an energy calculation increases rapidly, and so for reasonably sized systems such as those described in this study, expansion beyond the MP4 level is rare.

The implementation of perturbation theory, at least as it pertains to systems with non-degenerate states, is to "mix in" states other than the ground state. In the alternative configuration interaction (CI) approach, electron correlation is treated by adding terms that represent promotion of electrons from occupied to unoccupied molecular orbitals. The HF term and the additional terms each represent a particular electronic configuration (the ground, and excited states), and the wavefunction and electronic structure can be conceptualized as the result of interaction of these configurations [113, 118]. In other words, small fractions of excited states are mixed with the ground state to give a correlated wavefunction (Ψ_{CI}).

$$\Psi_{\mathrm{CI}} = c_1 \Psi_1 + c_2 \Psi_2 + c_3 \Psi_3 + \ldots\ldots\ldots c_{\mathrm{n}} \Psi_{\mathrm{n}} \qquad (\mathrm{Eq.\ 2.10})$$

Ψ_1 represents the ground state electronic configuration; $\Psi_2, \Psi_3 \ldots \Psi_{\mathrm{n}}$ represent wavefunctions for excited state configurations, and $c_1, c_2 \ldots c_{\mathrm{n}}$ are expansion (weighting) coefficients. The incorporation of excited states results in the decrease in the total energy of the system.

Full CI considers every possible electronic state of a given system, and is only possible for very small molecules, because the promotion of electrons into unoccupied orbitals can generate huge number of states unless we only have few electrons and orbitals, or choose a subset of the electrons and orbitals to determine the possible excited states (the active space, as used in complete active space (CAS-SCF) methods). If a CI calculation includes only single excitations it is denoted a CI Singles

(CIS) calculation, and such calculations are often used to obtain the optimized geometry of the first excited state, but cannot be used for ground state calculations. Higher order excitations may also be used, thus a CI calculation that uses double excitations may be denoted CID, and can be used to find ground state wavefunctions. Because some singly excited states may interact with doubly excited states, the method denoted CISD may be used. Similarly, the effect of triple excitations (which are not directly calculated, since the number of terms increases markedly, but treated as a perturbation) are included in methods such as coupled cluster (CCSD(T)) and quadratic CI (QCISD(T)) methods. The inclusion of multi-configurational self-consistent field (MCSCF) methods such as these, result in higher accuracy calculations of molecular energy, but at considerable computational cost for large systems. There are other electronic structure methods that are reliable and cost-effective. One such commonly used method is Density Functional Theory (DFT).

2.1.3 Density Functional Methods

Density Functional Theory (DFT) adopts a somewhat different approach to the HF methods, in that the total energy is expressed in terms of the total electron density, rather than a wavefunction [119]. The electron density (ρ) in the system may be given by the following expression (the Born interpretation of the wavefunction, although in the case below this is expressed in modulus, rather than complex conjugate form):

$$\rho = \sum_{i=1}^{n} n_i |\Psi_i|^2 \qquad \text{(Eq. 2.11)}$$

where n_i is number of electrons populating molecular orbital Ψ_i. The utilization of electron density simplifies the dimensionality of the system: the wavefunction of an *n*-electron molecule is a function of 4*n* variables for each electron; three spatial coordinates and one spin coordinate. On the other hand, the electron density is a function of only three spatial coordinates. This provides a considerable advantage to DFT: in about the same time needed for an HF calculation one can often obtain results of about the same quality as more expensive MP2 calculations.

Electron density is defined as the integral over the spin coordinates of all populated Kohn-Sham orbitals [114, 119-123]. The Hamiltonian describes the total energy of the coordinate system (*x*, *y*, *z*). The total energy may be defined as a sum of energetic terms (Eq. 2.12):

$$E=E^{T}+E^{V}+E^{J}+E^{XC} \qquad \text{(Eq.2.12)}$$

The components of (Eq. 2.12) may be described as follows:

- E^T is the kinetic energy term for the electron density (assuming a Born-Oppenheimer approximated system),
- E^V is a potential energy term for interactions of the electron density with nuclei, as well as nuclear repulsion terms,
- E^J is the electron-electron repulsion term (the coulomb self-interaction of the electron density), and
- E^{XC} is a term that accounts for the remaining energy: exchange energy arising from the antisymmetry of the quantum mechanical wavefunction (exchange functional, E^X) and dynamic correlation in the motions of the individual electrons (correlation functional, E^C):

$$E^{XC}(\rho) = E^{X}(\rho) + E^{C}(\rho) \qquad \text{(Eq.2.13)}$$

E^{XC} also typically includes a correction to the kinetic energy that accounts for the fact that E^{T} is typically calculated using a uniform electron gas approximation.

The first three terms have well defined functionals that describe the interactions, the fourth does not. Thus, there a number of forms of Density Functional Theory (DFT) models, that differ in how they describe the exchange-correlation functional. The most widely used functionals are so-called hybrid functionals, that combine a weighted exchange component from Hartree-Fock models (K_{ij} terms of Equation 1.10), with weighted approximate exchange and correlation functionals (Equation 2.14).

$$E_{hybrid}^{XC} = c_{HF}E_{HF}^{X} + c_{DFT}E_{DFT}^{XC} \qquad \text{(Eq. 2.14)}$$

There are a number of functionals that have been derived for the exchange-correlation terms that involve no parametrization. Models that use c_{HF}, c_{DFT} = 0.5 are known as half-and-half models. The two DFT models used in this study are denoted B3LYP [124] and BH&HLYP [125]:

B3LYP is a three-parameter model (weighting factors *a*, *b*, *c* determined empirically) that is defined as follows:

$$E_{B3LYP}^{XC} = (1-a)E_{LSDA}^{X} + aE_{HF}^{X} + b\Delta E_{B88}^{X} + (1-c)E_{LSDA}^{C} + cE_{LYP}^{C} \qquad \text{(Eq. 2.15)}$$

and in (Eq. 2.15) the terms are defined as follows:

$E_{HF}^{X} =$ Hartree − Fock exchange term

$E_{LSDA}^{X} =$ Exchange term: local spin density approximation (LSDA)

$E_{B88}^{X} =$ Exchange term: Becke generalized gradient approximation (GGA)

$E_{LSDA}^{C} =$ Correlation term: LSDA

$E_{LYP}^{C} =$ Correlation term: Lee − Yang − Parr four − parameter GGA

LSDA and GGA refer to specific approaches to approximating the exchange-correlation functional (Appendix II). The BH&HLYP model is defined as follows:

$$E_{BHandHLYP}^{XC} = 0.5E_{LSDA}^{X} + 0.5E_{HF}^{X} + 0.5\Delta E_{B88}^{X} + E_{LYP}^{C} \quad (\text{Eq. } 2.16)$$

Density functional theory provides an alternative model that allows for relatively rapid, inexpensive calculation of molecular properties. However, because of the parametrizations built into some of these models, they are no longer variational, and still do not provide energies of chemical accuracy.

2.1.4 Composite Methods

How can the degree of accuracy for molecular energies required to accurately predict the thermochemistry and kinetics be achieved? One possibility is to use extremely high levels of theory (MPn, CI or other MC-SCF models) in conjunction with large, flexible basis sets for defining atomic and molecular orbitals (Figure 2.1), which should approach the exact solution of the Schrödinger Equation.

Unfortunately, such an approach is very computationally expensive, and is limited to the smallest systems. An alternative approach relies on the observation that beyond a relatively modest level of theory and basis set, the optimized geometry of a molecule changes very little with significant changes in computational method. Thus, it should be possible to calculate the geometry of a molecule at a relatively modest and computationally inexpensive level of theory, and then obtain high accuracy energies by combining the results of several energy (single point) calculations. Such composite methods combine high levels of theory applied to small basis sets with methods that

employ lower level of theory with large basis sets [114]. The effects are assumed to be additive.

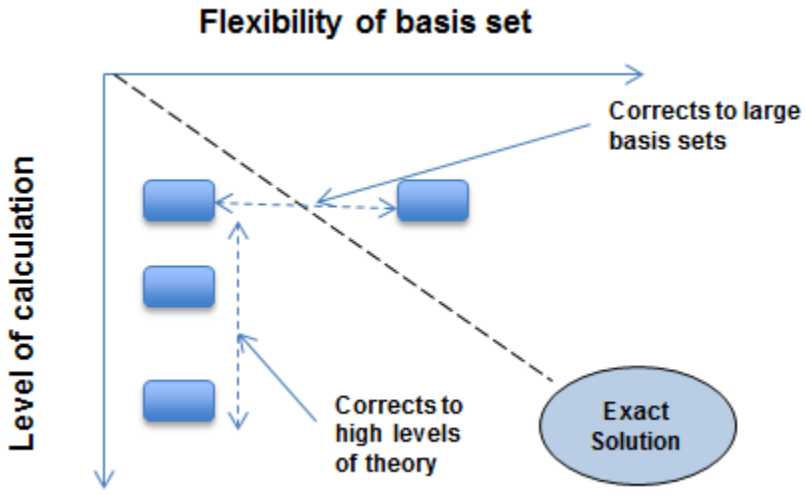

Figure 2.1: Complete Basis set limit. Interaction between basis set and correlation method require proper treatment of both for accurate calculations. All the corrections are assumed to be additive.

A variety of different compound methods have been developed to accurately model the thermodynamic quantities [113]. Some of the first methods developed were the Gaussian-n (Gn) methods of Pople *et al*., which yielded high accuracy results, but still at considerable cost [113, 126-128]. Re-parametrization of these methods allowed the formulation more computationally accessible methods that used MP2 instead of MP4 energies. Other Gn methods, such as the GnMP2 and GnMP2(RAD(ical)) methodologies are parametrized specifically for systems with unpaired electrons, and they have been used with some success to model free radical additions to alkenes (see Chapter 1).

An alternative approach, utilized in this study, is the Complete Basis Set (CBS) expansion of Petersson *et al*., which runs a sequence of calculations to estimate the

overall energy of the system. The base energy is calculated at a high level of theory, using a relatively modest basis set. Corrections are applied by subsequent calculations performed at lower levels of theory but with more extensive basis sets: the corrections are assumed to be additive, and are applied to the base energy. Two efficient computational models have been developed which employ smaller basis sets for higher orders of perturbation theory: CBS-4 and CBS-Q [113, 129, 130]. Both CBS-Q and CBS-4 have been found to reproduce the energies in benchmark data with relatively small errors, 1.0 and 2.0 kcal/ mol mean absolute deviation (MAD) from experiment, respectively [130]. These methods enter the realm of what is called “chemical accuracy” by computational chemists. A variant on the CBS-Q methodology, denoted CBS-QB3, differs mainly in the fact that the optimized geometry used for the single point energies in the former is obtained using MP2 methods, whereas in the latter it is obtained by DFT (B3LYP) methods.

There have been different studies [114, 129-131] performed to compare composite methods such as CBS-4, CBS-Q, G2(MP2) and G2, both with each other, as well as available experimental heats of formation, bond dissociation energies, gas phase acidities, and proton affinities. The CBS-4 composite method achieves a MAD less than 2 kcal/mol for substantially less computational cost than any other method. CBS-Q and G2 model tend to be more accurate, with CBS-Q values taking about half as long to compute compared to G2 theory.

Therefore, one may construct an approximate hierarchy of methods (Figure 2.2), depending on a number of factors including system size, computational expense, and accuracy. The choice of method also depends on the quantity being calculated.

Acceptable geometries and vibrational frequencies may be obtained at relatively modest levels of theory, whereas energies require more computationally expensive methods.

↓ Increasing computational cost ↓ Increasing Accuracy	older Empirical models	Ab initio methods	DFT Methods	Composite methods
			Xα	
	MM2, AM1, PM1, PM2			
		HF		
		MP2	B3LYP, PWK, BH&HLYP	
		MP3, MP4		
		CISD, CISD(T)		
		CCSD, CCSD(T)		
				CBS-4
				CBS-Q, G2(MP2)
				CBS-APNO, G2, G3(MP2)
				G3
				:
				:
				:
				Exact solution

Figure 2.2: Approximate hierarchy of computational methods in terms of their accuracy in computing thermochemical data.

2.1.5 Basis Sets

Basis sets are the group of mathematical functions that are used to describe the shape of the atomic orbitals in a molecule, recalling that molecular orbitals are computed by linear combination of atomic orbitals, and that non-hydrogenic atoms do not yield analytical solutions to the Schrödinger Equation. The GAUSSIAN program suite, as its name suggests, uses combinations of Gaussian functions (often termed Gaussian type functions or GTF) to model the form of an atomic orbital (even for

hydrogen). The accuracy of a calculation is at least partly dependent on the basis set used – a more extensive and flexible basis set will yield better results, but at the expense of greater CPU time.

In this study, the split valence basis sets formulated by Pople and others [132] were used. A split valence basis set allows a user to specify the number of GTFs to use for core and valence electrons separately, a useful formalism since most models of chemical bonding treat core orbitals as being largely unperturbed by the formation of bonds, whereas valence orbitals may be significantly perturbed. The notation used for a double zeta split valence basis sets is K-LMG, where K is the number of GTFs used to model each core s and p-type inner shell orbitals (these combinations are often referred to as Gaussian type orbitals (GTO). The valence shell orbitals are split into inner and outer valence orbitals to provide more flexibility in the basis set; thus, L is the number of GTFs used to model inner valence s- and p- type GTOs and M is the number of GTFs used to model outer valence s- and p-type GTOs. Finally, G indicates that GTOs are used.

By way of illustration, the 6-31G basis set has each core orbital composed of a linear combination of six GTF, while each valence orbital is split into two components, outer and inner, which are in turn composed of three and one GTOs, respectively. Enhanced flexibility in the basis may be achieved using triple zeta split valence basis sets, which generate an additional layer in the valence shell, *e.*g. 6-311G. Higher-order (quadruple zeta and above) basis sets may also be employed, but at an increase in computational cost.

Polarization: Basis sets may be further modified to include higher order terms that may be used to characterize the polarizability of the electron distribution in the atom. Thus, the flexibility of a basis set modelling a p-orbital may be enhanced by including a Gaussian function with the characteristics of a d-orbital. Polarization is often indicated in a basis set description by an asterisk (*), or by a specification of the types of polarization added. Thus, for example, the 6-311G(d,p) basis set adds d-type functions to heavy atoms and p-type functions to hydrogen.

Diffuse functions: Pople basis sets can also be modified by letting the electron move far away from nucleus, creating diffuse orbitals. This modification is particularly useful (and necessary) for systems containing lone pairs or negative charge [133], and is indicated by + in the basis set designation. Thus, in the 6-311++G(d,p) basis set, the first “+” indicates the inclusion of a set of diffuse p and s-type orbitals to heavy atoms, while the second “+” indicates large s-type orbitals on hydrogen.

2.2 Calculated Properties of Molecules from Computational Chemistry

2.2.1 Molecular Geometries

The energy of the molecular system varies with changes in the molecular geometry specified by its potential energy surface (PES). During a reaction, the molecular system may explore a large region of the PES, but there are certain stationary points on the surface that are of critical importance (Figure 2.3). It should be noted that Figure 2.3 is a three-dimensional representation of a (3*N*-6)-dimensional hypersurface, where *N* is the number of atoms in the (non-linear) molecule.

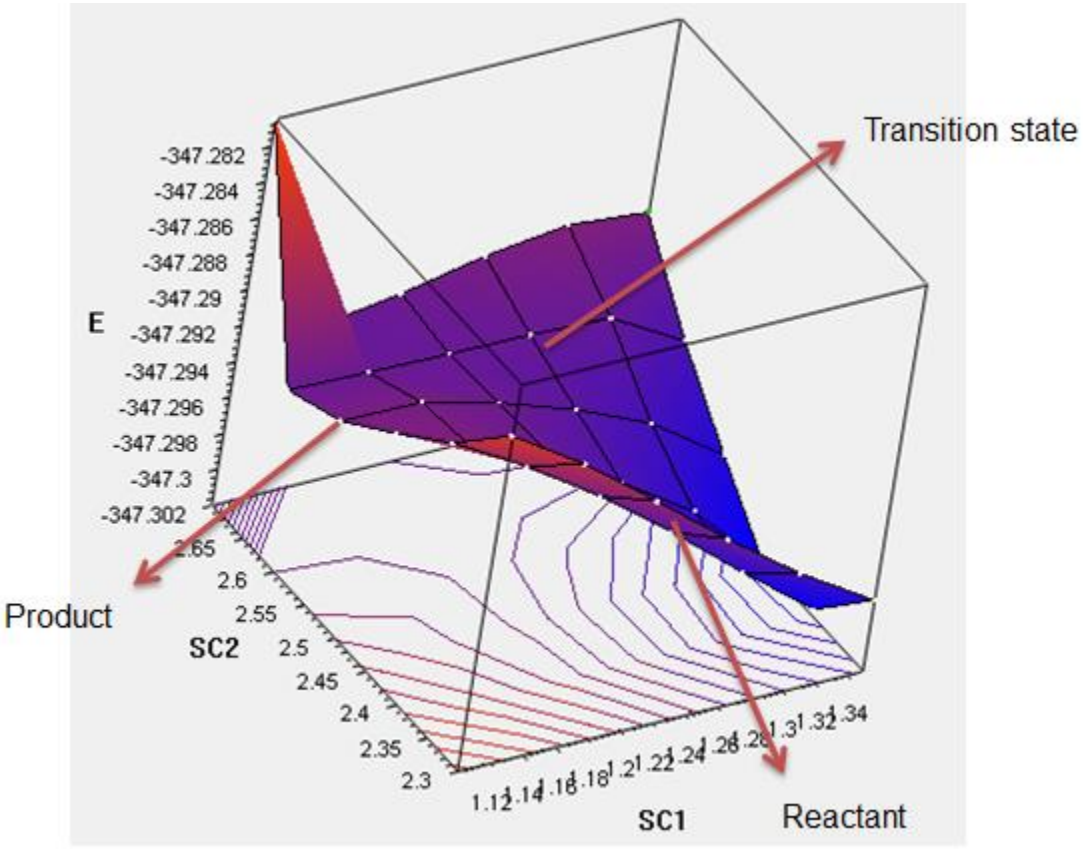

Figure 2.3: Representative potential energy surface (PES), showing presence of reactant and product valleys, and transition state (activated complex) saddle points.

Reactant and Product valleys. The optimized geometries of reactant and product lie at minima on the PES where the following conditions apply for all *q* (*q* represents the 3N-6 coordinates or degrees of freedom):

$$\frac{\partial E}{\partial q} = 0;\ \frac{\partial^2 E}{\partial q^2} > 0$$

GAUSSIAN contains a number of algorithms for determining the optimized geometry for a species, based on an initial starting "guess" for that geometry, based on iterative variation in *q*, calculating the first derivatives at each *q* until the values drop below certain convergence criteria, at which point the geometry is said to be optimized. In systems where various conformations may exist as minima, conformational space was explored to ensure that the optimized geometries corresponded to the lowest energy structures.

First order saddle points. First order saddle point structures have chemical relevance on the PES, as they correspond to transition states – critical geometries a system must attain for reaction to occur (see section 2.5). These are situated at geometries for which

$$\frac{\partial E}{\partial q} = 0;\ \frac{\partial^2 E}{\partial r^2} > 0\ ;\ \frac{\partial^2 E}{\partial s^2} < 0$$

Where *s* is a single coordinate in *q*, referred to as the reaction coordinate, and *r* represents the remaining (3*N*-7) orthogonal coordinates. Saddle points are more difficult to locate via the gradient minimization algorithm employed by GAUSSIAN, and so a very good initial "guess" for this geometry is required. For addition of hydroxyl radical to the ring, saddle points were located by systematic extension of the C-O bond of the product, allowing the remainder of the geometry to be optimized at each point (a

relaxed coordinate scan). The saddle point geometries were optimized from the highest energy point of these approximate reaction coordinate scans.

Typically molecular geometries are relatively insensitive to the level of theory employed, and so it is possible to obtain geometries at moderate levels of theory (B3LYP/6-31G(d)), that may be used for single point energy calculations at higher levels of theory (such as CBS-Q calculations). In this study, it was found that for reactions such as hydroxyl radical atom abstraction, the choice of model does have an impact on geometry (see Chapter 4). Rotational moments of inertia may be readily calculated from molecular geometries for use in thermochemical and kinetic determinations (see below).

2.2.2 Vibrational Frequencies

Once a stationary point has been found by geometry optimization, the calculation of vibrational frequencies is performed to determine whether the stationary point corresponds to a minimum, a saddle point, or a higher-order saddle point (which has limited chemical significance). A non-linear polyatomic molecule has 3*N*-6 vibrational degrees of freedom, each with a characteristic frequency ν (in cm^{-1} or wavenumbers), in the infra-red region of the spectrum given by:

$$\nu = \frac{1}{2\pi c}\sqrt{\frac{k}{\mu}} \qquad (\mathrm{Eq.}\ 2.17)$$

Equation 2.1 is derived from the harmonic oscillator model, which assumes that the PES at the stationary point is adequately modelled as a quadratic (Hookean) function in all 3*N*-6 dimensions, the major difference being that the molecular system is quantized.

The constant *c* is velocity of light, μ is the reduced mass of the molecular vibration, and *k* is the force constant for the vibration, which in turn is a measure of the second derivative of the PES with respect to the coordinate describing the vibrational motion (which need not be a Cartesian or internal coordinate, and is more typically a composite coordinate obtained from the "pure" coordinates via Normal Mode Analysis).

Thus, it may be shown that a non-linear minimum energy structure has 3*N*-6 vibrational frequencies which are real (see section 2.2.2, above). A saddle point (or transition state) structure has 3*N*-7 real vibrational frequencies, and one imaginary frequency that corresponds to the reaction coordinate.

The distribution of energy throughout vibrational degrees of freedom (vibrational modes) also contributes to the thermochemistry and kinetics of the system (see below). Like geometries, vibrational frequencies may be calculated at relatively modest levels of theory, but tend to overestimate values obtained by experiment [134]. The group of Radom and others [135-138] have investigated the ability of differing levels of theory to compute harmonic vibrational frequencies, as well as zero-point energies (ZPE, the energy of the ground state at 0K, since the lowest energy level of the harmonic oscillator is not at the bottom of the potential well) for vibrational motion, and have suggested a set of empirical correction factors for calculated vibrational frequencies at different levels of theory (Table 2.1).

Table 2.1 Scaling factors for frequencies, zero-point energies and thermochemistry for various levels of theory [135].

	Scale Factor			
Method	**Frequency**	**ZPE**	**S_{298K}**	**$\Delta H_{vib,298K}$**
HF/6-31G(d)	0.9062	0.9135	0.8978	0.8902
MP2/6-31G(d)	1.0139	0.9670	1.0178	1.0059
BLYP/6-31G(d)	1.0627	1.0135	1.0683	1.0648
B3LYP/6-31G(d)	1.0007	0.9813	1.0029	1.0004
BH&HLYP/6-31G(d)	0.9484	0.9446	0.9449	0.9400
BH&HLYP/6-31+G(d,p)	0.9581	0.9498	0.9510	0.9453

2.2.3 Thermochemistry

With appropriate geometries, vibrational frequencies and ZPE in hand, an accurate determination of the energy of the reacting system was obtained using the Complete Basis Set (CBS-Q) expansion methodology of Petersson *et al.*[129, 130, 139] Two methodologies were considered: the CBS-QB3 methodology, and a CBS-Q energy calculation based on geometries obtained at the BH&HLYP/6-31G(d,p) level of theory. These differ only by the methods used to calculate the optimized geometries and vibrational frequencies.

The CBS-QB3 methodology is based on a sequence of calculated single point energies, each intended to address a specific component of the overall energy [140, 141] .The energies are calculated as follows:

- Geometry optimization and vibrational frequency and ZPE calculation at the B3LYP/6-31G(2d,d,p) level of theory. This basis set includes 2d polarization on Na-Ar, a single d on Li-Ne, and p on H, He.

- Single point energy (E_{MP2}) at MP2/6-311+G(3d2f,2df,2p) and CBS extrapolation. The CBS extrapolation is based on the observation that the calculated MP2 correlation energy exhibits limiting behavior based on the number of orbitals used, and the complete basis set limit may be estimated by extrapolation from more limited bases.
- Single point energy at MP4(SDQ)/6-31+G(d(f),p), where the basis set includes d-polarization for atoms Li-Ar, f polarization on selected atoms Na-Ar, and p on H, He. This calculation captures the effects of truncation of the perturbation expansion (note that MP2 energy is automatically calculated as part of an MP4 calculation).
- Single point energy at CCSD(T)/6-31+G† (basis set is 6-31G orbitals, with modified d-polarization functions on heavy atoms, and diffuse functions) . This calculation is intended to capture the effects of triple excitations. Note that again, MP2 and MP4SDQ energies are calculated as part of a CCSD(T) calculation.

The total energy is given by:

$$E_{\mathrm{CBS-QB3}} = E_{\mathrm{MP2}} + \Delta E_{\mathrm{MP4}} + \Delta E_{\mathrm{CCSD(T)}} + \Delta E_{\mathrm{ZPE}} + \Delta E_{\mathrm{CBS}} + \Delta E_{\mathrm{emp}} + \Delta E_{\mathrm{int}} \quad (\mathrm{Eq.\,2.18})$$

where ΔE_{CBS} is the complete basis set correction to the MP2 single point energy, and ΔE_{ZPE} is the vibrational zero-point energy. ΔE_{MP4} is a higher order Møller-Plesset correction given by:

$$\Delta \mathrm{E}_{\mathrm{MP4}} = \mathrm{E}_{\mathrm{MP4(SDQ)}} - \mathrm{E}_{\mathrm{MP2}} \quad (\mathrm{Eq.\,2.19})$$

for the MP4SDQ and MP2 energies calculated as part of the MP4(SDQ)/6-31+G(d(f),p) single point. $\Delta E_{CCSD(T)}$ is given by:

$$\Delta E_{\mathrm{CCSD(T)}} = E_{\mathrm{CCSD(T)}} - E_{\mathrm{MP4(SDQ)}} \quad (\mathrm{Eq.\,2.20})$$

Again, both terms are calculated as part of the CCSD(T) single point. Finally, the term ΔE_{int} corrects for spin contamination in the MP2 energy, and an empirically parametrized correction, ΔE_{emp} is applied which accounts for the effects of near degenerate orbitals (note that the MP2 approach assumes non-degenerate orbitals).

Thus, we have an accurate energy for the molecule at 0K that compares well with benchmark G*n* calculations with lower computational cost. [140-143] However at temperatures above 0K, the total energy of the system includes additional thermal energy that is distributed amongst the 3*N* degrees of freedom in the system: 3 translational, 3 rotational, and 3*N*-6 internal vibrations.

$$E_{\text{molecule}} = E_{\text{elec}} + E_{\text{ZPE}} + E_{\text{Vib}} + E_{\text{Rot}} + E_{\text{transl}} \qquad (\text{Eq. } 2.21)$$

To obtain macroscopic thermodynamic data (enthalpies, entropies and free energies), it is necessary to consider large ensembles of molecules at different energies, with a very large number of possible distributions of those thermal energies among their degrees of freedom. Such systems may only be described statistically.

In a large group of molecules *N*, the fraction n_i with energy E_i above the energy at 0K may be given by Eq. 2.22 [116]

$$\frac{n_i}{N} = \frac{g_i e^{\frac{-E_i}{kT}}}{q} \qquad (\text{Eq. } 2.22)$$

where g_i represents the degeneracy of states with energy E_i, k is the Boltzmann constant, T is (absolute) temperature, and q is the molecular partition function, which represents the number of available energy states at a given temperature (Eq. 2.23)

$$q = \sum_i g_i e^{\frac{-E_i}{kT}} \qquad (\text{Eq. } 2.23)$$

Given that it is a function of energy, one may assume that the partition function

has a number of components (one makes the further assumption that these are separable, ie. uncoupled):

$$q_{\text{molecule}} = q_{\text{elec}} \cdot q_{\text{Vib}} \cdot q_{\text{Rot}} \cdot q_{\text{transl}} \quad \text{(Eq. 2.24)}$$

The electronic partition function includes the possibility that excited states may be thermally populated. However, since energy gaps between electronic states are typically large, in most cases the electronic component is assumed to be very close to 1, and is generally ignored.

The vibrational partition function is based on the energy levels of a harmonic oscillator, and therefore has limitations in cases where there is significant anharmonicity in the vibrational potential (low frequency torsional modes, and at high temperatures. For a system of 3*N*-6 harmonic oscillators, the vibrational partition function can be shown to be [116]

$$q_{vib} = \prod_{i=1}^{3N-6} \left(1 - e^{-h\nu_i / kT}\right)^{-1} \quad \text{(Eq. 2.25)}$$

where ν_i correspond to the scaled calculated harmonic frequencies (section 2.3), and *h* is Planck's constant.

The rotational partition function is estimated for a non-linear rigid rotor by the following expression (Equation 2.26) [116]:

$$q_{rot} = \frac{1}{\sigma}\left(\frac{kT}{hc}\right)^{\frac{3}{2}}\left(\frac{\pi}{ABC}\right)^{\frac{1}{2}} \quad \text{(Eq. 2.26)}$$

where σ is symmetry number, and A, B and C are rotational constants, which are in turn functions of the moments of inertia around the three primary rotational axes, I_A, I_B and I_C. The values of *I* are determined based on the masses of the atoms and the geometry of the molecule.

The translational partition function is given by Eq. 2.27 [116]:

$$q_{trans} = \left(\frac{2\pi mkT}{h^2}\right)^{\frac{3}{2}} V \qquad (\text{Eq. } 2.27)$$

where *m* is the mass of the molecular system, and *V* corresponds to a unitary macroscopic volume. The translational densities of states are very large, even at lower temperatures.

Macroscopic thermodynamic functions may be derived from partition functions: It may be shown [116] that the molar entropy of the system in molar volume *V* may be given by:

$$S = RT\left(\frac{\partial \ln q}{\partial T}\right)_V + R \ln q \qquad (\text{Eq. } 2.28)$$

where *R* is the ideal gas constant ($R = kN_A$, where N_A is Avogadro's number). Similarly, the molar internal thermal energy, *E* of the system is given by:

$$E = RT^2\left(\frac{\partial \ln q}{\partial T}\right)_V \qquad (\text{Eq. } 2.29)$$

Leading to molar enthalpy (assuming an ideal gas):

$$H=E+RT \qquad (\text{Eq. } 2.30)$$

and Gibbs free energy, G:

$$G=H-TS \qquad (\text{Eq. } 2.31)$$

From these expressions, it is possible to determine the relative thermochemical stabilities of reactants, products and intermediates along the reaction pathways (including along the way any changes in ZPE, and in the calculated molecular energies), and calculate enthalpies, entropies and free energies of reaction (ΔS_R, ΔH_R and ΔG_R respectively), the latter of which may be used to estimate the position of

chemical equilibria in the reaction by

$$K_{eq} = e^{-\Delta G_R/RT} \qquad \text{(Eq. 2.32)}$$

where K_{eq} is the equilibrium constant for reaction at temperature(T).

2.2.4 Kinetics

Transition state theory is an attempt to identify the principal features governing the magnitude of a rate constant in terms of a model for a reaction (or the elementary step of a reaction mechanism) in which reactant(s) is/are converted to product(s).

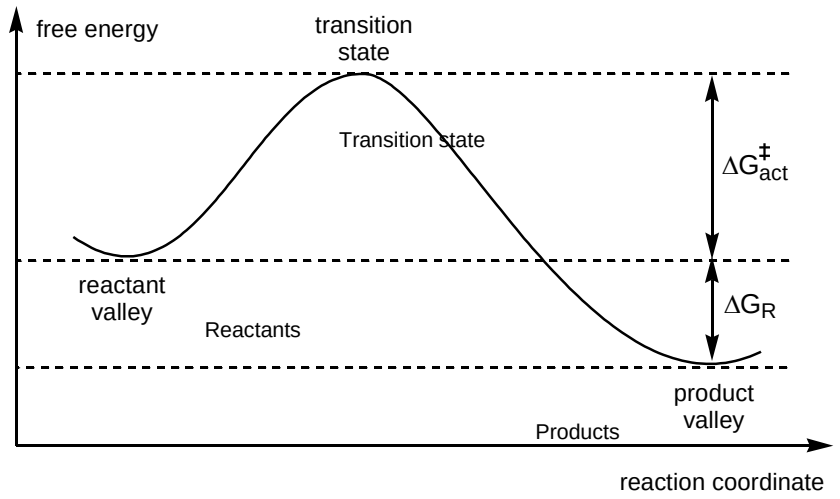

Figure 2.4: A reaction profile for an elementary step. The horizontal axis is the reaction coordinate and vertical axis is free energy.

The transition state represents a critical geometry that the reacting system must attain (with an associated free energy) in order for reaction to occur. Transition state theory also assumes that any trajectory that reaches the transition state will react without re-crossing. Thus, an overall unimolecular reaction

$$\mathrm{A} \xrightarrow[\mathrm{k_{uni}}]{} \mathrm{B}$$

May be written as a pseudo-equilibrium (given that the transition state has very short lifetime (nanoseconds), at most on the order of a molecular vibration) between reactant A and transition state $A^{\ddagger}$:

$$A \underset{K^{\neq}}{\leftrightarrow} A^{\neq} \underset{k_1}{\rightarrow} B$$

It is worth noting at this point that we are assuming that the rate of collisional activation/deactivation with a bath gas (Lindemann-Hinschelwood model) or solvent is high relative to the rate of reaction (in gas phase we are assuming reaction at the high pressure limit).

$K^{\neq}$ can be expressed in terms of the partition functions for the activated complex and reactant:

$$K^{\neq} = \frac{[A^{\neq}]}{[A]} = e^{\frac{-\Delta G^{\neq}}{RT}} = \frac{q^{\neq}}{q_A} e^{\frac{-E_0}{RT}} \qquad (\text{Eq. } 2.33)$$

where $q^{\neq}$ and q_A are the partition functions for the transition state and reactant respectively, and E_0 the potential barrier for reaction. The vibrational partition function of $q^{\neq}$ has one less degree of vibrational freedom than the reactant, since one vibrational mode has become imaginary in the transition state (the reaction coordinate). So, instead of 3N−6 degrees of vibrational freedom, the transition state has 3N−7 degrees of vibrational freedom.

If we treat the transition state as a molecule that decays unimolecularly with rate constant k_1 it can be shown that:

$$\mathrm{k}_1 = \frac{kT}{h}\mathrm{e}^{\frac{-\Delta \mathrm{G}^{\neq}}{\mathrm{RT}}} = \frac{kT}{h}\mathrm{e}^{\frac{-\Delta \mathrm{H}^{\neq}}{\mathrm{RT}}}\mathrm{e}^{\frac{\Delta \mathrm{S}^{\neq}}{\mathrm{R}}} \qquad (\mathrm{Eq.}\ 2.34)$$

and

$$\mathrm{k}_1 = \frac{kT}{h}\frac{\mathrm{q}^{\neq}}{\mathrm{q}_{\mathrm{A}}}\mathrm{e}^{\frac{-E_0}{\mathrm{RT}}} \qquad (\mathrm{Eq.}\ 2.35)$$

The typical parameters used to describe rate coefficients come from the Arrhenius equation:

$$k = A\mathrm{e}^{\frac{-E_A}{RT}} \qquad (\mathrm{Eq.}\ 2.36)$$

where *A* is the Arrhenius pre-exponential, and E_A is the activation energy. In this study, Arrhenius coefficients were calculated by determining the rate coefficient via (Eq. 2.34) at multiple temperatures in the range 273-333K, including 298K. Linear regression analysis of ln(*k*) as a function of 1/T yield values of the Arrhenius parameters.

Rate coefficients were calculated using the following expression

$$\mathrm{k}_1 = \frac{kT}{h}(c^o)^{1-m}\mathrm{e}^{\frac{-\Delta \mathrm{G}^{\neq}}{\mathrm{RT}}} \qquad (\mathrm{Eq.}\ 2.37)$$

where *k* and *h* are Boltzmann`s and Planck`s constants respectively, R the ideal gas constant, m is the molecularity of the reaction (in the case of cyclization and fragmentation reactions unimolecular, bimolecular for addition reaction), and $\Delta \mathrm{G}^{\neq}$ is the free energy of activation for reaction. The concentration factor c^0 , essentially a conversion factor, converts the rate coefficient from the standard state of 1 mol of ideal gas at the specified temperature and pressure (P at 1 atm) to standard concentration units of mol/L and is equal to c^0 = P/ RT [143, 144].

2.3 Solvent Effects

Reactions in solvent are going to significantly differ from the gas phase reactions. There are physical differences in the solvent phase: there is a reduction in the freedom of motion of molecules (eg. the “mean free path” of translational motion). In addition, the rate of collisional activation and deactivation of intermediates by solvent molecules will be enhanced. Perhaps just as importantly, solvents may have dipole and quadrupole moments making them polar and/or polarizable, which significantly impacts the potential being experienced by the molecule. For example, electrostatic effects are often much less important for species placed in a solvent with a high dielectric constant than they are in gas phase [113, 145]. There are different approaches for modelling a solute molecule in a solvent.

***Explicit Solvent models*:** In this approach to model solvent effects is to surround the solute with a small number of explicit solvent molecules during the calculation. For example, we could optimize the structure in ground state by placing couple of solvent molecules near negative and positive charged centers. The magnitude of the solvent effects depends on different factors like number of water molecules and their placement. In addition, the addition of explicit solvent molecules increases the degrees of freedom in the system, and there may be many minimum energy structures that involve solvent-solute interactions, each with their own energy. Nor is it clear whether one or two solvent molecules provide sufficient description of a solvation sphere. Thus a distribution of solvated species (e.g. a Monte Carlo simulated system) might be required, which greatly increases the computational complexity of the project.

***Implicit Solvent models*:** An alternative approach is to describe solvation by its

average effect that mainly arises from dipolar interactions. In a Polarizable Continuum Model (PCM) model, the polar solute polarizes a surrounding dielectric medium. The polarized medium acts as a self-consistent reaction field (SCRF) that interacts with the solute. Calculations are performed in the presence of a solvent by placing the solute in a cavity formed from multiple overlapping spheres for each of the atoms within the molecule [146, 147].

The SMD solvation model calculates the free energy of solvation by (Eq.2.38) following equation:

$$\Delta G_{solvation}=\Delta G_{solvent}-\Delta G_{gas\text{-}phase} \qquad (Eq.2.38)$$

The SMD model attempts to use electron density to estimate the solvent accessible surface (SAS) and the atomic surface tensions to determine the cavitation and dispersion repulsion energies. This method is the best method to use when attempting to calculate $\Delta G_{solvation}$ for a molecule going from the gas-phase to the solvent as it attempts to actually calculate both the energy of cavitation and dispersion-repulsion energy. This method has been shown to produce solvation free energies of mean unsigned errors of 0.6-1.0 kcal/mol for neutral molecules, and mean unsigned errors of 4 kcal/mol for ions, whereas other SCRF solvation methods in Gaussian have mean unsigned errors of 1-6 kcal/mol for neutrals and 7-10 kcal/mol for ions [148].

It is important to note, however, the self-consistent reaction field (SCRF) approaches have the disadvantage that they are incapable of modelling systems with specific solvent solute interactions (e.g. strong hydrogen bonding with the solvent). Under such circumstances, explicit solvent approaches, while considerably more complex, may be necessary.

2.4 Computational Methods used in this Study

All calculations were carried out using the GAUSSIAN 09 program suite [149] running on the BSU College of Science and Humanities CSH Beowulf cluster, 32 Dell PowerEdge R420's with dual 2.6 GHz 8 core Xeon ES-2670, 62 GB RAM and 450 GB local disk storage. The cluster is managed with Rocks 6.0.2 and the nodes are running CentOS 6.3 linux. Input files were constructed and computational results from output files were visualized and interpreted using the GaussView 5.0.9 user interface. Geometry optimizations and frequency calculations were performed at the computationally inexpensive BH&HLYP/6-31G(d,p) level of theory. The structures of reactants, products, intermediates, and transition states were determined to have the appropriate number of imaginary frequencies (1 for transition states, 0 for all other structures). The high-accuracy complete basis set composite method CBS-Q, based upon BH&HLYP geometries was employed for energy refinement. Solvent effects on the reactivity of hydroxyl radical were probed in water, benzene and acetonitrile with SCRF=SMD calculations using geometries optimized at the BH&HLYP/6-31G(d,p) level of theory.

CHAPTER 3-RADICAL ADDITIONS TO ARENES

The reactions of hydroxyl radicals with relatively simple arenes may be characterized by three types of reactions: 1) addition to the arene ring; 2) hydrogen abstraction from the side chain; and 3) hydrogen abstraction from the ring (it should be noted that an alternative mode of reaction involving electron transfer is possible, but is not as amenable to study via MO methods). This chapter will consider the addition to arene rings; the following will consider hydrogen abstraction from benzylic positions. The aim of both chapters is to delineate some useful structure-reactivity relationships that may be used predictively for a broad range of arenes, including species that may exhibit harmful biological or environmental properties.

It is a well-established fact that the presence of substituents on a benzene ring can have a profound impact on the nature of the π-bonding in, and the reactivity of the ring [42, 97]. Arene reactivity provides some of the best illustrations of the effect of different functional groups. In particular, the dominant polar reaction of arenes, electrophilic aromatic substitution (S_EAr), proceeds via a carbocation intermediate the reactivity and outcomes of such reactions may be readily explained by the ability of functional groups to stabilize or destabilize positive charge (Scheme 3.1).

Electron donating groups such as NH_2 will enhance the reactivity of the arene ring (by increasing π-electron density), and stabilize positive charge arising from electrophilic attack at *ortho* and *para* positions, leading the group to selectively "direct" attacking electrophiles towards positions *ortho* or *para* to the functional group.

Scheme 3.1: Attack of electrophile on ring.

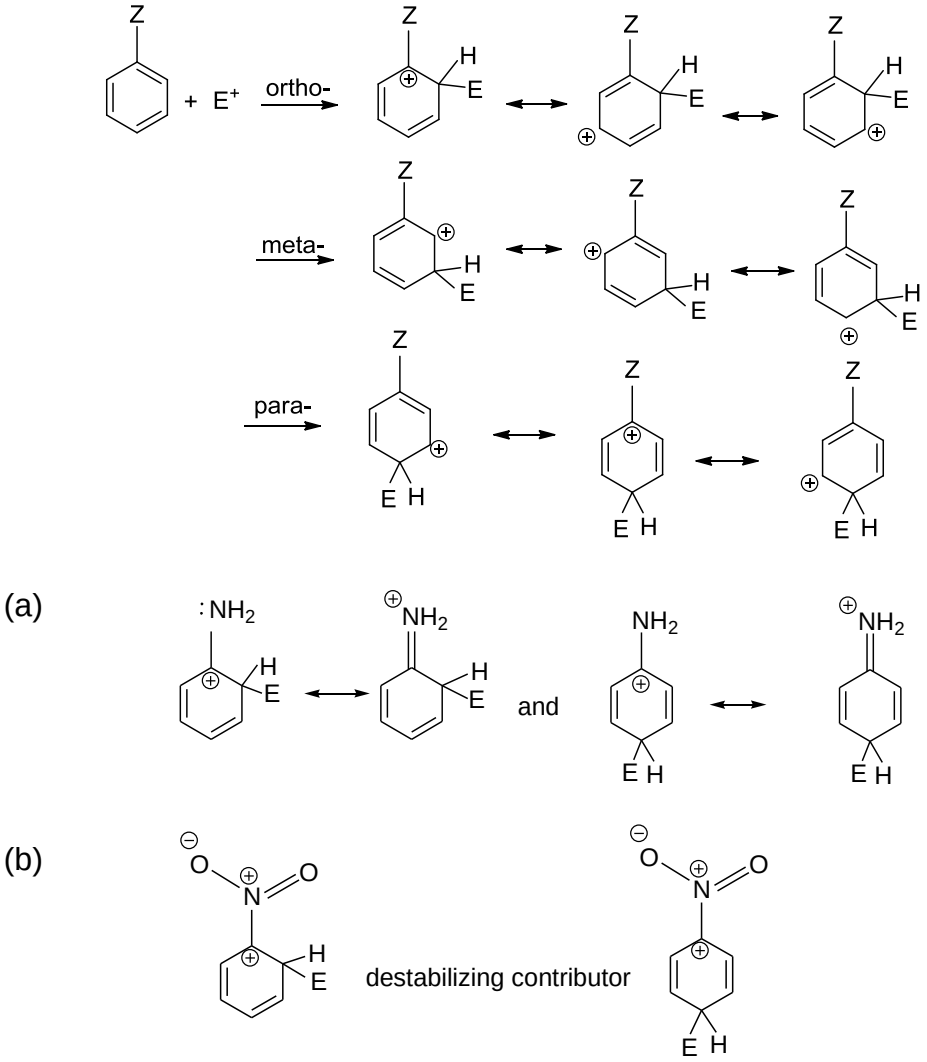

Electron withdrawing groups such as NO_2 will lower the reactivity of the arene ring and destabilize positive charge arising from electrophilic attack at *ortho* and *para* positions.

The group will selectively direct electrophiles to the position where its effects are minimized: the *meta* position. A small selection of functional groups (the halogens) will act to reduce the reactivity of the ring, but also direct *ortho* and *para*, and this may be readily explained using a combination of resonance and inductive effects [97].

If electron-donating groups stabilize carbocations, then it is reasonable to conclude that electron withdrawing groups stabilize carbanions, and there are experimental data that support such a position (Scheme 3.2).

Scheme 3.2: Attack of nucleophile on ring.

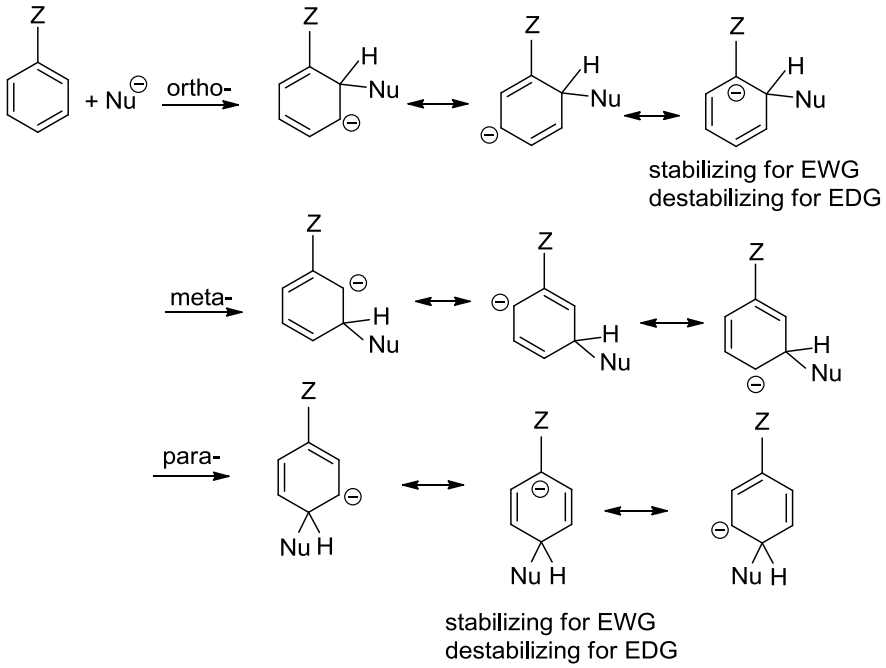

What then of free radical centers? It turns out that at least in principle, radical centers may be stabilized by both types of groups (Scheme 3.3). One would expect *ortho*- and *para*- substitution to be selectively favored for both electron donating

(Scheme 3.3(a) and withdrawing (Scheme 3.3 (b)) groups, since the radicals generated by such modes of attack are stabilized by the functional group.

Scheme 3.3: Attack by free radical on the ring.

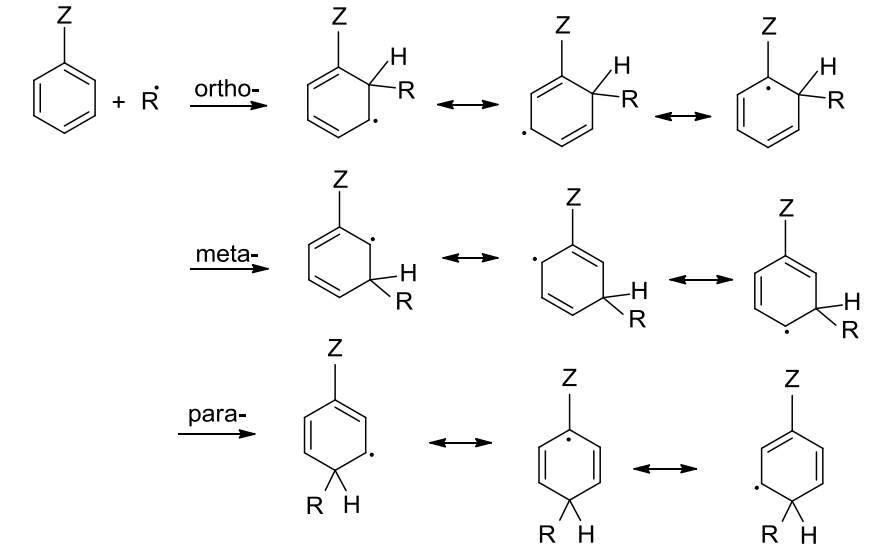

(a)

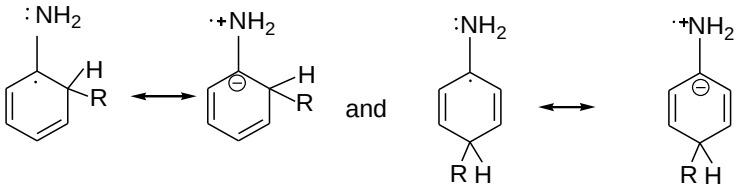

(b)

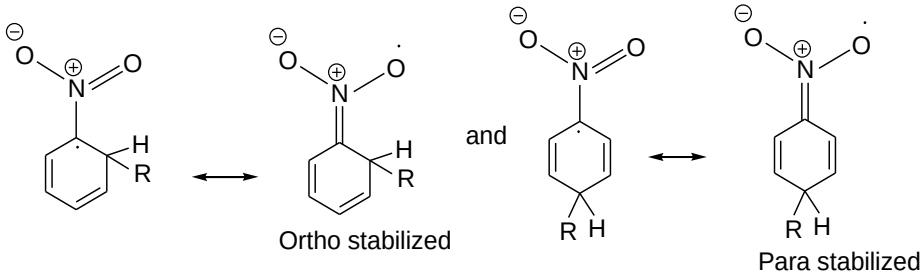

In this study, model compounds that consisted of monosubstituted benzene rings are selected; they represent a range of functional groups with electron donating and withdrawing properties from which we may be able to derive trends in reactivity and selectivity (Scheme 3.4).

Scheme 3.4: The structure and name of the substrates.

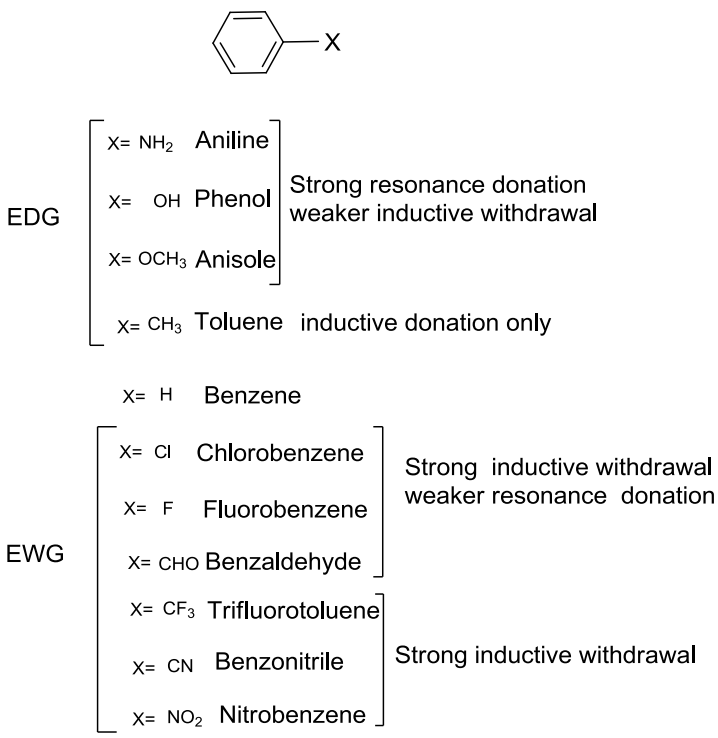

3.1 Geometries

As there are a number of potential sites where hydroxyl radical can attack, the geometries for reactants, transition states and products were optimized at B3LYP/6-31G(d) and BH&HLYP6-31G(d,p) level of theory and then high level calculations were performed at CBS-QB3 level of theory for B3LYP/6-31G(d) optimized geometries and CBS-Q level of theory for BH&HLYP/6-31G(d,p) optimized geometries. Although geometry optimizations were performed at both levels of theory, discussion of the results will be limited to CBS-Q/BH&HLYP/6-31G(d,p) for consistency with geometry optimizations for the abstraction reactions. Geometries obtained with CBS-QB3/B3LYP/6-31G(d) differ from those from CBS-Q/BH&HLYP/6-31G(d,p) calculations, particularly with respect to hydrogen abstraction reactions. Therefore the CBS-

Q/BH&HLYP/6-31G(d,p) calculations were used for consistency and this is discussed further in chapter 5.

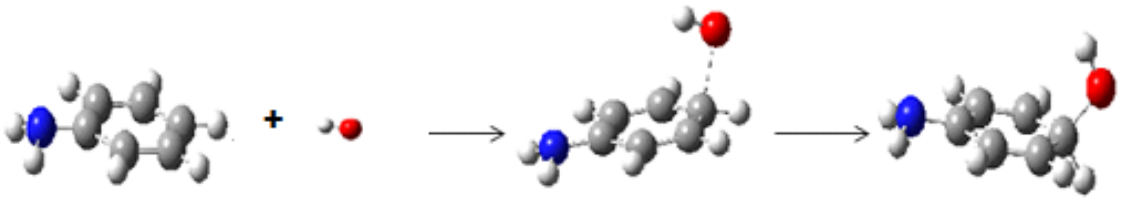

Figure 3.1: Hydroxyl Radical Addition Pathway for Aniline.

It is difficult to optimize the pre-reactive complex because the hydroxyl radical has rotational positions and have free rotations. Reactants were optimized separately. Therefore the investigation of geometry starts from geometries of the product, cyclohexadienyl radicals. When the hydroxyl hydrogen or oxygen is engaged in intermolecular hydrogen bonding, steric effects exerted upon its other reactant may control the rotamer position. As such steric factors can be expected for the arenes, therefore if hydrogen of hydroxyl radical is above or below the ring that rotamer position will have the lowest energy (Figure 3.1). The bond length extends through the transition state to the reactant valley i.e. reverse reaction is considered beginning with the product. The critical geometric parameters of the OH-arene adducts are shown in Table 3.1. Addition of hydroxyl radical to arene leads to the lengthening of the C-C bonds adjacent to the site of addition as compared to the corresponding reactant.

Table 3.1: Geometries for addition products-Cyclohexadienyl radical, gas phase for BH&HLYP/6-31G(d,p). 1-R_{CH}, 2-R_{OC}, 3-R_{OH},4-R_{CC},α-O---C---C

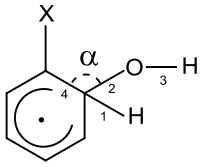

Functional groups on arenes		GEOMETRY				
		R_{CH} (Å)	R_{OC} (Å)	R_{OH}(Å)	R_{CC} (Å)	O---C---C (deg)
NH_2	o-	1.097	1.433	0.954	1.504	110.4
	m-	1.098	1.430	0.954	1.495	112.5
	p-	1.096	1.435	0.955	1.497	111.8
OCH_3	o-	1.089	1.433	0.956	1.503	110.8
	m-	1.097	1.429	0.954	1.498	110.8
	p-	1.096	1.433	0.954	1.496	111.8
OH	o-	1.097	1.422	0.954	1.496	111.4
	m-	1.098	1.428	0.954	1.497	111.8
	p-	1.096	1.432	0.955	1.498	111.8
CH_3	o-	1.099	1.428	0.953	1.506	112.2
	m-	1.098	1.428	0.954	1.497	112.2
	p-	1.097	1.429	0.954	1.496	112.1
H		1.098	1.427	0.954	1.497	112.2
Cl	o-	1.096	1.421	0.956	1.501	112.2
	m-	1.097	1.424	0.955	1.499	111.1
	p-	1.097	1.425	0.955	1.497	111.3
F	o-	1.097	1.421	0.955	1.488	111.8
	m-	1.097	1.425	0.955	1.498	112.2
	p-	1.096	1.429	0.955	1.500	111.7
CHO	o-	1.098	1.425	0.959	1.507	112.7
	m-	1.098	1.424	0.956	1.496	111.9
	p-	1.098	1.421	0.954	1.498	112.5
CN	o-	1.096	1.417	0.956	1.510	111.8
	m-	1.097	1.422	0.955	1.496	111.0
	p-	1.097	1.420	0.954	1.497	111.5
CF_3	o-	1.094	1.423	0.955	1.507	112.7
	m-	1.097	1.424	0.955	1.498	111.6
	p-	1.098	1.422	0.954	1.497	112.3
NO_2	o-	1.095	1.411	0.957	1.501	113.2
	m-	1.097	1.422	0.955	1.498	111.3
	p-	1.099	1.418	0.954	1.499	112.4

For the *ortho* substituted products, the C-C bond lengths are increased by about 0.11 Å relative to the reactant arenes which reflects that there is a decrease in bond order, as the π-electron density of the arene is partly transferred to the newly formed O-C bond. Similar C-C bond extensions are observed for *meta* and *para* substituted products. The distance of the newly formed C-O bonds in all of the products range from 1.411 to 1.435 Å. The presence of electron donating group on the benzene ring if compared to unsubstituted benzene ring shows that there is an increase in the O-C bond length. If the unsubstituted benzene ring is compared to the benzene rings with electron withdrawing groups the O-C bond length decreases, which is due to resonance and inductive effects.

The geometric parameters of monosubstituted benzene ring transition states (Figure 3.2) were compared to unsubstituted benzene ring transition states.

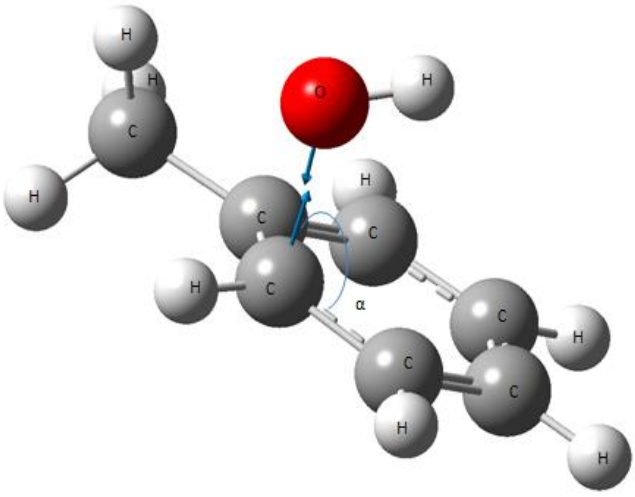

Figure 3.2: Transition state for addition of hydroxyl radical to toluene. Blue arrows show the displacement vectors for the reaction coordinate.

The geometries of the OH-arene addition transition states are shown in Table 3.2.

Table 3.2: Geometries for addition transition states for hydroxyl radical on arenes- gas phase for BH&HLYP/6-31G(d,p).

Functional groups on arenes		GEOMETRY					
		R_{CH} (Å)	R_{OC} (Å)	R_{OH}(Å)	R_{CC} (Å)	O---C---C (deg)	ν_{imag} (cm^{-1})
NH_2	o-	1.075	1.999	0.961	1.422	98.3	397.69i
	m-	1.074	1.944	0.961	1.415	104.0	520.1i
	p-	1.074	1.978	0.961	1.416	102.2	448.32i
OCH_3	o-	1.072	1.951	0.960	1.421	100.7	471.23i
	m-	1.074	1.954	0.961	1.421	103.8	510.63i
	p-	1.073	1.960	0.961	1.414	101.9	477.98i
OH	o-	1.075	1.958	0.962	1.415	100.4	511.78i
	m-	1.074	1.937	0.961	1.416	103.5	530.52i
	p-	1.073	1.959	0.961	1.416	101.9	480.6i
CH_3	o-	1.076	1.961	0.961	1.425	100.5	477.08i
	m-	1.075	1.951	0.961	1.419	102.2	504.95i
	p-	1.074	1.956	0.961	1.417	101.9	493.38i
H		1.075	1.944	0.961	1.419	101.8	514.17i
Cl	o-	1.074	1.948	0.962	1.416	102.8	513.01i
	m-	1.074	1.939	0.962	1.419	102.2	527.57i
	p-	1.074	1.949	0.962	1.418	101.8	512.22i
F	o-	1.075	1.940	0.962	1.408	101.9	540.36i
	m-	1.074	1.940	0.962	1.419	102.8	529.1i
	p-	1.074	1.943	0.962	1.419	102.0	511.17i
CHO	o-	1.076	1.964	0.964	1.422	100.4	540.9i
	m-	1.074	1.929	0.962	1.415	101.5	529.43i
	p-	1.074	1.964	0.962	1.421	101.6	509.14i
CN	o-	1.073	1.951	0.962	1.424	102.5	522.37i
	m-	1.074	1.931	0.962	1.417	101.3	535.15i
	p-	1.074	1.957	0.962	1.418	101.4	517.55i
CF_3	o-	1.074	1.935	0.962	1.419	102.9	534.45i
	m-	1.074	1.938	0.962	1.419	101.2	526.27i
	p-	1.074	1.939	0.962	1.419	101.6	530.96i
NO_2	o-	1.074	1.946	0.964	1.413	101.5	571.03i
	m-	1.074	1.927	0.962	1.417	101.1	540.61i
	p-	1.074	1.944	0.962	1.419	101.4	533.47i

The hydroxyl radical is positioned nearly parallel to the ring. The C-O bond distances are in range of 1.999-1.927Å. The transition states have much longer C-O

bonds as compared to the C-O bonds in the corresponding OH-arene products. The C-C bonds adjacent to the site of addition in the transition state are much shorter as compared to the C-C bonds in the corresponding OH-arene products. This signifies that the decrease in C-O bond distance is the reaction coordinate.

For the *ortho* transition state, the C-C bond lengths are increased by about 0.03 Å as compared to the separated reactants and the C-C bond lengths of the products are increased by about 0.11 Å as compared to the separated reactants. According to Hammond Postulate, the structural similarity between the transition states and their corresponding reactants indicates an “early” transition state. Similar C-C bond characteristics are observed for attack at *meta* and *para* positions.

For the three isomeric modes of attack it can be seen that there is not much change in the bond angles but there is variation in the bond lengths. For electron donating group like NH_2, *ortho* has longest O-C and C-C bond distance followed by *para* and then *meta,* but this is not true for all of the functional groups.

The Hammond postulate states that varying the structure of the transition state can vary the enthalpy of the reaction [150]. Therefore if there is change in geometric structure it would change the energy of transition state and therefore the activation energy and reaction rate as well. The broad similarities in transition state geometries allows us to assume certain similarities in entropy change going from reactant to transition state to product.

3.2 Energies

CBS-Q/BH&HLYP/6-31G(d,p) calculations were performed to find the energies of the transition state, products and the separated reactants. The free energy of reaction and free energy of activation were calculated relative to the combined free energies of separated reactants (Figure 3.3).

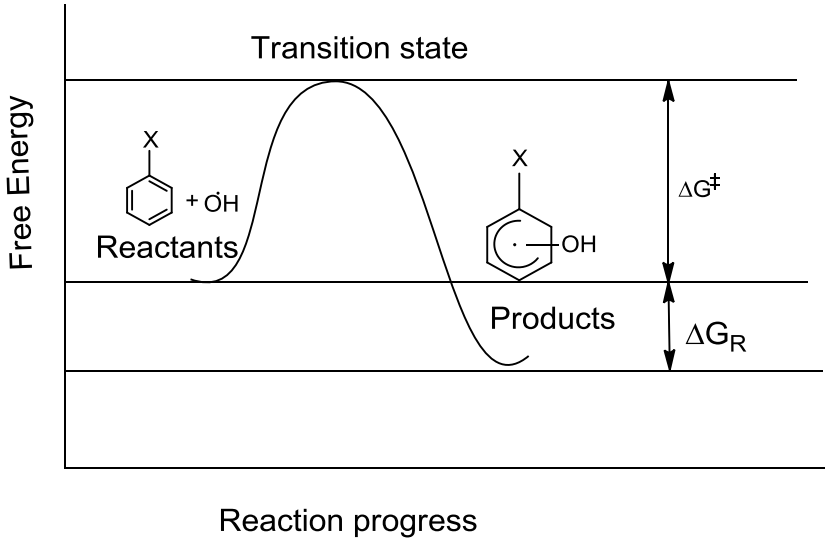

Figure 3.3: Reaction profile for finding free energy of reactants (ΔG_R) and free energy of transition state ($\Delta G^{\neq}$) for addition reaction.

The free energy of reaction (ΔG_R) and free energy of activation ($\Delta G^{\neq}$) are summarized in Table 3.3. The free energies of reaction for radical adducts were determined relative to the combined energies for infinitely separated arene rings and hydroxyl radical. ZPEs are scaled values obtained from the geometry optimizations, and entropies and enthalpies were calculated using the methods discussed in Chapter 2, again using scaled appropriately vibrational frequencies.

The energies were obtained for addition of hydroxyl radical from both CBSQ//BH&HLYP/6-31+G(d,p) and CBS-QB3 level of theory shown in Table 3.3 and

Table 3.4 to compare the similarities and differences for trends in both levels of theory. Tables 3.3 and 3.4 indicate that the free energy of activation increases from electron donating groups to electron withdrawing groups. Therefore, an arene substituted with electron donating groups will in general react faster with the hydroxyl radical compared to those substituted with electron withdrawing groups.

Table 3.3: Free energies of reaction and activation at the CBS-Q//BH&HLYP/6-31+G(d,p) level of theory (gas phase) for hydroxyl radical addition, relative to isolated reactants.

Functional group	ΔG_R Ortho (kcal/mol)	ΔG_R Meta (kcal/mol)	ΔG_R Para (kcal/mol)	$\Delta G^{\neq}$ Ortho (kcal/mol)	$\Delta G^{\neq}$ Meta (kcal/mol)	$\Delta G^{\neq}$ Para (kcal/mol)
$-NH_2$	-14.5	-9.4	-12.3	3.5	7.4	5.1
$-OCH_3$	-14.7	-12.5	-12.9	4.6	7.2	6.1
-OH	-10.8	-9.4	-10.7	4.4	7.9	6.3
$-CH_3$	-11.6	-11.0	-11.5	7.2	8.2	7.5
-H	-7.7	-7.7	-7.7	7.8	7.8	7.8
-Cl	-10.3	-7.5	-8.7	7.9	8.5	7.8
-F	-9.2	-7.8	-7.5	8.8	8.3	7.6
-CHO	-11.0	-8.4	-12.8	8.1	8.5	7.6
-CN	-14.2	-10.2	-13.7	8.7	8.9	8.2
$-CF_3$	-8.1	-8.4	-7.5	9.6	9.1	8.8
$-NO_2$	-9.3	-8.6	-10.8	9.2	8.9	8.7

Table 3.4: Free energy energies of reaction and activation at CBS-QB3 level of theory (gas phase) for hydroxyl radical addition to arenes relative to isolated reactants.

Functional group	ΔG_R Ortho (kcal/mol)	ΔG_R Meta (kcal/mol)	ΔG_R Para (kcal/mol)	$\Delta G^{\neq}$ Ortho (kcal/mol)	$\Delta G^{\neq}$ Meta (kcal/mol)	$\Delta G^{\neq}$ Para (kcal/mol)
-NH_2	-12.6	-7.6	-10.3	5.7	8.5	6.7
-OCH_3	-8.8	-8.5	-8.9	6.0	8.1	7.3
-OH	-10.9	-7.4	-8.8	8.6	8.9	7.5
-CH_3	-8.5	-7.5	-8.5	7.9	8.5	8.0
-H	-7.6	-7.6	-7.6	8.8	8.8	8.8
-Cl	-10.4	-7.4	-8.7	9.1	9.5	8.9
-F	-9.2	-7.7	-7.5	10.0	9.3	8.7
-CHO	-13.5	-7.0	-11.2	9.1	9.5	8.8
-CN	-11.0	-7.1	-10.6	10.4	10.0	9.4
-CF_3	-7.7	-7.1	-7.7	10.5	9.6	9.5
-NO_2	-11.4	-7.1	-9.3	10.4	10.0	9.8

Figure 3.4 shows that the free energies of activation calculated at both levels of theory show a strong correlation. The free energies of activation for CBS-Q/BH&HLYP/6-31G(d,p) are slightly higher than CBS-QB3. However, given the broad similarities in molecular geometries observed between the two levels of theory, it is reasonable to assume that the structure-reactivity and selectivity relationships observed at one level of theory also generally apply to the other and this indeed the case. Thus, all subsequent discussion will refer to the dataset obtained at the CBS-Q//BH&HLYP/6-

31G(d,p) level of theory.

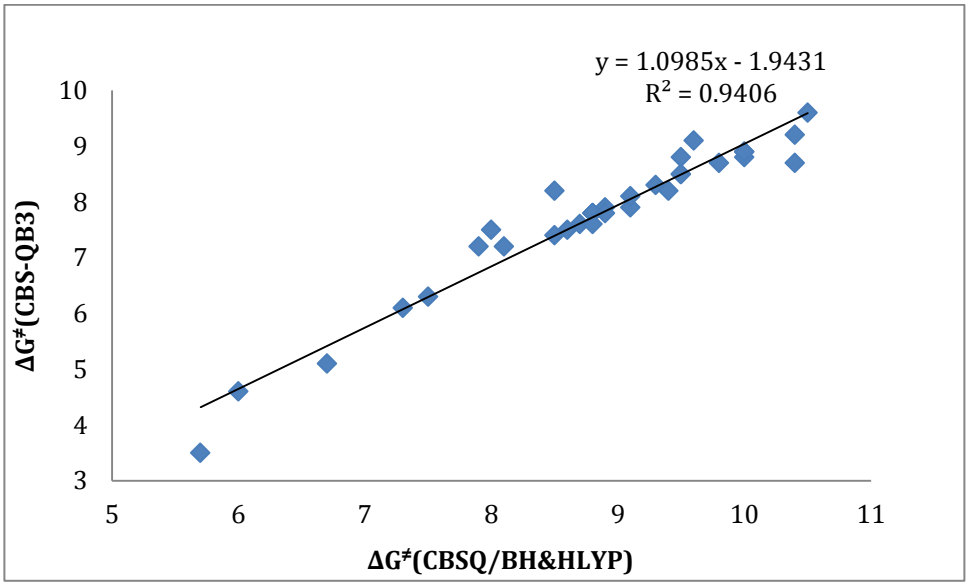

Figure 3.4: Comparison of the free energy of transition state ($\Delta G^{\neq}$) in kcal/mol for addition reactions for CBS-QB3 and CBS-Q//BH&HLYP/6-31+G(d,p) level of theory.

The reaction profile (Figure 3.5) for aniline (an electron donating group) shows that the *ortho* products are more favored than the *para* and *meta* products which is consistent with the previous discussion. The free energy of activation is 3.5 kcal/mol for *ortho* attack, and 5.1 and 7.4 kcal/mol for attack at the *para* and *meta* positions respectively. In contrast, the reaction profile (Figure 3.6) for trifluorotoluene (inductively electron withdrawing with no potential resonance stabilization) indicates that the *meta* product is increasingly favored, and preferred relative to the *ortho* product, but not the *para* product. The free energy of activation is 9.6 kcal/mol for attack at the *ortho* position, and 8.8 and 9.1 kcal/mol for attack at the *para* and *meta* positions respectively. The *para* position remains favorable because the inductive effect of the $-CF_3$ group is minimized.

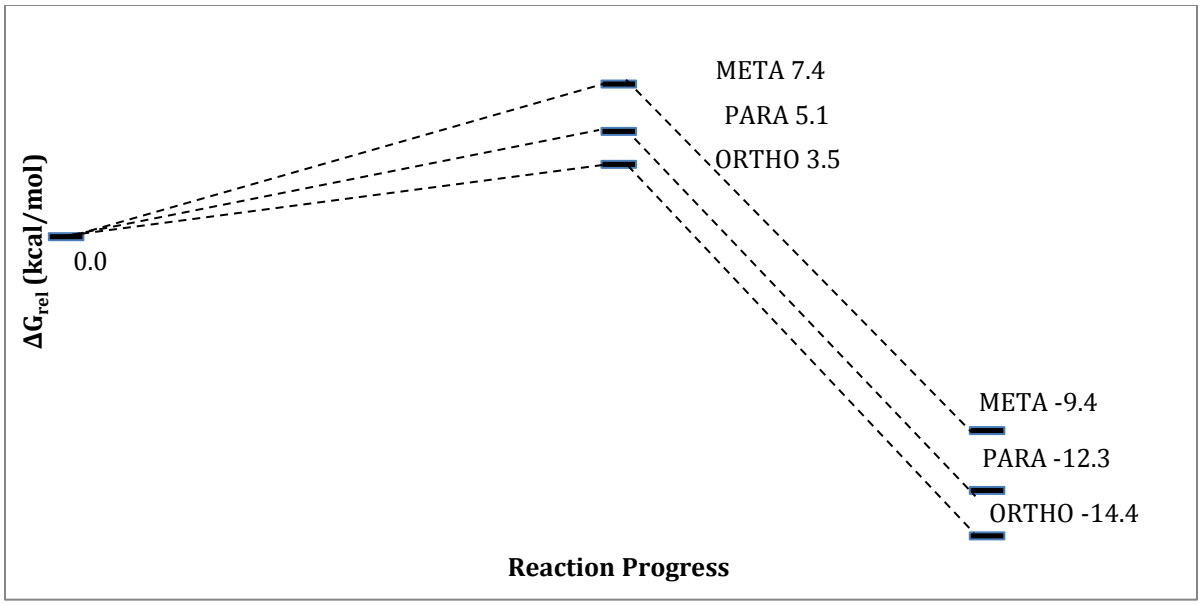

Figure 3.5 : Comparison of gas phase ΔG (298K) values for hydroxyl radical addition to Aniline (electron donating group $–NH_2$) (kcal/mol) at the CBS-Q//BH&HLYP/6-31+G(d,p)level of theory. All energies are relative to separated species at same level of theory.

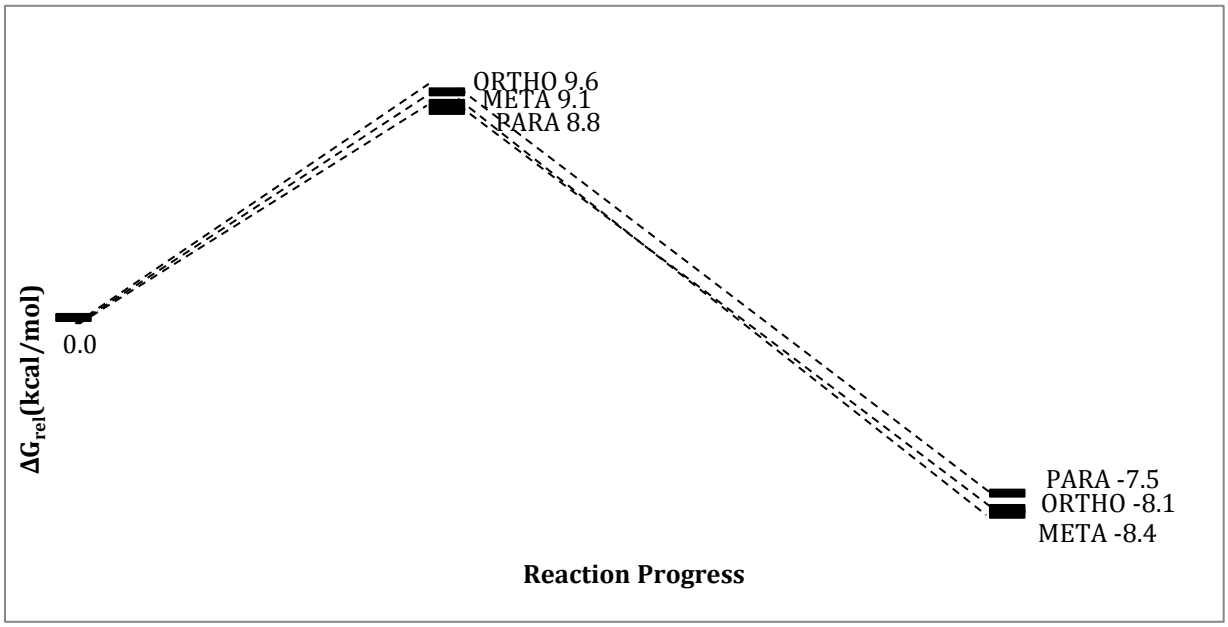

Figure 3.6 : Comparison of gas phase ΔG (298K) values for hydroxyl radical addition to Trifluorotoluene (electron withdrawing group $–CF_3$) (kcal/mol) at the CBS-Q//BH&HLYP/6-31+G(d,p)level of theory. All energies are relative to separated species at same level of theory.

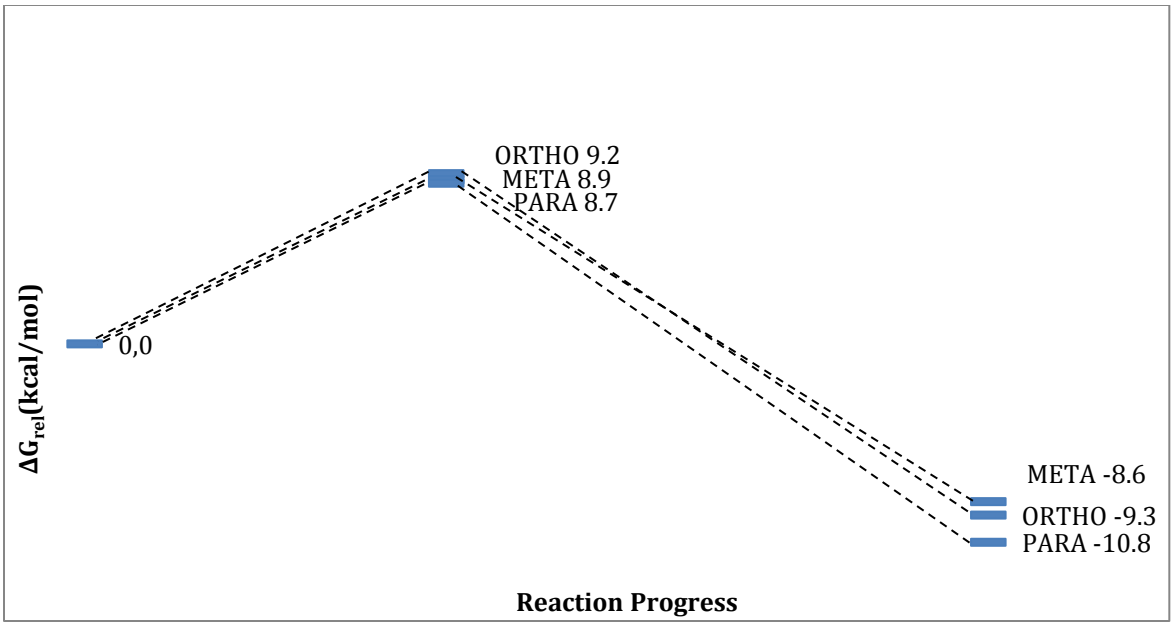

Figure 3.7 : Comparison of gas phase ΔG (298K) values for hydroxyl radical addition to nitrobenzene (electron withdrawing group $–NO_2$) (kcal/mol) at the CBS-Q//BH&HLYP/6-31+G(d,p)level of theory. All energies are relative to separated species at same level of theory.

The reaction profile (Figure 3.7) for nitrobenzene (inductively electron withdrawing, but potentially resonance stabilizing) shows that the free energy for transition state is 9.2, 8.7 and 8.9 kcal/mol for attack at the *ortho*, *para* and *meta* positions respectively. The preference for *para* over *meta* substitution may be explained by resonance stabilization effects, but the same argument cannot explain the reduced activity toward *ortho* attack relative to both *meta* and *para*. It would appear that the reaction is not governed purely by radical stabilization effects - polar effects may play a significant role.

Table 3.5 shows the rate coefficients calculated for each reaction. The Arrhenius equation states that rate coefficient depends upon the activation energy, pre-exponential factor, and the temperature. The geometries found for the transition states

are structurally similar, with small variations in bond lengths (Table 3.2), which means to good approximation, the entropy changes in the systems as they evolve from reactant to transition state are similar. The pre-exponential factors may be assumed, to good approximation, to be the same for all of these reactions. Therefore, the rate coefficient or the relative rate coefficient for these reactions depends upon the activation energies. The rate coefficients for electron donating groups are generally larger than those for electron withdrawing groups, consistent with calculated free energies of activation.

Table 3.5 also includes calculated product distributions, which are estimated from the weighted mean of the rate coefficients, weighted by the number of possible sites of attack (for example, Eq. 3.1)

$$\%(ortho) = 100 \times \frac{2k_{ortho}}{\left(2k_{ortho} + 2k_{meta} + k_{para}\right)} \qquad \text{(Eq. 3.1)}$$

Combined attack at both *ortho* and *para* positions are more favorable than *meta* position, which is consistent with the previous computational and experimental studies discussed earlier in chapter 1 for toluene [42], fluorobenzene [101], chlorobenzene [102] and phenol [18]. This observation is also consistent with the resonance contributors drawn in Figure 3.3. However, attack at *ortho* position becomes increasingly disfavored for groups that are strongly inductively withdrawing (including those groups that are resonance stabilizing for free radicals), whereas attack at *meta* position becomes increasingly favored. Additional structure–reactivity relationships were investigated to better understand this effect.

Table 3.5: Rate coefficients and % product distributions for gas phase hydroxyl radical addition to arenes.

Functional group	k_{298} ($dm^3mol^{-1}s^{-1}$)			% product distribution at 298K		
	Ortho	***Meta***	***Para***	***Ortho***	***Meta***	***Para***
$-NH_2$	1.73E+10	2.15E+07	1.06E+09	97	0	3
$-OCH_3$	2.69E+09	3.28E+07	2.19E+08	95	1	4
-OH	3.41E+09	9.35E+06	1.36E+08	98	0	2
$-CH_3$	3.17E+07	5.72E+06	1.91E+07	68	12	20
-H	1.23E+07	1.23E+07	1.23E+07	40	40	20
-Cl	9.68E+06	3.62E+06	1.19E+07	50	19	31
-F	2.03E+06	5.17E+06	1.61E+07	13	34	53
-CHO	6.66E+06	3.62E+06	1.58E+07	37	20	43
-CN	2.54E+06	1.75E+06	6.02E+06	35	24	41
$-CF_3$	5.52E+05	1.27E+06	2.10E+06	19	44	37
$-NO_2$	1.02E+06	1.78E+06	2.45E+06	25	44	31

3.3 Structure-Reactivity Relationships

Hydroxyl radical addition depends on different functional groups on the benzene ring and there are a number of potential factors that may influence the rates of addition: electronic effects, polar effects, steric effects, and thermodynamic stabilization (radical stabilization and bond strength effects).

Bond strength effects: The approximate geometric structure of a transition state can be predicted by comparing its energy with the neighboring species along the reaction coordinate. According to the Hammond postulate [150], the structure of transition state resembles reactant, product, or intermediate that is closest in energy. For exothermic reactions, the transition state is closer in energy to reactants than to products. Therefore the transition state is assumed to be more similar to the reactants than products – an "early" transition state. For endothermic reactions the transition state is closer in energy to products than reactants and therefore the transition state is going to be more similar to products –a "late" transition state. The Hammond postulate is reflected in the Bells-Evans-Polanyi principle [151], which postulates that the difference in activation energy between two reactions of the same family is proportional to the difference of their enthalpy of reaction. The Evans-Polanyi model assumes that the transition states are structurally similar for all the reactions and the pre-exponential factors of Arrhenius equation are effectively the same for all the reactions of the particular family [150]. Thus, the entropies of reaction and entropies of activation are not drastically different and, there exists a linear relationship between the activation energies (E_a) and enthalpies of reaction (ΔH_R), where the more stable product is formed via the lower-energy transition state [152, 153].

$$E_a = E_0 + \alpha \Delta H_R \qquad \text{(Eq.3.2)}$$

In (Eq. 3.2), E_0 is the activation energy of a reference reaction of same class, and α is a weighting factor that reflects the position of the transition state along the reaction coordinate, ($0 < \alpha < 1$). If α is large (> 0.5), then the transition state is "late" whereas if α is small (< 0.5) then the transition state is "early" [154]. Any linear

relationship provides an efficient way to find the activation energy of many reactions in distinct families.

Table 3.6 shows that the enthalpies of activation for electron donating groups are smaller than those for electron withdrawing groups. For the three sites of potential attack the enthalpies of reaction and activation show behavior that is qualitatively similar to that exhibited by calculated free energies (Table 3.3). This is consistent with a family of reactions where the TΔS term of the free energy is similar.

Table 3.6: Enthalpy of reaction, enthalpy of activation for hydroxyl radical addition to arenes.

Functional group	ΔH_R Ortho (kcal/mol)	ΔH_R Meta (kcal/mol)	ΔH_R Para (kcal/mol)	$\Delta H^{\neq}$ Ortho (kcal/mol)	$\Delta H^{\neq}$ Meta (kcal/mol)	$\Delta H^{\neq}$ Para (kcal/mol)
-NH_2	-14.4	-9.2	-11.1	0.9	5.7	3
-OCH_3	-15.7	-16.6	-13.8	3.2	5.3	4.2
-OH	-13.1	-8.8	-10.1	1.9	6.2	4.4
-CH_3	-11.2	-10.3	-10.7	3.8	5.3	4.8
-H	-9.7	-9.7	-9.7	5.3	5.3	5.3
-Cl	-12.4	-10	-10.8	5.8	6.1	5.4
-F	-11.4	-10.1	-9.7	7.2	6.2	5.5
-CHO	-10.3	-8.9	-13	6.1	6.5	5.5
-CN	-15.9	-12	-15.2	6.6	6.6	5.8
-CF_3	-11.2	-9.8	-10.1	6.7	6.1	6.2
-NO_2	-15.1	-9.1	-11.6	7	6.9	6.5

The data in Figure 3.8 does not exhibit any clear Bell-Evans-Polanyi behavior, suggesting that the stability of the product is not a controlling factor in the kinetics of hydroxyl radical addition reactions. This in turn suggests that (a) the transition state bears relatively little structural resemblance to the products (the transition state is "early"), and (b) other factors, such as those described above, may play a more dominant role.

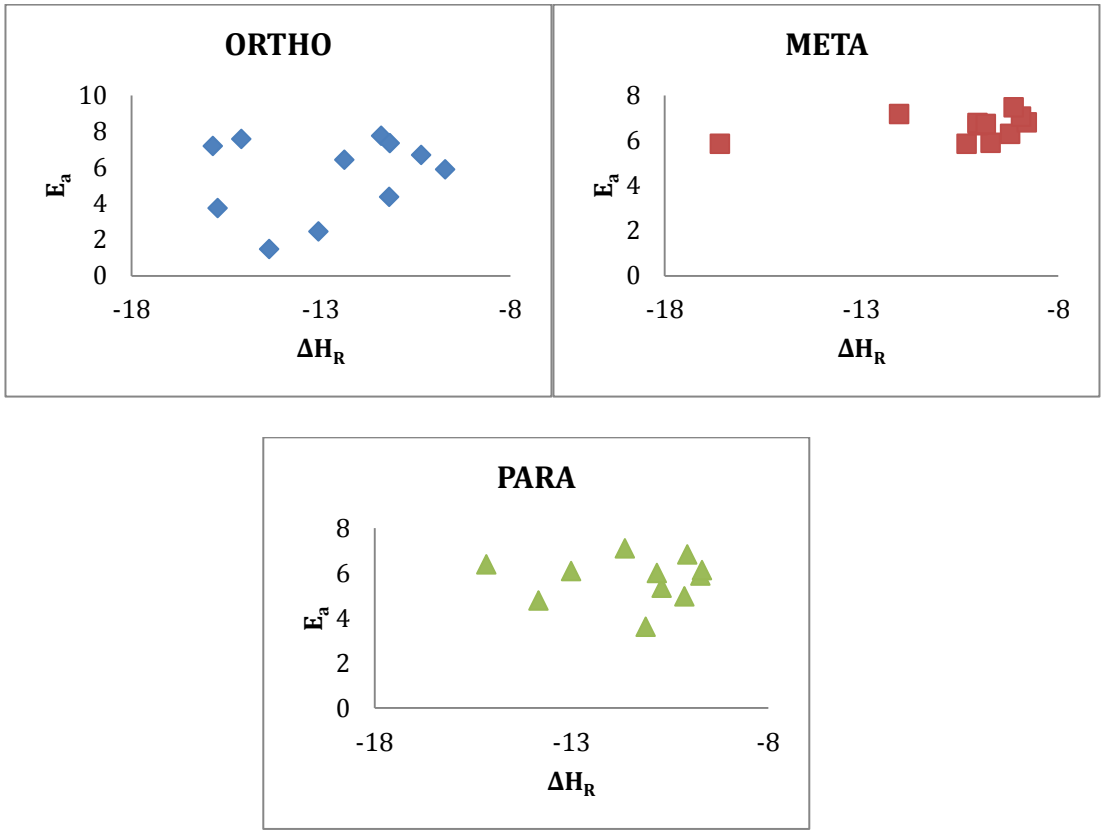

Figure 3.8: Evans-Polanyi plots for addition of hydroxyl radical to arenes where both activation energy at 298K and enthalpy of reaction are measured in kcal/mol.

Radical Stabilization Energies (RSE): It would appear from the previous discussion that the addition of hydroxyl radical is not strongly dependent upon the thermochemistry of the reaction. However, the effect of intrinsic radical stabilization of

the formed adduct radical was also investigated. The effect of substituents on the stability of free radicals is important in understanding the nature of reactions involving radicals as reactants, products, or intermediates. The radical stabilization energy (RSE) reflects the stability of a radical relative to its unsubstituted analog, and probes the effects of substituted functional groups directly.

Bond dissociation energy is often used as a measure of radical stability. If for example, to quantify the stability of hydroxymethyl radical, the bond dissociation energy of the methanol C-H bonds can be used. This is synonymous to calculating the reaction energy for the reaction:

$$CH_3OH \rightarrow C\dot{H}_2OH + \dot{H}$$

While the energy of reaction reflect stability of product radicals but not for reactants, as the electron correlation energies will differ in closed shell reactant and open shell products. Thus, free radical stability is not solely reflected by bond strengths.

RSEs are often determined using isodesmic reactions, hypothetical chemical processes in which the number of bonds of each formal type remain the same on each side of chemical equation but with changes occurring in their mutual relationships. The enthalpy of an isodesmic reaction is a measure of deviations from the additivity of bond energies, due to selective stabilization or destabilization of an intermediate by the functional group. The use of numerical values for the enthalpy of isodesmic reactions, involving the compounds being examined and their models, is a simple but effective tool for search and quantitative estimation of the diverse effects of stabilization/destabilization [155]. A positive RSE indicates that a functional group exerts a selectively stabilizing effect on the radical relative to the unfunctionalized parent, and

a negative number indicates a destabilizing effect. Free radicals are electron deficient and any factor that helps to donate electron density to half-filled orbital or to withdraw that electron will stabilize the radical. Therefore using an appropriate isodesmic reaction will simplify the situation because isodesmic reactions are written so that correlation effects largely cancel.

$$CH_3OH + C\dot{H}_3 \rightarrow C\dot{H}_2OH + CH_4$$

This isodesmic hydrogen transfer reaction between methanol and methyl radical can be constructed as the difference between the heat of formation of products and reactants, and thus the differential stability of the methyl and the hydroxymethyl radical [156]. Therefore the radical stabilization energies in the reaction of arene with hydroxyl radical can be calculated by comparing the heats of formation of products and the reactants to study the effect of substituents on the stability of free radicals which are involved in the reaction.

Radical stabilization energy was calculated by two different methods for an species substituted with electron donating (NH_2), electron withdrawing (CN) and weakly inductively donating ($-CH_3$) to compare the results from both the methods: method 1 and method 2 are shown in Scheme 3.5, and the calculated RSEs in Table 3.7.

Scheme 3.5: Isodesmic reactions used to estimate the radical stabilization energies for functional groups (X) at *ortho*, *meta* and *para* position.

(a) Method 1

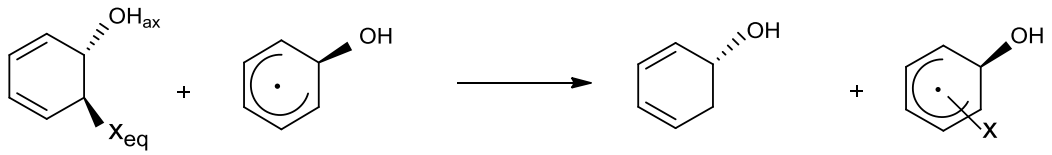

(b) Method 2

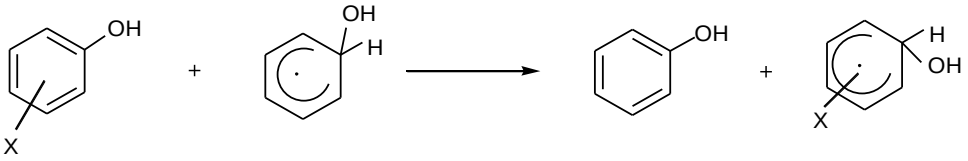

Table 3.7: Calculated radical stabilization energies (0 K,kcal/mol) for addition reactions with method 1 and method 2.

Functional group		RSE	
		Method 1	Method 2
OCH_3	o-	6.15	0.16
	m-	2.52	-2.06
	p-	4.51	-0.72
CH_3	o-	2.49	-0.92
	m-	1.12	-2.73
	p-	1.33	-0.11
CN	o-	3.13	-0.30
	m-	-0.37	0.67
	p-	2.80	-4.48

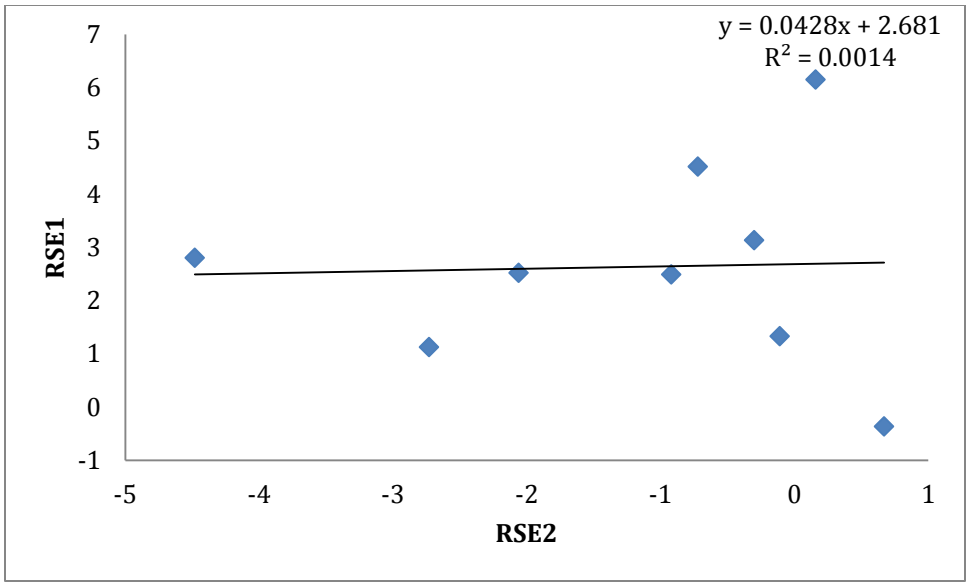

Figure 3.9: Comparison of Radical stabilization energy (0K, kcal/mol) for scheme 3.5 for toluene, anisole and benzonitrile.

Figure 3.9 show that the methods do not correlate with each other. Method 2 indicates that *ortho* products are destabilized relative to *meta* and *para* products. This may be a reflection of the fact that in method 2, selective stabilization of the starting materials may occur when the functional group is allowed to interact with the aromatic ring in the starting substituted phenol, but a non-aromatic system in the products. In method 1, the functional group X interacts with non-aromatic systems in both reactant and products.

Radical stabilization energies were calculated using method 1 (Scheme 3.5(a)) because it minimizes the steric strain and *ortho* interactions, but also avoids selective stabilization of the reactants. Table 3.8 shows that electron donating groups give positive stabilization energy at all the possible sites of addition of hydroxyl radical, and that stabilization by electron withdrawing groups also occurs, particularly for *ortho* and

para addition, but is more sensitive to the effects of destabilization by inductive withdrawal (-F, -CF_3 and –NO_2). Table 3.8 shows that the lone pair donor functional groups (OH, NH_2, and OCH_3) all stabilize the radical center. The overall interaction between the radical center and the lone pair orbital of functional group is a net one electron stabilization. The energy gap between the interacting cyclohexadienyl molecular orbital (MO) and the 2p orbital of the donating atom increases across first row of periodic table (going from NH_2 to OH), [156] which is reflected in the decreasing stabilization energies.

Table 3.8: Calculated radical stabilization energies energy (0K, kcal/mol) for addition reactions.

Functional group	Ortho	Meta	Para
-NH_2	8.37	4.58	6.68
-OCH_3	6.15	2.51	4.51
-OH	4.46	2.57	2.93
-CH_3	2.49	1.12	1.33
-Cl	0.30	-1.85	-1.33
-F	-0.48	-1.40	-2.57
-CHO	5.09	1.74	5.60
-CN	3.13	-0.37	2.80
-CF_3	-2.28	-3.94	-3.85
-NO_2	-1.86	-3.08	-1.36

A methyl substituent is also predicted to give rise to radical stabilization. This occurs as a result of hyperconjugation in which the radical orbital interacts with an occupied π-type and a vacant π*-type orbital of the methyl group. This orbital interaction is similar to that occurring between orbital and a π-acceptor substituent, but the resulting stabilization is smaller because the energy difference between the lone pair and sigma bond is large. Hyperconjugation due to the methyl substituent involves the three C-H bonds.

All substituents other than NO_2, F, and CF_3 stabilize the radical. The destabilization is caused due to the dominance of the inductively electron-withdrawing fluorine or nitro atoms acting on the electron-deficient radical center. This electron-withdrawal effect apparently exceeds any stabilizing resonance, or in the case of $–CF_3$ hyperconjugative interaction. The CF_3 substituent is slightly more destabilizing than F and NO_2, due to the presence of three C-F bonds.

Figure 3.10 shows the plots of enthalpy of activation as a function of RSE calculated for substituted cyclohexadienyl radicals by method 1. The kinetics of attack at the *meta* position show almost no dependence on the calculated RSE. In the case of *ortho* and *para* attack, it is possible that a linear relationship may exist, but there is a significant degree of scatter in the data (R^2 = 0.48 and 0.47 for *ortho* and *para* attack respectively). It is worth noting that the largest variations from a linear relationship occur for those substituents that are resonance stabilizing but electron withdrawing (-CN and –CHO) in both cases. However, it is clear that radical stabilization of the product does not provide a reliable structure-reactivity relationship for these early transition state

reactions.

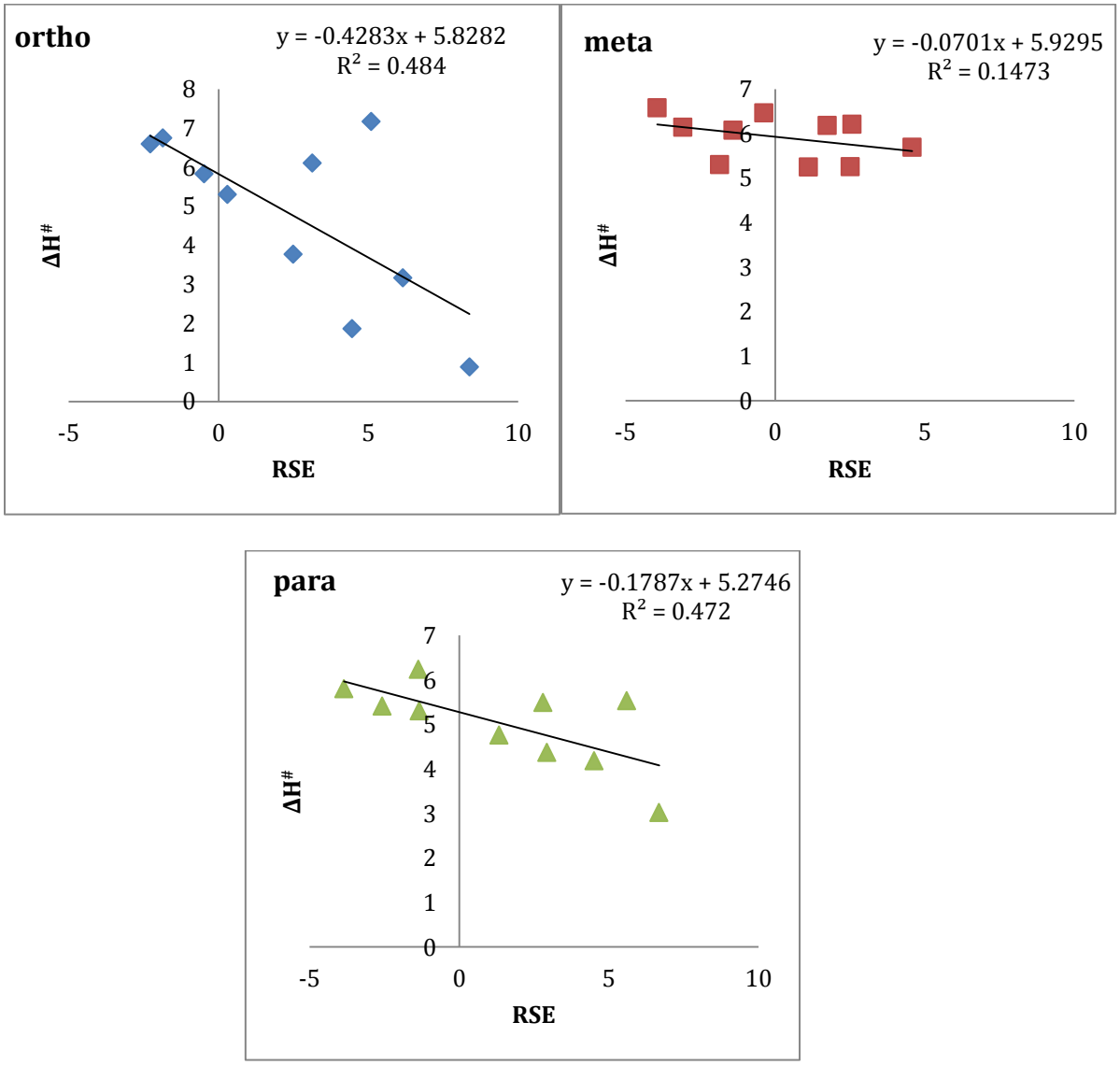

RSE vs $\Delta H^{\neq}$	Slope	R^2	INTERCEPT
ortho	-0.43	0.48	5.83
meta	-0.07	0.15	5.93
para	-0.18	0.43	5.27

Figure 3.10: Radical stabilization energy (0K, kcal/mol) vs enthalpy of activation (kcal/mol) plots and lines of best fit for the addition of hydroxyl radical on arenes.

Frontier molecular interactions: The FMO approach is based on the reactivity of two reactants as they approach and begin bonding, which is treated in terms of perturbation; the largest perturbation will arise from the orbitals closest in energy i.e. the gap between HOMO (highest occupied molecular orbital) and LUMO (lowest unoccupied molecular orbital) of the reacting species. In case of free radical, SOMO (singly occupied molecular orbital) plays the role of HOMO or LUMO. Although in this case of hydroxyl radical, it's probably going to act as an electron acceptor (LUMO) since gain of electron by hydroxyl radical and form a nucleophile is much easier than donating a electron and form electrophile. The overlap of these two atomic orbitals leads to formation of a new "bonding" molecular orbital [157]. The atomic orbitals of reactants: arene and hydroxyl radical, combine with each other by coulombic interactions and form a new molecular orbital. The following expression may be derived for FMO theory for reacting A and B reactants [158]

$$\Delta E = C\left\{\sum_{A}^{occ}\sum_{B}^{unocc}\frac{1}{(E_A - E_B)} + \sum_{A}^{unocc}\sum_{B}^{occ}\frac{1}{(E_A - E_B)}\right\} \qquad (\text{Eq. } 3.3)$$

where ΔE is the interaction energy between reactants A and B, and *C* represents the degree of overlap between molecules A and B, and is assumed to be constant for similar reactions. The interactions that raise the HOMO or lower the LUMO (Figure 3.11) will facilitate the reaction, while those that lower the HOMO or raise the LUMO will inhibit the reaction.

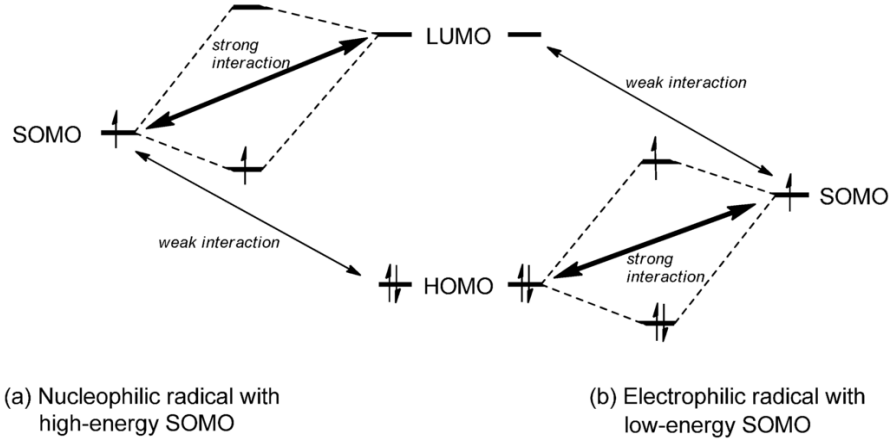

Figure 3.11: Interaction between HOMO, LUMO and SUMO.

FMO theory predicts the relative energies of an early transition state by approximating the slope of the reaction path diagram at the reactant i.e. first derivative of the energy with respect to motion along the reaction path. If derivative of energetic contribution of the HOMO/LUMO interaction with respect to the overlap of orbitals forming bonds, the following expression can be obtained by truncated perturbation theory [159]:

$$\Delta E \propto C\left\{\frac{1}{E_{HOMO,nuc} - E_{LUMO,elec}}\right\} \qquad (\text{Eq. } 3.4)$$

As the geometries for these reactions are similar, it may be assumed that *C* is similar for all of the reactions. In these reactions the arene acts as nucleophilic species (*nuc*), and hydroxyl radical as an electrophile (*elec*) with a singly occupied molecular orbital (SOMO). Higher HOMO energies result in higher interaction energies and a faster rate of reaction. The energy of the SOMO is going to be same for hydroxyl radical, since hydroxyl radical behaves as the electrophile. A smaller HOMO-SOMO energy gap will lead to a faster rate, as orbitals of similar energy will overlap more effectively.

The HOMO energies for arenes can be determined from their ionization potentials (IP, Table 3.9). Koopmans' theorem states that the first ionization potential is equal to the negative of the orbital energy of HOMO [160]. The measured ionization energy can either be vertical or adiabatic ionization energy. The vertical ionization energy is used in case the ion is in the same geometry as the neutral. The adiabatic ionization energy is used in which the ion is in its lowest energy, relaxed geometry. Vertical ionization energy were used in this study [161].

Table 3.9: Rate coefficient ratios for hydroxyl radical addition and ionization potentials.

Functional group X =	$\log(k_x/k_H)$			IP arene[a] (ev)
	ortho	meta	para	
-NH_2	3.15	0.24	1.94	7.72
-OCH_3	2.34	0.43	1.25	8.20
-OH	2.44	-0.12	1.05	8.49
-CH_3	0.41	-0.33	0.19	8.82
-H	0	0	0	9.24
-Cl	-0.10	-0.53	-0.01	9.07
-F	-0.78	-0.38	0.12	9.20
-CHO	-0.26	-0.53	0.11	9.50
-CN	-0.68	-0.84	-0.31	9.73
-CF_3	-1.35	-0.99	-0.77	9.68
-NO_2	-1.08	-0.84	-0.70	9.94

[a]Reference [161]

Figure 3.12 shows plots of the logarithm of relative rate coefficients (a measure of differences in $\Delta G^{\ddagger}$) as a function of arene IP. The relative rate coefficients for an arene substituted with functional group –X (k_X) are determined relative to the unsubstituted system, benzene (k_H). The plots show a linear dependence of relative rate coefficients on the HOMO energy for attack at all three sites, with systems with electron donating groups exhibiting higher reactivity than those with electron withdrawing groups. The magnitude of the effect of substitution is much greater for *ortho* and *para* attack than it is for *meta* attack.

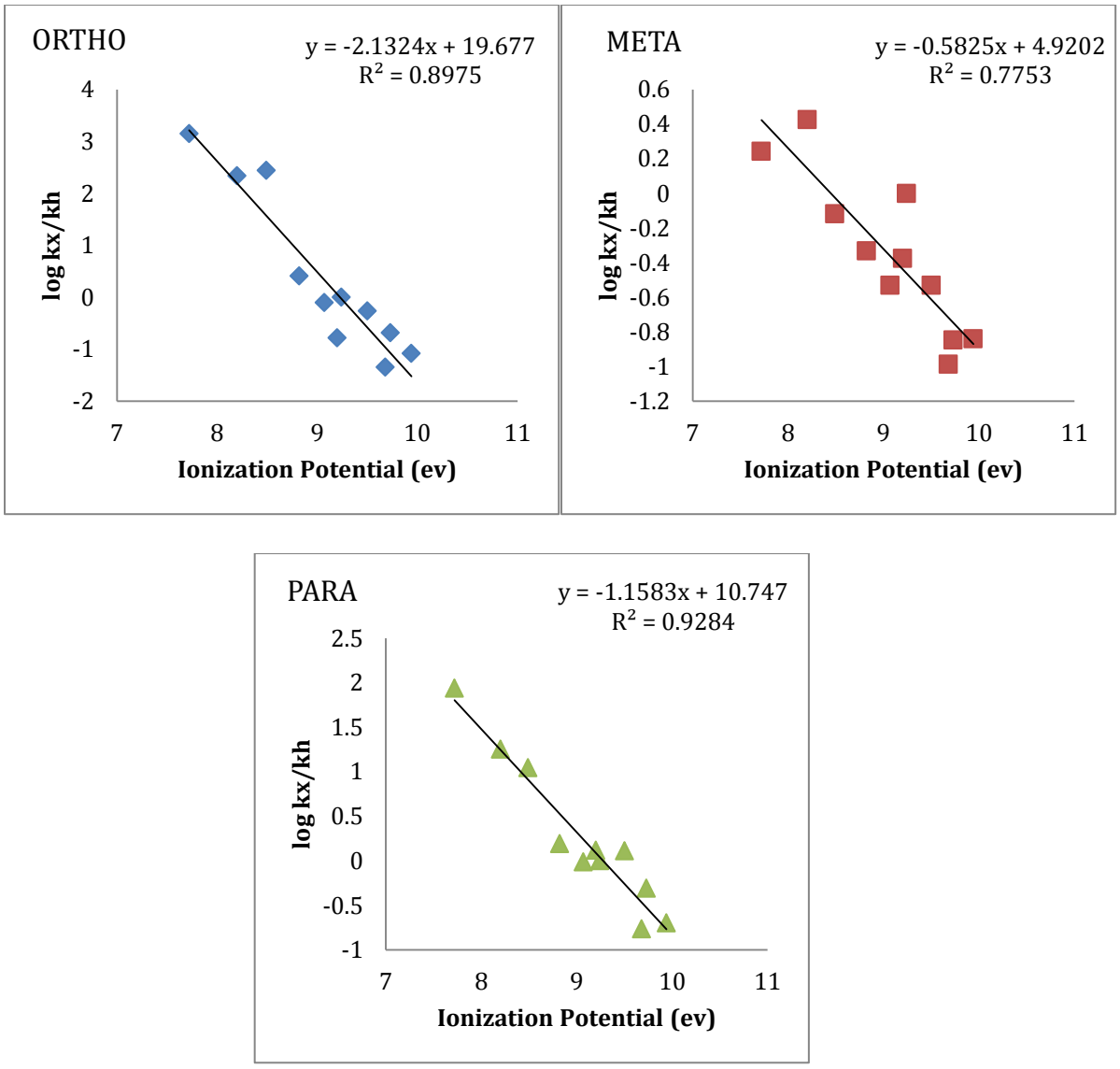

IP vs log(k_x/k_H)	Slope	R^2	INTERCEPT
ortho	-2.13	0.90	19.7
meta	-0.58	0.78	4.90
para	-1.16	0.93	10.7

Figure 3.12: Frontier molecular orbital theory correlation for addition of hydroxyl radical to arenes.

Similar behavior has been observed experimentally for alkylated arenes [44, 45], and is believed to reflect the fact that the attack of hydroxyl radical on an arene has a

significant degree of charge transfer character in the transition state. That is, to some extent the charge distribution in the transition state resembles a hydroxide anion interacting with the radical cation of the arene. The radical cation is the species generated by ionization of the arene. This observation also implies that polar effects may exert greater influence on the reaction rate.

Polar effects can originate with functional groups and be transmitted to the reacting atoms. If there is an electron withdrawing group on the benzene ring it will shift the electron density towards itself and a charged electrophilic species can preferentially at *meta* positions as we can see in Figure 3.1. If there is electron donating group on the benzene ring it will shift the electron density towards the ring and the hydroxyl radical can add at *ortho* and *para* positions. Natural Population Analysis (NPA) methods were used to probe the polar effects for each of the stationary points to determine the charge and spin density on each atom of the systems. The calculations were performed for the single-point energy calculations at the BH&HLYP/6-31+G(d,p) level of theory using the BH&HLYP/6-31+G(d,p) geometries but it did not provide any clear relationships between relative rate coefficients and either charge or spin density at the potential sites of attack.

Hammett correlations: Polar effects on free radical reactions can be studied by the Hammett equation (Eq. 3.3) [162].

$$log\frac{k_X}{k_H} = \sigma\rho \qquad \text{Eq.3.3}$$

The rate coefficients k_X and k_H are rate for reactions of substituted (with substituent –X) and unsubstituted arenes respectively, σ is a parameter dependent on the nature and

position of the substituent on the aromatic ring (Table 3.10) and ρ is a reaction parameter that reflects the reaction's sensitivity towards substituent effects.

Table 3.10: Standard hammett substituent parameters for addition reactions.

Functional group	σ_m [a]	σ_p [a]
-NH_2	-0.16	-0.66
-OCH_3	0.11	-0.27
-OH	0.12	-0.37
-CH_3	-0.06	-0.17
-H	0	0
-Cl	0.37	0.23
-F	0.34	0.06
-CHO	0.35	0.42
-CN	0.62	0.66
-CF_3	0.43	0.54
-NO_2	0.73	0.78

[a]Reference [83]

A Hammett plot for this reaction is shown in Figure 3.13, which includes substituent parameters for groups on both the *meta* and *para* positions. Note that most Hammett plots do not include *ortho* parameters, due to the complicating influences of steric and internal hydrogen bonding effects in the benzoic acid systems that define σ. The plot exhibits a clear linear relationship, and the slope of the linear fit has a negative value, which is consistent with the notion that hydroxyl radical behaves as electrophilic

species, that positive charge builds up in the ring in the in the transition state and the rate is accelerated by electron donating groups [162].

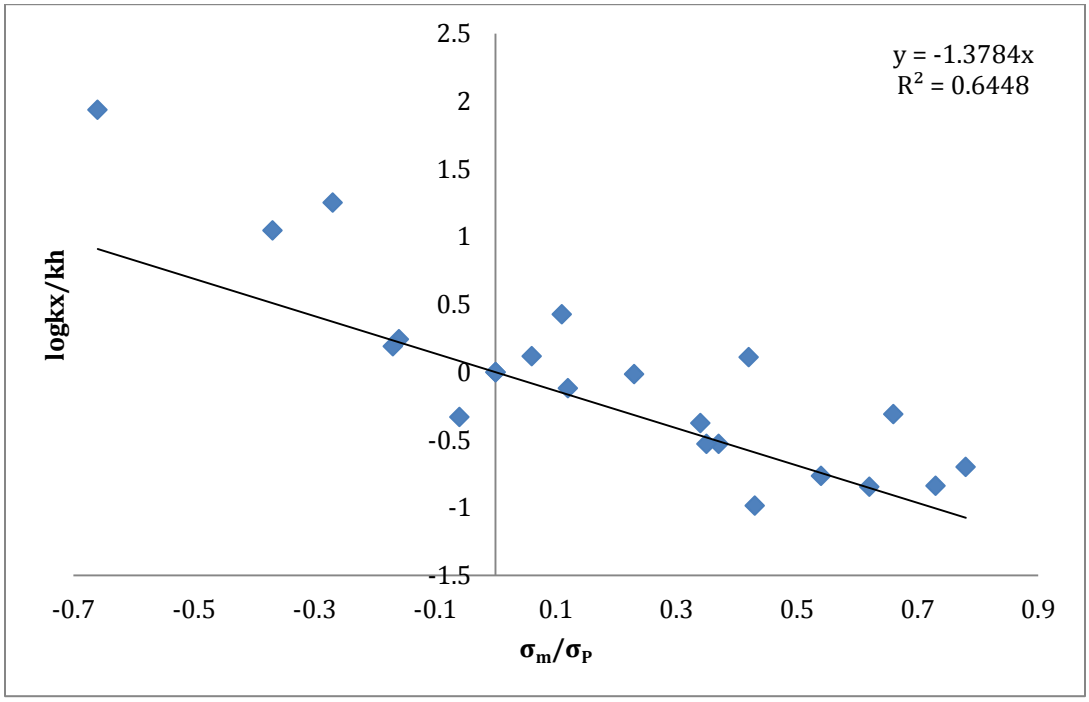

Figure 3.13: Correlation for relative rate for hydroxyl radical addition to arenes with Hammett substituent parameters.

Figure 3.13 shows that strong electron groups do not fall on the line, which suggests that arenes with these functional groups in the *para* position act as stronger nucleophiles than would be expected from the σ values. The correlation of activation energy and Hammett substituent constant should also give a similar type of relationship as expected from the Arrhenius equation [163] (Figure 3.14), which shows a positive trend for the activation energy showing that the transition state stabilized by electron donating groups, results in lowering of activation energy. Again, strongly electron-donating groups in the *para* position appear to diverge from the line of best fit for this relationship. These arenes have an additional rate enhancing effect predicted from the

standard *σ* values. This enhancement is possibly due to polar effects.

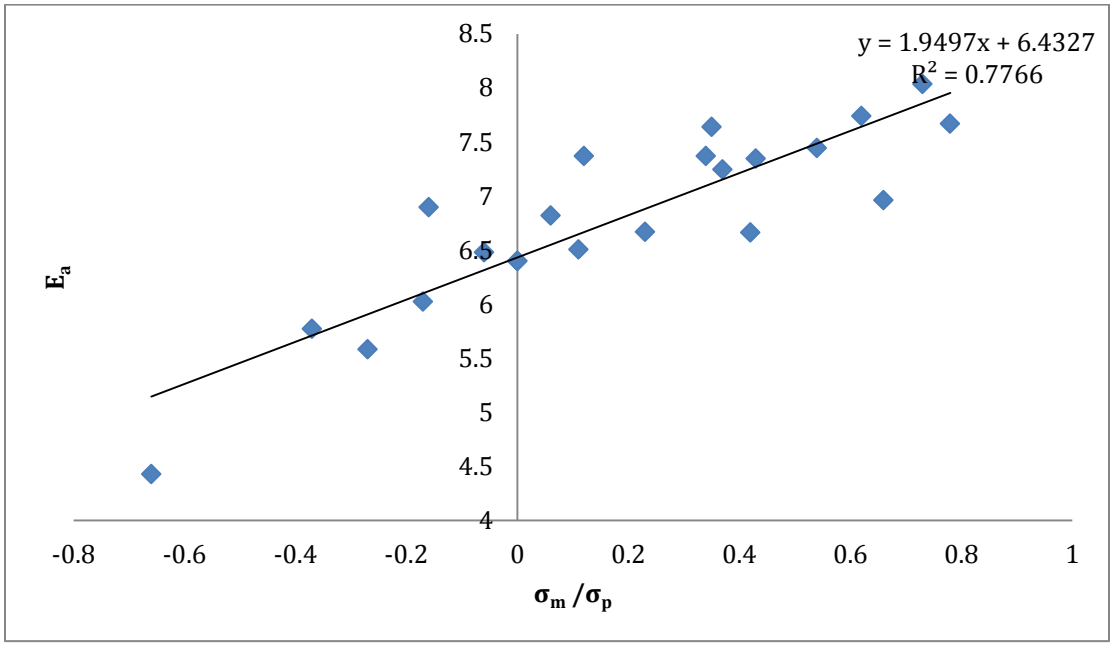

Figure 3.14: Correlation of activation energy in kcal/mol for addition of hydroxyl radical with Hammett substituent parameters.

To assess the additional polar effect, substituent parameters σ^-, σ^+, $\sigma^\bullet$, was employed. σ^- is used to describe nucleophilic substitution reactions (σ^-, ie. the benzene ring acting as an electron acceptor). The numerical value of σ^- is greater than the Hammett σ value for a given electron withdrawing group (Table 3.11). Consequently, for arene nucleophilic substitutions, a much better correlation should be observed if σ^- is plotted against relative rate. Figure 3.15 shows only para σ^- values (*meta* values are not available for most of the functional groups). It did not show correlation with nucleophilic substituent parameters which is consistent with the idea that this reaction behaves more like an electrophilic substitution.

Table 3.11: Alternate hammett substituent parameters for addition reactions.

Functional group	σ^{-}_{p} [a]	σ^{+}_{m} [a]	σ^{+}_{p} [a]	$\sigma\bullet_{m}$ [b]	$\sigma\bullet_{p}$ [b]
-NH_2	-0.15	-0.16	-1.30	-	0.7
-OCH_3	-0.26	0.047	-0.78	-0.02	0.27
-OH	-0.37	-	-0.92	-	0.26
-CH_3	-0.17	-0.066	-0.31	0.03	0.16
-H	0	0	0	0	0
-Cl	0.19	-0.39	0.11	-0.03	0.11
-F	-0.03	0.352	-0.07	-0.02	-0.06
-CHO	1.03	-	0.73	-	0.64
-CN	1.00	0.562	0.66	-0.13	0.47
-CF_3	0.65	0.520	0.61	-0.08	0.05
-NO_2	1.27	0.674	0.79	-0.11	0.57

[a]Reference [83]. [b]Reference [164]

In a similar vein, *para* substituents, which contain a pair of electrons that can come into direct resonance with electron-deficient reaction center, can also have rate-enhancing effects. In cases like these, where the reaction center becomes electron-deficient and develops a positive charge (an electrophilic addition), an electron-donating substituent at *para* position is directly involved in resonance stabilization. For this purpose, a new reaction parameter is employed, denoted as σ^{+} for electrophilic substitution reactions (Table 3.11). The values thus obtained give a much better correlation for electrophilic substitution. Figure 3.16 shows a strong linear dependence

with improved goodness of fit R^2 values over the dependence observed with standard Hammett parameters, which confirms the electrophilic nature of the hydroxyl radical.

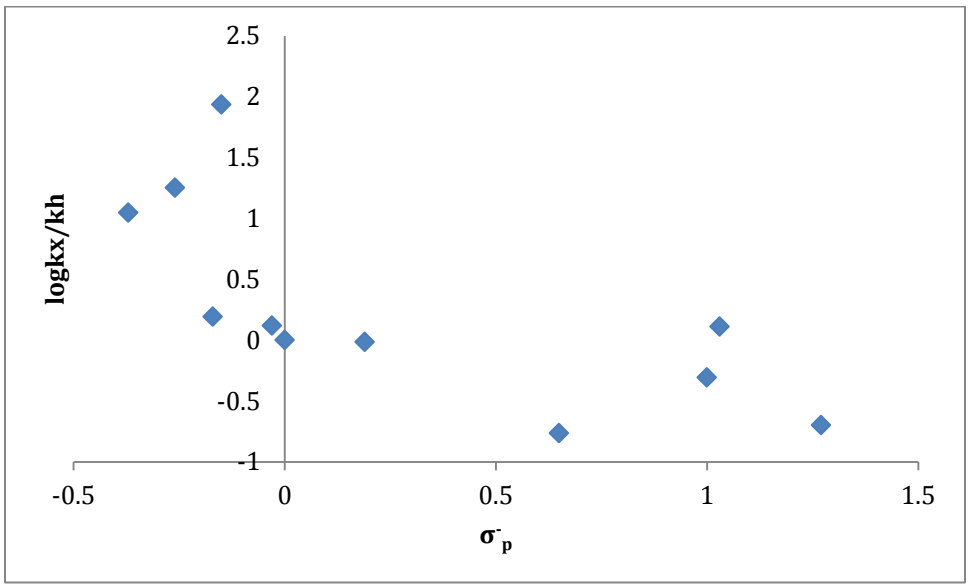

Figure 3.15: Correlation for relative rate for hydroxyl radical addition to arenes with nucleophilic substituent parameters.

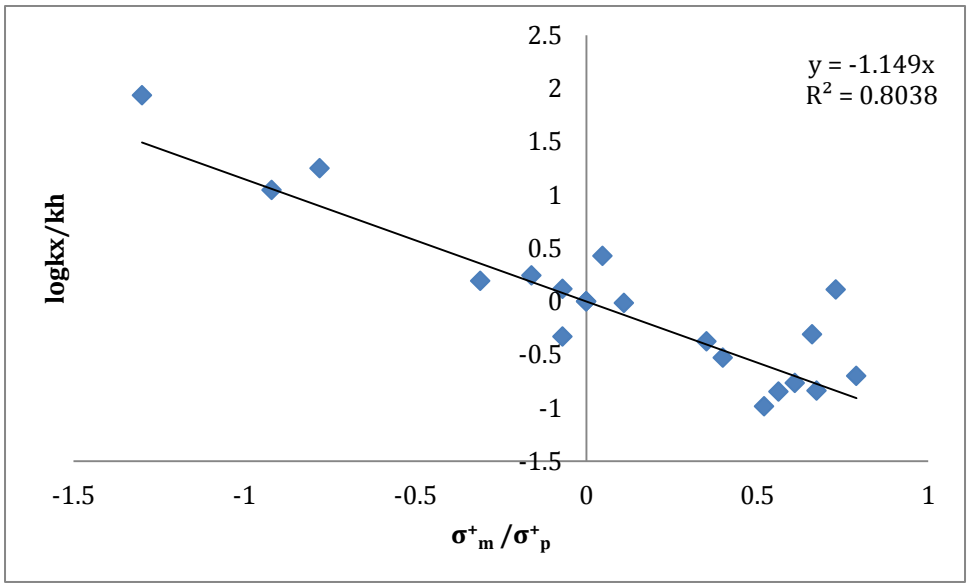

Figure 3.16: Correlation for relative rate for hydroxyl radical addition to arenes with electrophilic substituent parameters.

To study radical stabilization effects, a σ• factor introduced by Creary *et al*., based on the observed kinetics of rearrangement of methylenecyclopropane systems may be used in correlations (see Table 3.11). The rearrangement proceeds via a benzyl radical intermediate, which may not provide the best model for a cyclohexadienyl system. Figure 3.17 does not show a clear linear relationship: once again, it is notable that the apparent "outliers" with relative rate coefficients that are significantly lower than would be predicted from σ•, are those corresponding to inductively withdrawing, resonance stabilizing groups (-CN, -CHO and $–NO_2$) in the para position. This observed behavior confirms the notion that radical stabilization is not the only factor that controls the rate of addition of hydroxyl radical (see Radical Stabilization Energies), but polar effects must also be considered.

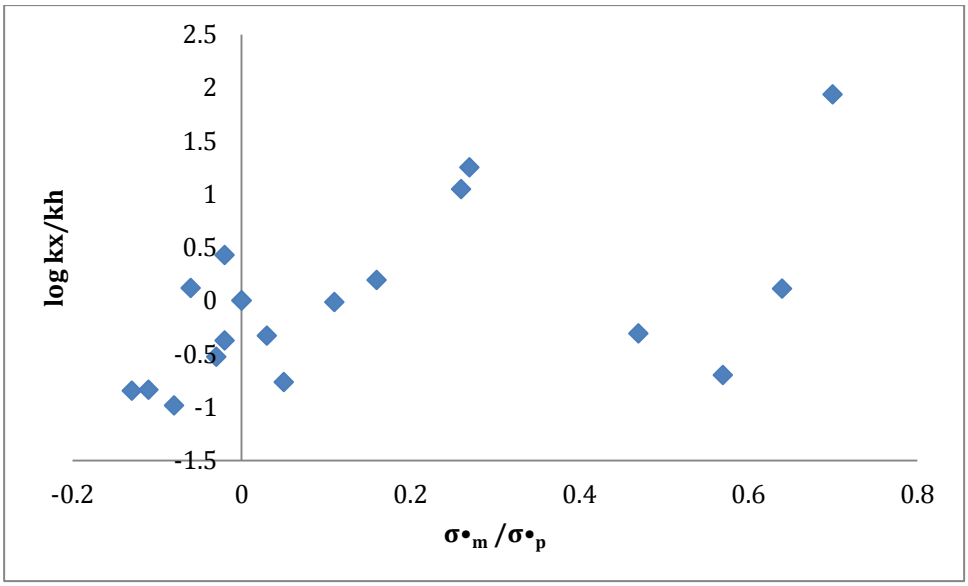

Figure 3.17: Correlation for relative rate for hydroxyl radical addition to arenes with radical substituent parameters.

***Steric effects*:** The addition of hydroxyl radical also depends upon the steric factors. If there is any steric hindrance in the addition it raises the energy required to reach the transition state for the reaction. The transition state becomes energetically more difficult to attain as the size of the group increases to the position of addition, which therefore decreases the rate constant of the reaction.

The Hammett equation describes the influence of polar and resonance effects at *para* and *meta* positions. The effect of both steric and polar factors at *ortho* positions cannot be readily treated by the Hammett equation. Taft [165] introduced a modification to Hammett equation which also accounts for steric factors (Equation 3.5):

$$\log\left(\frac{k_X}{k_{CH_3}}\right) = \rho^*\sigma^* + \delta E_s \qquad \text{(Eq. 3.5)}$$

Where the log term is the ratio of the rate of substituted reaction compared to the reference reaction (-CH_3 substituent, rather than –H), σ^* is a polar substituent constant, E_s is the steric substituent constant, ρ^* is the sensitivity factor for the reaction to polar effects and δ is the sensitivity factor for the reaction to steric factors.

When Taft's σ_o* values are changed to a σ_o scale with hydrogen as the standard, by assuming $\sigma_o=\sigma_p$ for CH_3 , it is seen that in various other cases $\sigma_o \sim \sigma_p$ (see Table 3.10). This assumes that the polar effects of substituents operate equally at the *ortho* and *para* positions. The generality of this approach has yet to be established, but steric factors can be estimated using deviations from linearity in correlations using σ_p. It can be seen in Figure 3.18 that when the relative rates for *ortho* attack are plotted against Hammett substituent parameter for *para* substitution, they exhibit a linear dependence with the largest outlier corresponding to a small, highly electronegative group exerting strong inductive withdrawal (-F).

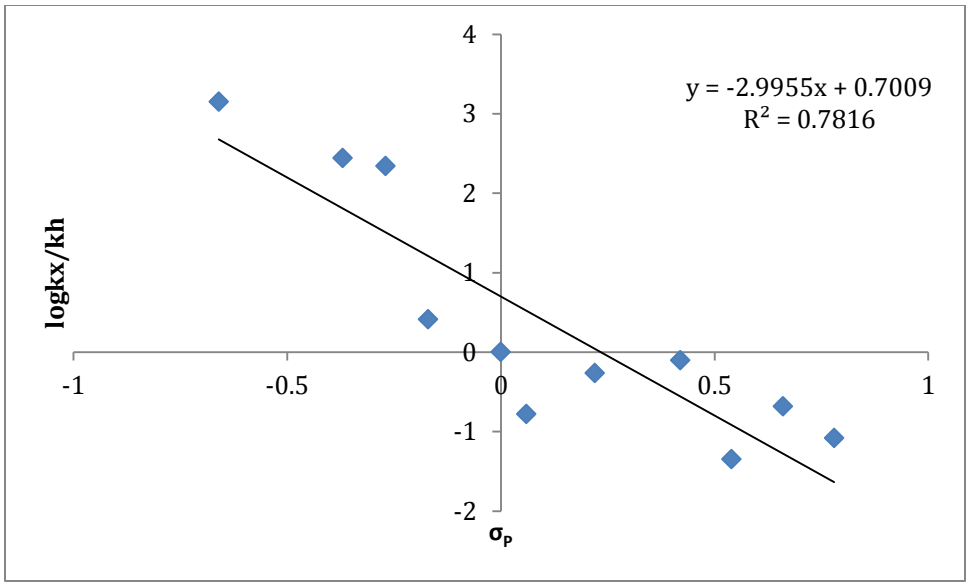

Figure 3.18: Correlation for relative rate for hydroxyl radical addition on *ortho* position to arenes with Hammett substituent parameters.

It is difficult to draw definitive conclusions, since none of the groups considered are sterically bulky, but the lack of large deviations from linearity in Figure 3.18 supports the hypothesis that the effect of steric crowding in the transition state is relatively small, which is not unreasonable since the hydroxyl radical approaches from above the plane of the ring. This correlation does not account for other possible interactions, such as hydrogen bonding in *ortho* substituted systems.

To summarize, there are a number of potential sites where hydroxyl radical may attack an aromatic ring. Calculations were performed to determine the structures and properties of potential intermediates and products formed. Addition of hydroxyl radical at *ortho* and *para* positions in the aromatic ring is favorable overall, but addition at *ortho* becomes less favorable in cases where electron withdrawing groups are present, and addition at *meta* becomes more favored in such systems. A frontier molecular orbital-

based model suggests that in all three possible modes of attack the transition state is early, and more structurally similar to the reactants than products. The charge on hydroxyl radical becomes more negative upon progressing from reactant to transition state and at same time the charge on aromatic ring becomes more positive. The positive charge appears to accumulate at *ortho* and *para* positions as expected from resonance theory. Hammett correlations indicate that stabilization of positive charge in the ring at the transition state is important, supporting the notion that the transition state for addition has significant charge transfer character. Under such circumstances polar effects play a major role in these types of reactions.

CHAPTER 4-SOLVENT EFFECTS ON THE RADICAL ADDITIONS TO ARENES

Since many organic reactions occur in solution, it is important to be familiar with the ways that solvents affect the rates of reaction. The most environmentally relevant solvent system is water. Water as we know is an unusual solvent. Water is highly polar molecule that exhibits hydrogen bonding i.e. specific solvent- solvent interactions. So it has strong, highly directional interaction that will lead to short-range structure, even in liquid phase. Water is also capable of significant ion dipole (solvation sphere) and dipole-dipole or hydrogen bonding interactions with solutes: one can envision hydrogen bonding interactions between water and hydroxyl radical or water and hydroxylated organics i.e. specific solvent- solute interactions. Again, such interactions are directional and lead to short–range structure.

There are important differences between protic solvents, those which contain hydrogens that form hydrogen bonds and can exchange rapidly (such as those bonded to oxygen, nitrogen, or sulfur), and aprotic solvents, in which all hydrogen is bound to carbon. Solvents that fall into the nonpolar aprotic class are not very effective at

stabilizing the development of charge separation. These molecules have small dipole moments and do not have hydrogens capable of forming hydrogen bonds. Reactions that involve charge separation in the TS therefore proceed more slowly in this class of solvents than in protic or polar aprotic solvents. The reverse is true for reactions in which species having opposite charges come together in the TS. Therefore the data have been obtained in benzene (non-polar, aprotic), acetonitrile (polar, aprotic),and water (polar, protic). It is important to note that the models used in this study assume that the solvent is a structureless dielectric continuum. Therefore, these studies will be able to capture the continuum properties of water, but will be unable to model specific solvent-solute interactions.

The effect of solvent on hydroxyl radical addition to arenes was performed using Self Consistent Reaction Field (SCRF) approaches, with the SMD solvation model (see chapter 2). This method allows ΔG of solvation to be computed by taking the difference in energies, between gas phase and SMD calculations for the system. The results for water, benzene, and acetonitrile as solvent, are summarized in Tables 4.1, 4.2, 4.3, respectively**.**

Table 4.1: Free energies for addition and reaction for hydroxyl radical addition to arenes in water (BH&HLYP/6-31G(d,p), SMD).

Functional group	ΔG_R Ortho (kcal/mol)	ΔG_R Meta (kcal/mol)	ΔG_R Para (kcal/mol)	$\Delta G^{\neq}$ Ortho (kcal/mol)	$\Delta G^{\neq}$ Meta (kcal/mol)	$\Delta G^{\neq}$ Para (kcal/mol)
-NH_2	-15.58	-12.00	-14.77	-0.52	3.35	-1.57
-OCH_3	-12.77	-12.76	-13.25	2.43	3.45	1.20
-OH	-14.56	-12.09	-13.38	2.19	3.92	1.14
-CH_3	-14.27	-13.17	-13.58	1.92	2.87	2.01
-H	-12.78	-12.78	-12.78	3.23	3.23	3.23
-Cl	-13.81	-12.83	-13.57	3.54	4.26	3.29
-F	-13.26	-12.83	-12.44	4.59	4.23	4.31
-CHO	-17.46	-11.51	-16.60	4.42	4.41	4.19
-CN	-15.14	-12.03	-15.46	4.38	4.79	4.53
-CF_3	-12.67	-12.84	-13.17	4.71	4.33	4.73
-NO_2	-16.91	-11.49	-16.00	5.76	5.45	5.49

Table 4.2: Free energies for addition and reaction for hydroxyl radical addition to arenes in acetonitrile (BH&HLYP/6-31G(d,p), SMD).

Functional group	ΔG_R Ortho (kcal/mol)	ΔG_R Meta (kcal/mol)	ΔG_R Para (kcal/mol)	$\Delta G^{\neq}$ Ortho (kcal/mol)	$\Delta G^{\neq}$ Meta (kcal/mol)	$\Delta G^{\neq}$ Para (kcal/mol)
-NH_2	-15.06	-10.86	-13.59	1.58	5.49	1.43
-OCH_3	-12.44	-11.63	-12.34	3.57	5.12	3.18
-OH	-14.11	-10.94	-12.33	4.28	5.76	3.30
-CH_3	-13.11	-12.06	-12.47	3.70	4.82	4.07
-H	-11.79	-11.79	-11.79	5.01	5.01	5.01
-Cl	-13.25	-11.84	-12.57	5.11	5.78	5.15
-F	-12.53	-11.87	-11.44	6.37	5.82	5.05
-CHO	-17.15	-10.63	-15.50	5.80	5.85	5.38
-CN	-14.12	-11.13	-14.55	5.65	6.15	5.77
-CF_3	-11.96	-11.91	-12.26	6.07	5.81	6.16
-NO_2	-16.23	-10.93	-14.84	6.94	6.51	6.37

A comparison of all the data in different solvent fields demonstrates that the activation barriers are lower in water than in benzene and acetonitrile.

$$\Delta G^{\neq}_{water} < \Delta G^{\neq}_{benzene} \sim \Delta G^{\neq}_{acetonitrile}$$

The activation barrier for addition of hydroxyl radical in presence of solvent is on average 1.9 and 1.6 kcal/mol lower in water than in acetonitrile and benzene respectively. These results are in good agreement with the experimental observations [44, 46], which show that the rates of reaction for hydroxyl radical with arenes are enhanced in water relative to acetonitrile.

Table 4.3: Free energies for addition and reaction for hydroxyl radical addition to arenes in benzene (BH&HLYP/6-31G(d,p), SMD).

Functional group	ΔG_R Ortho (kcal/mol)	ΔG_R Meta (kcal/mol)	ΔG_R Para (kcal/mol)	$\Delta G^{\neq}$ Ortho (kcal/mol)	$\Delta G^{\neq}$ Meta (kcal/mol)	$\Delta G^{\neq}$ Para (kcal/mol)
-NH_2	-15.97	-10.89	-13.24	0.60	5.26	1.86
-OCH_3	-13.56	-11.40	-12.06	2.83	4.74	3.26
-OH	-14.70	-10.48	-12.10	4.76	5.78	3.44
-CH_3	-12.87	-11.86	-12.21	3.36	4.72	4.09
-H	-11.47	-11.47	-11.47	4.87	4.87	4.87
-Cl	-13.69	-11.49	-12.32	5.31	5.69	4.98
-F	-12.85	-11.57	-11.17	6.64	5.75	4.96
-CHO	-18.07	-10.51	-15.18	5.68	5.97	5.17
-CN	-14.37	-10.80	-14.20	6.05	6.24	5.61
-CF_3	-12.55	-11.62	-11.92	6.31	5.76	5.99
-NO_2	-16.65	-10.73	-13.94	6.75	6.56	6.26

It should be noted that water in principle acts as a hydrogen bond donor and may preferentially stabilize the transition state for reaction via specific solvent-solute interactions such as hydrogen bonds, whereas the acetonitrile and benzene will not. Such specific solvent-solute interactions lie outside the scope of the SMD model.

The relative rate coefficients in each solvent may be estimated from the free energies (Table 4.4).

Table 4.4: Relative rate coefficients at 298K ($mol^{-1}dm^3s^{-1}$) for hydroxyl radical addition to arenes in various solvents.

	log(k_X/k_H)					
Functional group		***water***			***acetonitrile***	
	ortho	***meta***	***para***	***ortho***	***meta***	***para***
-NH_2	2.76	-0.09	3.53	2.52	-0.36	2.64
-OCH_3	0.59	-0.16	1.49	1.06	-0.08	1.34
-OH	0.76	-0.51	1.54	0.54	-0.55	1.26
-CH_3	-0.23	-0.76	-0.04	0.96	0.14	0.69
-H	0.00	0.00	0.00	0.00	0.00	0.00
-Cl	-0.23	-0.76	-0.04	-0.07	-0.57	-0.10
-F	-1.00	-0.74	-0.79	-1.00	-0.60	-0.03
-CHO	-0.87	-0.87	-0.71	-0.59	-0.62	-0.27
-CN	-0.85	-1.15	-0.96	-0.47	-0.84	-0.56
-CF_3	-1.09	-0.81	-1.11	-0.78	-0.59	-0.84
-NO_2	-1.86	-1.64	-1.67	-1.42	-1.10	-1.00
	benzene			***Gas phase***		
	ortho	***meta***	***para***	***ortho***	***meta***	***para***
-NH_2	3.14	-0.29	2.22	3.15	0.24	1.94
-OCH_3	1.50	0.10	1.18	2.34	0.43	1.25
-OH	0.08	-0.67	1.05	2.44	-0.12	1.05
-CH_3	1.11	0.11	0.58	0.41	-0.33	0.19
-H	0.00	0.00	0.00	0.00	0.00	0.00
-Cl	-0.33	-0.61	-0.08	-0.10	-0.53	-0.01
-F	-1.30	-0.65	-0.07	-0.78	-0.38	0.12
-CHO	-0.59	-0.81	-0.22	-0.26	-0.53	0.11
-CN	-0.87	-1.01	-0.54	-0.68	-0.84	-0.31
-CF_3	-1.06	-0.66	-0.82	-1.35	-0.99	-0.77
-NO_2	-1.39	-1.25	-1.02	-1.08	-0.84	-0.70

Plots of relative rate coefficients for reaction at the *ortho* position as a function of the ionization potential of the arenes exhibit linear dependencies, and similar behavior may be observed for reactions at the *meta* and *para* positions (Figure 4.1).

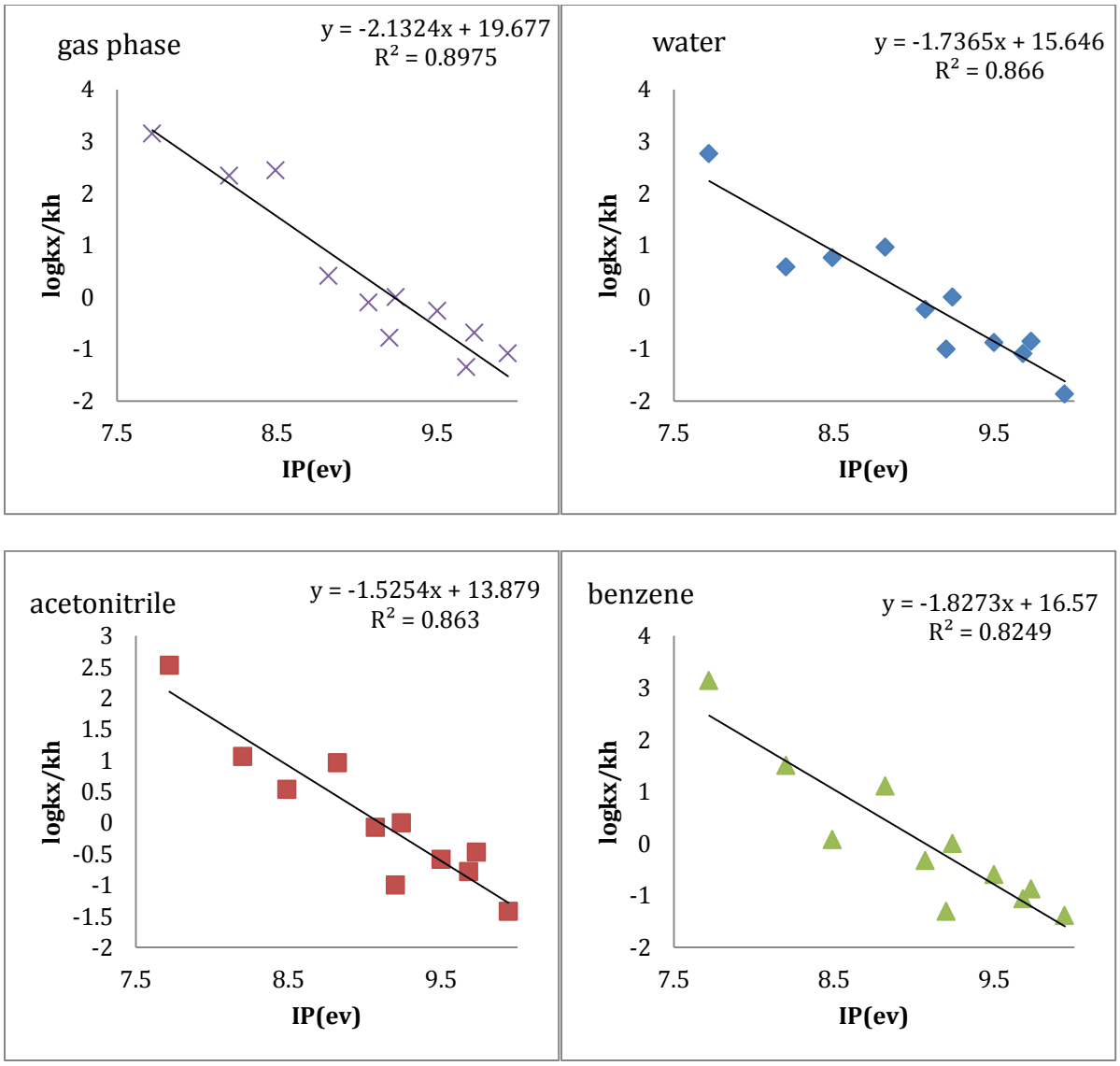

log(k_x/k_H) vs IP	Slope	R^2	INTERCEPT
Water	-1.74	0.87	15.6
Acetonitrile	-1.53	0.86	13.9
Benzene	-1.83	0.83	16.6
Gas phase	-2.13	0.90	19.7

Figure 4.1: Correlation of free energy of activation with Ionization Potential for *ortho* addition of hydroxyl radical to arenes in solvent system and gas phase.

The relationships show little variation which is remarkable when one considers that the ionization potentials (as proxies for the HOMO energies) were measured in the gas phase, and that charged species such as radical cations are far more susceptible to solvent effects than uncharged species. Ideally, a solution phase ionization potential would be determined by an electrochemical oxidation potential, and the gas phase IP is probably not an reliable reflection of the HOMO energies in solution.

Figure 4.2 shows the rate coefficients as a function of standard hammett substituent parameters obtained from chapter2. The slope of the hammett plots (Figure 4.2) have a negative value in all solvents and the gas phase, consistent with positive charge build up in the transition state, and the rates are accelerated by electron donating groups.

It is worth noting that the effect of solvent on the reactivity parameter ρ becomes more pronounced as the solvent becomes increasingly polar and capable of stabilizing a transition state which has a degree of charge separated character. Thus, rate enhancements observed in water are substantially greater than those observed in benzene.

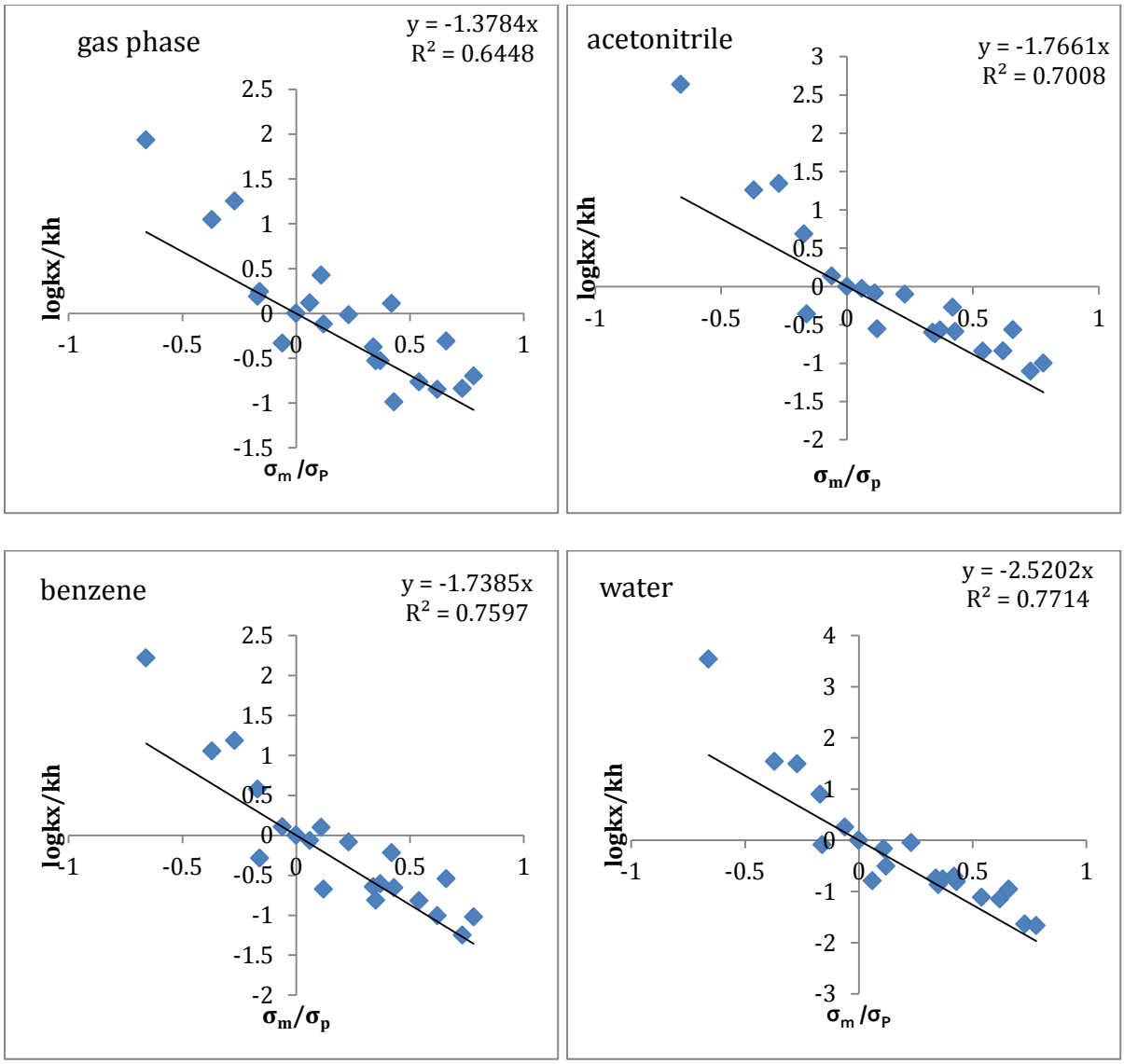

log(k_x/k_H) vs σ_m/σ_p	Slope	R^2
Water	-2.52	0.77
Benzene	-1.74	0.76
Acetonitrile	-1.77	0.70
Gas phase	-1.38	0.65

Figure 4.2: Correlation for relative rate for hydroxyl radical addition on *ortho* position to arenes with Hammett substituent parameters.

These structure-reactivity relationships for hydroxyl radical additions are entirely consistent with the fact that hydroxyl radical acts as an electrophilic species when reacting with electron rich arene rings in the gas phase, and in solution. For the addition of hydroxyl radical to the arenes, the radical stabilization effects are a contributing factor. However, polar factors are also important for these types of reactions. Polar solvents stabilize the charge separated transition state, and therefore reactions in water have lower energy transition states than those in benzene and acetonitrile.

CHAPTER 5: SIDE-CHAIN ABSTRACTIONS

As discussed in Chapter 1, there are three possible modes of reaction of hydroxyl radical to arenes: (a) addition to ring, (b) abstraction of hydrogen from side chains, and (c) abstraction of hydrogen from the ring. The kinetics of addition of hydroxyl radical to ring has been discussed in Chapters 3 and 4. Hydrogen abstraction from the side chain (Scheme 5.1), which is one of the reaction pathways that is important at high temperatures, is discussed in this chapter.

Scheme 5.1: Hydrogen Abstraction reaction from the side chain of functionalized toluenes.

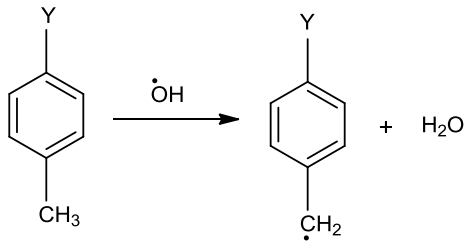

In order to verify the fact that addition pathway is the most dominant pathway, calculations were performed at the CBS-Q//BH&HLYP/6-31+G(d,p) level of theory for the hydrogen-atom abstraction reaction, which leads to the formation of benzyl radical.

Therefore, toluene compounds with a range of electron donating and withdrawing functional groups (H, NH_2, OCH_3, CHO, OH, CN, F, CF_3, NO_2), were selected for these studies.

5.1 Geometries

Geometry optimization for hydrogen abstraction from side chain was performed at both CBS-QB3 and CBS-Q//BH&HLYP/6-31+G(d,p) levels of theory. Using toluene as a model reaction to assess theoretical procedures, it was found that the optimized geometries for the benzyl radical product showed little variation between the two levels of theory employed. For example: both radicals were planar, and the C-C bond lengths between the ring and benzylic center were 1.403 Å and 1.407 Å for BH&HLYP and B3LYP optimizations respectively. However, the transition state geometries for hydrogen abstraction reactions with CBS-QB3 level of theory did not give similar geometries to those of CBS-Q//BH&HLYP/6-31+G(d,p) level of theory (Figure 5.1 and Table 5.1). For CBS-QB3 calculations, transition state structures had very low imaginary frequencies (Table 5.1(b)) as compared to CBS-Q//BH&HLYP/6-31+G(d,p) level of theory. The calculated reaction coordinate at the B3LYP/6-31G(d,p) level of theory (indicated by the atomic displacement vectors in Figure 5.1) does not correspond to that of a hydrogen abstraction reaction (typically a linear arrangement of C--H--O atoms with the hydrogen atom approximately equidistant between the two other atoms).

For the transition state at the CBS-Q//BH&HLYP/6-31+G(d,p) level of theory, vibrational frequencies and transition state geometry agree well with other studies that have been performed previously [166-175]. The CBS-Q//BH&HLYP/6-31+G(d,p) level of theory also improves the energetic and kinetic features of hydroxyl radical hydrogen abstraction reactions.

Table 5.1: Geometries of CBS-QB3/ B3LYP and CBS-Q//BH&HLYP/6-31+G(d,p) for hydrogen abstraction transition state of Toluene.

Level of theory	Geometry			Imaginary frequencies (cm^{-1})	Zero point energies (kcal/mol)	ΔH_{vib} (kcal/mol)
	R_{CH} (Å)	$R_{O\cdots H}$ (Å)	O---H---C (deg)			
CBS-QB3/B3LYP	1.109	2.793	109.8	386i	83.15	89.99
CBS-Q/BH&HLYP	1.191	1.372	174.8	1323i	88.52	93.27

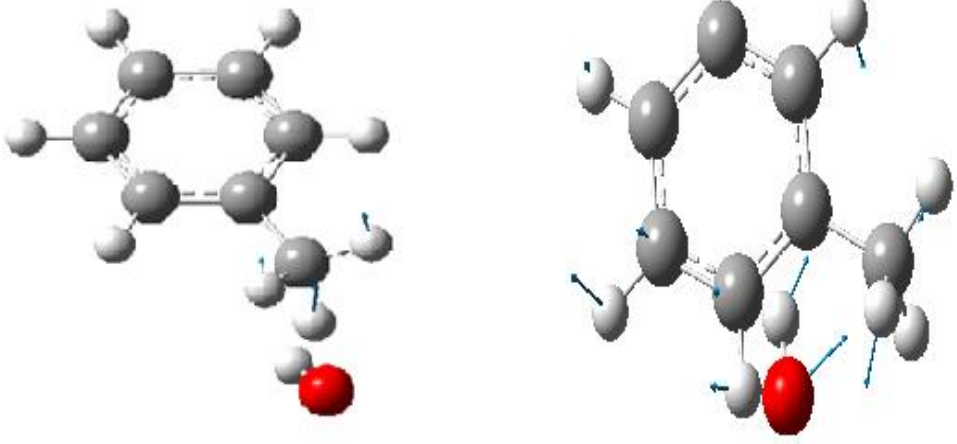

(a) (b)

Figure 5.1: (a) Optimized Transition state structure at BH&HLYP/6-31+G(d,p) for the side chain H abstraction. (b) Optimized Transition state structure at CBS-QB3 for the side chain H abstraction. Blue arrows correspond to the atomic translation vectors for the reaction coordinate.

The data indicate that transition state geometries for hydrogen abstraction from the side chain depend on the level of theory. As CBS-QB3 does not appear to provide useful geometries, the CBS-Q//BH&HLYP/6-31+G(d,p) level of theory was used for both hydroxyl addition and hydrogen abstraction from the ring for consistency and to compare the results [96]. The optimized geometrical parameters of transition state at BH&HLYP/6-31+G(d,p) are transition state are shown in Table 5.2. Transition states were confirmed by normal mode analysis to have one imaginary frequency that is the mode corresponding to the transfer of hydrogen atom to hydroxyl to form a water molecule.

Table 5.2: Geometrical parameters of transition states for hydrogen abstraction from the side chain.

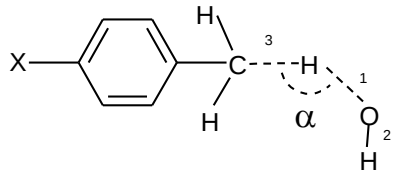

Functional group	GEOMETRY			
	$R_{O\cdots H,1}$ (Å)	$R_{OH,2}$ (Å)	$R_{C—H}$ (Å)	O---H---C (°)
-NH_2	1.390	0.963	1.184	176.2
-OCH_3	1.376	0.963	1.189	176.3
-OH	1.373	0.963	1.190	176.5
-H	1.356	0.963	1.195	176.0
-F	1.355	0.963	1.196	176.7
-CHO	1.343	0.963	1.200	177.2
-CN	1.338	0.963	1.202	177.5
-CF_3	1.339	0.963	1.202	176.9
-NO_2	1.335	0.963	1.203	176.0

The data in Table 5.2 indicate that there is no significant difference in the bond angles and bond lengths, as might be expected since the substituent at the *para* position is a significant distance from the reactive center. The calculated C-H distances in the transition states are smaller than O-H distances, which implies that the transition state is early which, according to Hammond`s postulate, resembles the reactants.

5.2 Energies

The free energies of reaction (ΔG_R) and activation ($\Delta G^{\#}$) were calculated at the CBS-QB3//BH&HLYP/6-31+G(d,p) level of theory, and are summarized in Table 5.3. It is apparent from these results that the activation barrier for the abstraction pathway has a larger free energy of activation when compared to addition reactions, particularly with respect to systems substituted by electron donating groups.

Table 5.3: Free energies of reaction and activation calculated at CBS-Q//BH&HLYP/6-31+G(d,p) level of theory for hydrogen atom abstraction.

Functional group	$\Delta G^{\neq}$ (kcal/mol	ΔG_R (kcal/mol)	$\log(k_x/k_H)$	IP (ev)
-NH_2	8.08	-26.54	0.05	7.72
-OCH_3	6.84	-26.65	0.96	8.2
-OH	8.36	-26.07	-0.15	8.49
-H	8.15	-23.63	0	8.82
-F	8.21	-23.29	-0.04	9.2
-CHO	7.89	-24.63	0.19	9.5
-CN	8.25	-24.25	-0.07	9.73
-CF_3	7.99	-25.65	0.12	9.68
-NO_2	9.13	-23.76	-0.72	9.94

Therefore it may be concluded that the addition pathway should be the dominant pathway for the reaction of hydroxyl radical with arene at 298 K. An FMO-based correlation using the vertical IP data for the substituted systems (Table 5.3) does not exhibit a reliable linear relationship (Figure 5.2). This is probably a function of two factors: firstly, the substituent is removed from the reactive center, diminishing its effect. The second factor to consider is that the IP represents promotion of an electron out of the arene π-system. Since the abstraction reaction nominally does not involve the π-system, a strong relationship cannot be anticipated.

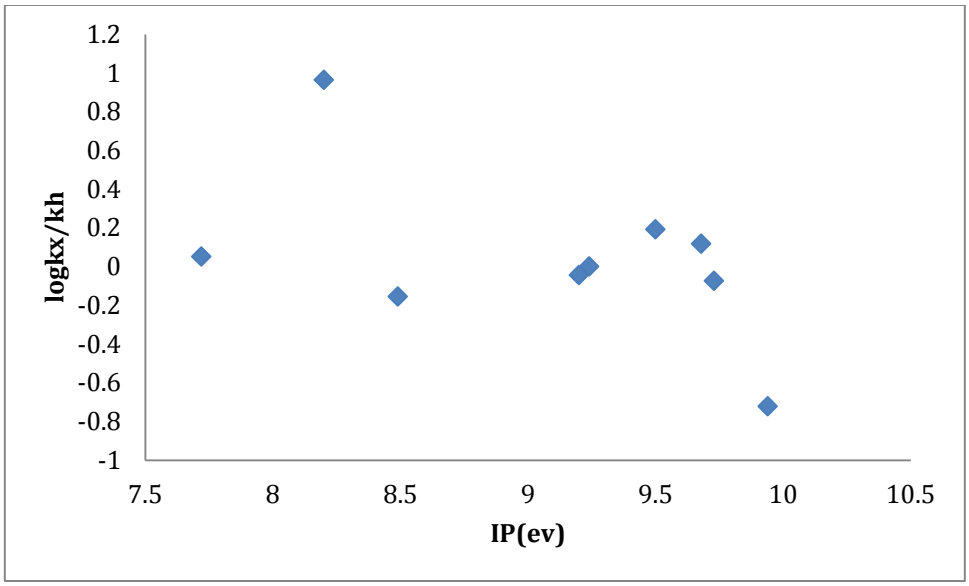

Figure 5.2: FMO-based plot for rate of abstraction of hydrogen from side chain of arenes as a function of the IP of the substituted arene.

The abstraction of hydrogen atom from side chain of arenes can also depend upon the product radical stabilization. We might not expect that polar effects play as great a role in these reactions as they do in addition reactions. The effect of substituents on the stability of free radicals is important in understanding the nature of reactions involving radicals as reactants, products or intermediates. Once again, this may be studied by considering an appropriate isodesmic reaction, such as the one shown in Scheme 5.2.

Scheme 5.2: Isodesmic reaction scheme for radical stabilization energies for hydrogen abstraction.

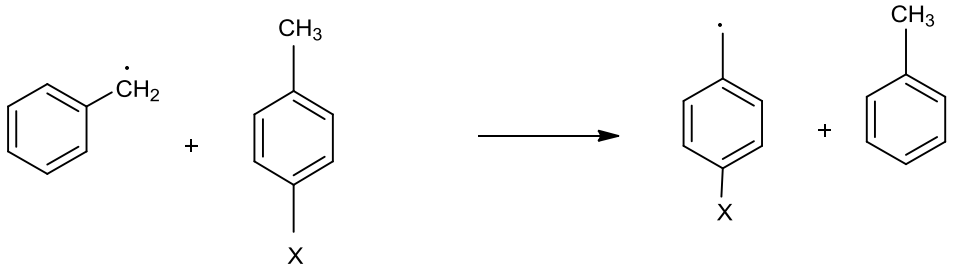

Table 5.4: Free energy of activation and calculated radical stabilization energies, and hammett substituent constants for hydrogen atom abstraction.

Functional group	$\Delta G^{\neq}$ (kcal/mol)	$\log(k_x/k_H)$	RSE (0K, kcal/mol)	σ_p	$\sigma\bullet$	$\sigma+$
$-NH_2$	8.08	0.05	1.06	-0.66	0.7	-1.3
$-OCH_3$	6.84	0.96	0.31	-0.27	0.27	-0.78
-OH	8.36	-0.15	0.28	-0.37	0.26	-0.92
-H	8.15	0	-0.07	0	0	0
-F	8.21	-0.04	-0.46	0.06	-0.06	-0.06
-CHO	7.89	0.19	0.74	0.42	0.64	0.73
-CN	8.25	-0.07	0.19	0.66	0.47	0.66
$-CF_3$	7.99	0.12	-0.76	0.54	0.05	0.61
$-NO_2$	9.13	-0.72	-0.30	0.78	0.57	0.79

The free energy of activation shows little dependence on the computed radical stabilization energies (Figure 5.3), the only functional groups exhibiting significant

variation being $–NO_2$ and $–OCH_3$. The reasons for this are unclear, but once again the relatively little impact of p-substituents may arise from their distance from the reactive center, and the fact that if the transition state for the reaction is early, there may be insufficient orbital overlap between the aromatic π-system, and the breaking C-H σ-bond for resonance stabilization from the para substituent to be significant.

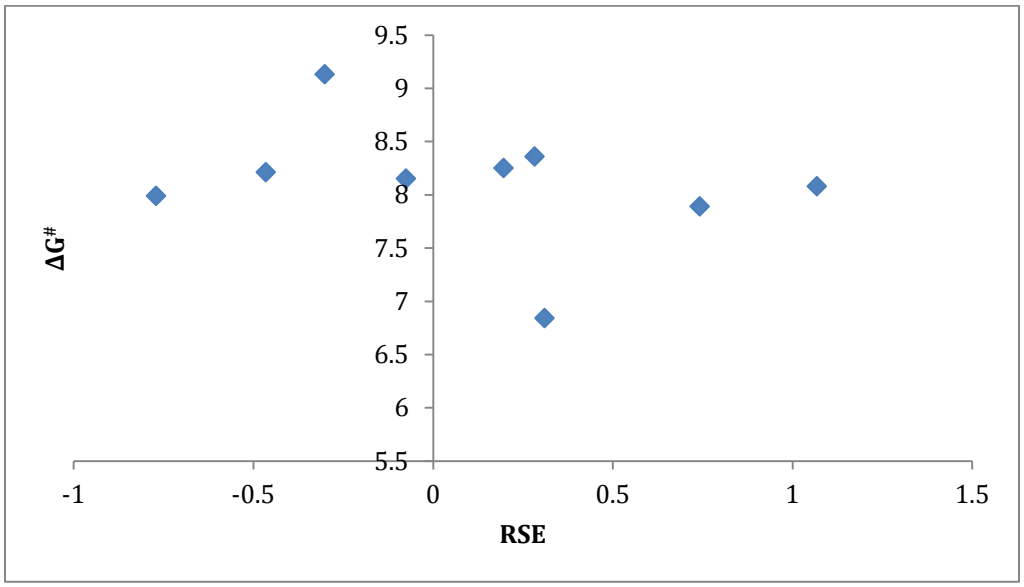

Figure 5.3: Radical stabilization correlations for abstraction of hydrogen atom from side chain of arenes.

Hammett correlations for *p*-substituted toluenes similarly show weak dependencies. Although it is difficult to draw definitive conclusions, the fact that linear regression analysis yields a negative gradient *may* indicate a buildup of positive charge at the benzylic carbon in the abstraction transition state (Figure 5.4). If so, the transition state is stabilized by electron donating groups, and is consistent with the notion that the hydroxyl radical behaves as an electrophilic species and that may also be some degree of charge separation in the abstraction transition state.

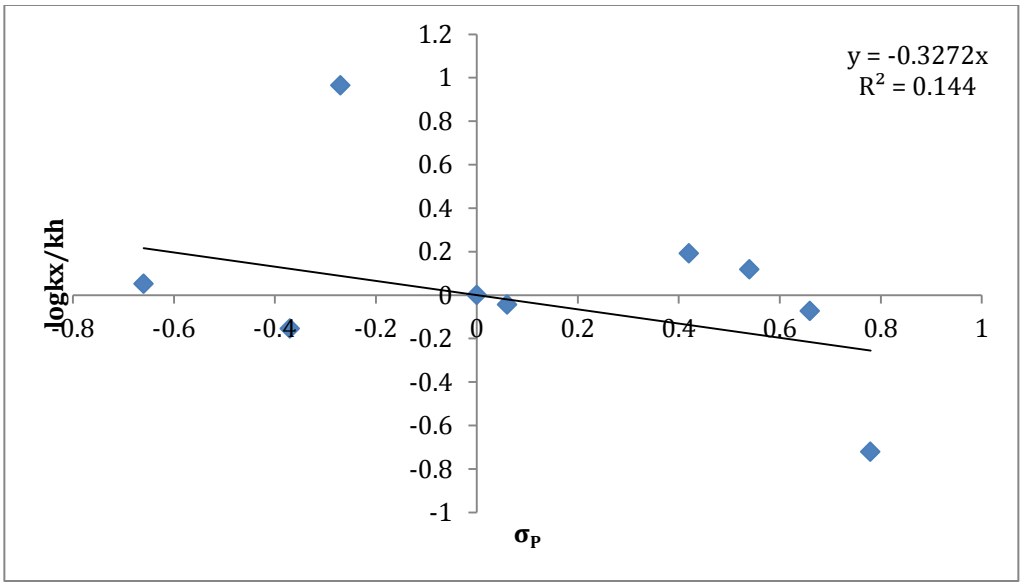

Figure 5.4: Plot of Hammett correlations for abstraction of hydrogen atom from side chain of arenes.

Since the product of the reaction is a benzylic radical, one might expect that if radical stabilization terms dominate, a strong correlation with Creary's σ• substituent constant (Table 5.4) would be apparent, particularly as this substituent scale is defined by a reaction that generates benzylic radicals. In fact, the correlation (Figure 5.5) shows limited dependence on radical stabilization, suggesting that radical stabilization may not the only factor that governs hydrogen abstraction from the side chain. Note also the similarity in correlation curves for σ• and RSE (Figures 5.3 and 5.5 respectively). If however, polar effects are more dominant, we might expect to see a stronger correlation for the electrophilic addition derived substituent parameter σ+ (Figure 5.6). This is not observed, although it is worth pointing out that *p*-substitution may not necessarily provide a particularly sensitive model, given its distance from the reactive site.

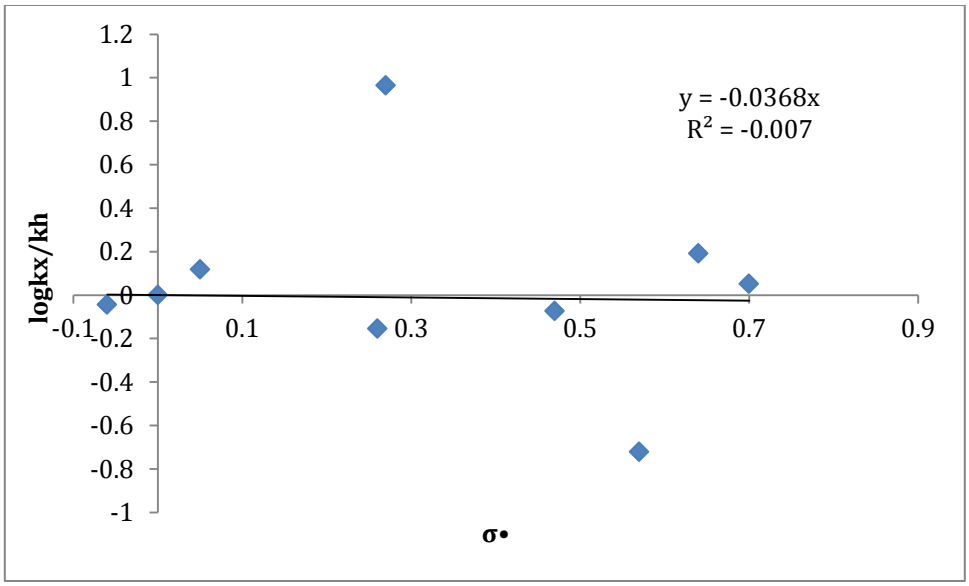

Figure 5.5: Correlations of relative rate constant with radical substituent parameters for hydrogen atom abstraction from substituted arenes.

The side chain abstraction occurs through a complex mechanism, but it can be seen from the above discussed observations that the abstraction is not the dominant pathway. The addition pathway is the most dominant pathway at 298K as compared to the hydrogen abstraction from the side chain.

CHAPTER 6-CONCLUSIONS, BROADER IMPACTS AND FUTURE WORKS

6.1 Conclusions

It has been discussed in previous chapters that computational methods with different levels of theory have been used to determine the selectivity and reactivity of addition of hydroxyl radical to arenes, and hydrogen abstraction from side chains. Hydroxyl radical reactions are not 'clean' reactions, so to understand the reactivity and selectivity an important aspect of this study was to examine the reactions without interference from any side reactions.

This study allows us to draw the following conclusions:

(a) Rate coefficients for addition to arenes substituted with electron donating groups are higher than those substituted with electron withdrawing groups. The electron donating groups activate the ring yielding faster reactions whereas electron withdrawing groups will deactivate the ring yielding slower reactions.

(b) Rate coefficients and reaction profiles show that both electron donating and electron withdrawing groups were primarily *ortho* or *para* directors. With strongly electron withdrawing groups, *ortho* addition becomes increasingly disfavored, whereas addition to the *meta* position becomes increasingly favored.

(c) The structures of transition state for both addition and abstraction state resembles the structures of the reactants, rather than the products. The transition state may be considered “early”. Hydroxyl radical reactions in gas phase do not exhibit dependencies on the radical stabilization of the products.

(d) Frontier molecular orbital theory shows that the SOMO of hydroxyl radical reacts faster with molecules which have a higher energy HOMO, and confirms the electrophilic nature of hydroxyl radical. Observed relationships between relative rate coefficients and arene ionization potentials are consistent with charge separation in transition state, which will be subject to the influence of polar effects on the rate of reaction.

(e) The reactivity data for different reaction paths exhibits correlations with Hammett substituent parameters. Hammett plots show a negative correlation, which indicates a buildup of positive charge on the ring in the transition state. The negative trend is typical for electrophilic substitution reactions and further supports the hypothesis that the hydroxyl radical behaves as an electrophilic species.

(f) Polarizable continuum models for solvent effects helps to compare the results for the different solvents. The reactivity of hydroxyl radical is enhanced in water compared to benzene and acetonitrile.

(g) Hammett correlations in various solvents indicate that the polar effects that control reaction become more pronounced in polar solvents. Hammett plots in various solvents also support the fact that hydroxyl radical behaves as electrophile.

(h) Hydrogen abstraction reactions have higher activation barriers when compared to addition reactions, particularly for systems substituted with electron donating groups. Therefore abstraction products are not the major products compared to the addition products of hydroxyl radical at 298K.

6.2 Future work

Expansion of these studies with more complex arene rings: Seventy percent of the pollutants found in environment are aromatic and most of them are having fused or heterocyclic rings (e.g., phenothiazines) [1]. Reaction of hydroxyl radical with these rings is the first step for degradation of these pollutants as discussed in chapter 1. A number of theoretical studies were carried out to understand the reactions of hydroxyl radical reactions but it can be improved with supplementary information. The fused and heterocyclic rings, theoretical studies in both gas phase and solvent phase at same levels of theory would benefit to better understand the reactivity and selectivity of the hydroxyl radical in environment.

Abstraction from side chains: In this present study the abstraction from the side chain (i.e. methyl group at *para* position) is studied which is not a good model as seen in chapter 5. The abstraction of hydrogen from side chain, if methyl group is at *ortho* and *meta* position from the functional group can help to confirm the findings in present study. The abstraction from side chains other than methyl group, for example esters, hydroxyl, ethyl and propyl can be studied to better understand the hydrogen

abstraction process. Hydrogen abstraction can be performed in both gas phase and solvent systems to compare and confirm some of the findings in present study.

***NPO studies*:** Natural population analysis (NPO) has been developed to calculate atomic charges and orbital populations of molecular wave functions. NPO can be used to better describe the electron distribution in compounds. The analysis allows one to observe the change in spin density of pre-reactive complex going to transition state, which shows that either it is behaving like anion or cation, and what changes it make to the activation energy.

6.3 Broader impacts

Hydroxyl radicals are one of the most powerful oxidizing agents able to react with surrounding organic pollutants in the environment. The hydroxyl radicals are pervasive in the environment (natural waters, atmosphere, etc.), including biological systems where hydroxyl radical has an important role in immunity metabolism. The scope of present study was to understand the fundamental chemistry of the reaction of hydroxyl radical with arene (environmental pollutant) in environment. This will help to understand and model processes of environmental importance.

The present study shows that hydroxyl radicals are going to react faster with arene with electron donating groups as compared to electron withdrawing groups. This study also shows that the reactions are going to be faster in water as compared to acetonitrile, benzene and gas phase.

Hydroxyl radicals play an important role in the oxidation of various organic and inorganic compounds in gas phase and aqueous systems. The interaction of hydroxyl

radical with aqueous surfaces is particularly important for atmospheric chemistry, as many reactions of hydroxyl radical occur in or on aqueous surfaces.

Industries, transportation and biogenic emissions contain volatile organic carbons and benzene is one of them. Reactivity and selectivity of these compounds can help us to know the methods of the degradation of these pollutants. Various pesticides have different functional groups on the ring and can have different reactivity and selectivity depending upon the functional groups. The present study depicts that the pesticides which have electron donating group attached to the ring will react faster as compared to the pesticide with electron withdrawing group attached to the ring. Reactivity of benzene and toluene can also help to study the gas spills.

The model described would be theoretically useful in modeling the degradation of aromatic pollutants in environment. Incorporation of “real-world” problems, such as gas leakage, water purification, and dense clouds would assist in modelling the role of hydroxyl radicals in the environment.

APPENDIX I – ASYMMETRIC WAVEFUNCTIONS

Molecular orbital theory decomposes ψ into combination of molecular orbitals: ψ_1, ψ_2,……The simplest possible way of making ψ as a combination of these molecular orbitals is by forming their hartree product:

$$\psi(r) =: \psi_1,(r_1)\ \psi_2(r_2)\ldots\ldots\ \psi_n(r_n) \qquad \text{(Eq.A1)}$$

However, such a function is not antisymmetric, since interchanging two of r_i`s:equivalent to swapping the orbitals of two electrons, does not result in sign change. Hence, this hartree product is an inadequate wavefunction.

The simplest antisymmetric function that is a combination of molecular orbitals is a determinant. Before forming it, electron spin should be considered. Electrons can spin up (+1/2) or down (-1/2). Equation A1 assumes that each molecular orbital holds only one electron. However, most calculations are closed shell calculations, using doubly occupied orbitals, holding two electrons of opposite spin. Two spin functions can be defined as follows:

$$\alpha(\uparrow)=1 \quad \alpha(\downarrow)=0$$

$$\beta(\uparrow)=0 \quad \beta(\downarrow)=1 \qquad \text{(Eq.A2)}$$

The α function is 1 for sign up electron, and the β function is 1 when the electron is spin

down. The notation α(i) and β(i) designate the values of a and b for electron i; thus,$\alpha(1)$ is the value of α for the electron1.

Multiplying a molecular orbital function by α or β will include electron spin as the part of the overall electronic wavefunction ψ.

We can now build a closed shell wavefunction by defining n/2 molecular orbitals for a system with n electrons and then assigning electrons to these orbitals in pair of opposite spins

$$\psi = \frac{1}{\sqrt{n!}} \begin{vmatrix} \psi_1(r_1)\alpha(1) & \psi_1(r_1)\beta(1) & \psi_2(r_1)\alpha(1) & \psi_2(r_1)\beta(1) & \cdots & \psi_{\frac{n}{2}}(r_1)\beta(1) \\ \psi_1(r_2)\alpha(2) & \psi_1(r_2)\beta(2) & \psi_2(r_2)\alpha(2) & \psi_2(r_2)\beta(2) & \cdots & \psi_{\frac{n}{2}}(r_2)\beta(2) \\ \psi_1(r_3)\alpha(3) & \psi_1(r_3)\beta(3) & \psi_2(r_3)\alpha(3) & \psi_2(r_3)\beta(3) & \cdots & \psi_{\frac{n}{2}}(r_3)\beta(3) \\ \vdots & \vdots & \vdots & \vdots & \cdots & \vdots \\ \psi_1(r_n)\alpha(\mathrm{n}) & \psi_1(r_n)\beta(\mathrm{n}) & \psi_2(r_n)\alpha(\mathrm{n}) & \psi_2(r_n)\beta(\mathrm{n}) & \cdots & \psi_{\frac{n}{2}}(r_n)\beta(\mathrm{n}) \end{vmatrix} \quad (\mathrm{Eq.A3})$$

Each row is formed by representing all possible assignments of electron i to all orbital-spin combinations. The initial factor is necessary for normalization. Swapping two electrons corresponds to interchanging two rows of the determinant, which will have the effect of changing its sign.

APPENDIX II- Approximations for the exchange-correlation functionals of Density Functional Methods

The major problem with density functional theory is that the exact functionals for exchange and correlation are not known except for free electron gas. However, approximations exist which permit the calculation of certain physical quantities quite accurately. The most widely used approximations are as following:

- Local spin density approximation (LDA),
- Generalized gradient approximation (GGA) or
- Hybrid functional.

Local spin density approximation: it assumes that the charge density varies slowly so each small volume looks like a uniform electron gas. Exc[ρ], the so called exchange-correlation energy can be obtained by integrating uniform electron gas results:

$$E^{XC,LDA}(\rho) = \int \rho(r)\, V_{XC}\big[\big(\rho(r)\big)\big] d^3r \qquad (\mathrm{Eq.\,A4})$$

where, exchane-correlation potential v_{XC} is defined as the function derivative of E_{XC} with respect to p, i.e $v_{XC} = \delta E_{XC}/\delta\rho$.

Generalized gradient approximation: First step to go beyond LDA is the use of not only the information about the density at particular point (r), but to supplement density with information about the gradient of the charge density (∇) in order to account for the non-homogeneity of the true electron density. Thus, exchange-correlation energy can we written in following term:

$$E^{XC,GGA}(\rho) = \int \rho(r)\, V_{XC}[(\rho(r)\nabla)]d^3r \qquad (\text{Eq. A5})$$

Pure DFT methods are defined by pairing and exchange functional with a correlation functional. For example, BLYP functional pairs Becke`s gradient-corrected exchange functional with the gradient-corrected correlation functional of Lee, Yang and Parr.

Hybrid functional: It is combination of orbital-dependent HF and an explicit density functional (LDA/GGA).

$$E^{XC}_{hybrid} = c_{HF}E^{X}_{HF} + c_{DFT}E^{XC}_{DFT} \qquad (\text{Eq. A6})$$

where C`s are constants. For example, a becke style three parameter functional may be defined via following expression:

$$E^{XC}_{B3LYP} = E^{X}_{LDA} + c_o(E^{XC}_{HF} - E^{X}_{LDA}) + c_X\Delta E^{X}_{B88} + E^{C}_{VWN3} + c_C(E^{C}_{LYP} - E^{C}_{VWN3}) \qquad (\text{Eq.A7})$$

Here the parameter c_o allows mixture of Hartree-Fock and LDA local exchange to be used, C_x is Becke`s gradient correction to LDA exchange, VWN3 local correlation functional and it may be optionally corrected by the LYP correlation correction via parameter c_C.

Different functional can be constructed in the same way by varying the component functional for example by substituting the Perdew-Wang 1991 gradient-corrected correlation functional for LYP- and by adjusting the values of the three parameters.

BIBLIOGRAPHY

1. Atkinson, R. and J. Arey, *Atmospheric Degradation of Volatile Organic Compounds.* Chemical Reviews, 2003. **103**(12): p. 4605-4638.
2. Boggs, S., D. Livermore, and M.G. Seitz, *Humic substances in natural waters and their complexation with trace metals and radionuclides: A review*. 1985: Argonne National Laboratory.
3. Song, Y., M. Shao, Y. Liu, S. Lu, W. Kuster, P. Goldan, and S. Xie, *Source Apportionment of Ambient Volatile Organic Compounds in Beijing.* Environmental Science & Technology, 2007. **41**(12): p. 4348-4353.
4. Hites, R.A., G.A. Jungclaus, V. Lopez-Avila, and L.S. Sheldon, *Potentially Toxic Organic Compounds in Industrial Wastewaters and River Systems: Two Case Studies*, in *Monitoring Toxic Substances*. 1979, AMERICAN CHEMICAL SOCIETY. p. 63-90.
5. Böhnhardt, A., R. Kühne, R.-U. Ebert, and G. Schüürmann, *Indirect Photolysis of Organic Compounds: Prediction of OH Reaction Rate Constants through Molecular Orbital Calculations.* The Journal of Physical Chemistry A, 2008. **112**(45): p. 11391-11399.
6. Fayet, G., L. Joubert, P. Rotureau, and C. Adamo, *Theoretical Study of the Decomposition Reactions in Substituted Nitrobenzenes.* The Journal of Physical Chemistry A, 2008. **112**(17): p. 4054-4059.
7. Phousongphouang, P.T. and J. Arey, *Rate Constants for the Gas-Phase Reactions of a Series of Alkylnaphthalenes with the OH Radical.* Environmental Science & Technology, 2002. **36**(9): p. 1947-1952.
8. Washenfelder, R.A., N.L. Wagner, W.P. Dube, and S.S. Brown, *Measurement of Atmospheric Ozone by Cavity Ring-down Spectroscopy.* Environmental Science & Technology, 2011. **45**(7): p. 2938-2944.
9. Ferrer-Sueta, G. and R. Radi, *Chemical Biology of Peroxynitrite: Kinetics, Diffusion, and Radicals.* ACS Chemical Biology, 2009. **4**(3): p. 161-177.
10. Lobo, V., A. Patil, A. Phatak, and N. Chandra, *Free radicals, antioxidants and functional foods: Impact on human health.* Pharmacognosy Reviews, 2010. **4**(8): p. 118-126.
11. Blough, N.V. and R.G. Zepp, *Reactive Oxygen Species in Natural Waters*, in *Active Oxygen in Chemistry*, C.S. Foote, et al., Editors. 1995, Springer Netherlands: Dordrecht. p. 280-333.
12. Dormandy, T.L., *Free-radical reaction in biological systems.* Annals of The Royal College of Surgeons of England, 1980. **62**(3): p. 188-194.
13. Hernandez-Marin, E. and A. Martínez, *Carbohydrates and Their Free Radical Scavenging Capability: A Theoretical Study.* The Journal of Physical Chemistry B, 2012. **116**(32): p. 9668-9675.
14. Mezyk, S.P., T.J. Neubauer, W.J. Cooper, and J.R. Peller, *Free-Radical-Induced Oxidative and Reductive Degradation of Sulfa Drugs in Water: Absolute Kinetics and Efficiencies of Hydroxyl Radical and Hydrated Electron Reactions.* The Journal of Physical Chemistry A, 2007. **111**(37): p. 9019-9024.

15. Chen, Y. and E. Tschuikow-Roux, *Mechanism of hydrogen abstraction reactions by free radicals: simple metathesis or involving intermediate complex?* The Journal of Physical Chemistry, 1993. **97**(15): p. 3742-3749.
16. Buxton, G.V., C.L. Greenstock, W.P. Helman, and A.B. Ross, *Critical Review of rate constants for reactions of hydrated electrons, hydrogen atoms and hydroxyl radicals (□OH/□O− in Aqueous Solution.* Journal of Physical and Chemical Reference Data, 1988. **17**(2): p. 513-886.
17. Zavitsas, A.A. and A.A. Melikian, *Hydrogen abstractions by free radicals. Factors controlling reactivity.* Journal of the American Chemical Society, 1975. **97**(10): p. 2757-2763.
18. Wu, P., J. Li, S. Li, and F.-M. Tao, *Theoretical study of mechanism and kinetics for the addition of hydroxyl radical to phenol.* Science China Chemistry, 2011. **55**(2): p. 270-276.
19. Shiroudi, A., M.S. Deleuze, and S. Canneaux, *Theoretical study of the oxidation mechanisms of naphthalene initiated by hydroxyl radicals: the O2 addition reaction pathways.* Physical Chemistry Chemical Physics, 2015. **17**(20): p. 13719-13732.
20. Tripathi, G.N.R., *Electron-Transfer Component in Hydroxyl Radical Reactions Observed by Time Resolved Resonance Raman Spectroscopy.* Journal of the American Chemical Society, 1998. **120**(17): p. 4161-4166.
21. Koppenol, W.H. and J.F. Liebman, *The oxidizing nature of the hydroxyl radical. A comparison with the ferryl ion (FeO2+).* The Journal of Physical Chemistry, 1984. **88**(1): p. 99-101.
22. Schwarz, H.A. and R.W. Dodson, *Equilibrium between hydroxyl radicals and thallium(II) and the oxidation potential of hydroxyl(aq).* The Journal of Physical Chemistry, 1984. **88**(16): p. 3643-3647.
23. Klaning, U.K., K. Sehested, and J. Holcman, *Standard Gibbs energy of formation of the hydroxyl radical in aqueous solution. Rate constants for the reaction chlorite (ClO2-) + ozone .dblarw. ozone(1-) + chlorine dioxide.* The Journal of Physical Chemistry, 1985. **89**(5): p. 760-763.
24. Gligorovski, S., R. Strekowski, S. Barbati, and D. Vione, *Environmental Implications of Hydroxyl Radicals (•OH).* Chemical Reviews, 2015. **115**(24): p. 13051-13092.
25. Tully, F.P., *Laser photolysis/laser-induced fluorescence study of the reaction of hydroxyl radical with ethylene.* Chemical Physics Letters, 1983. **96**(2): p. 148-153.
26. Meier, U., H.H. Grotheer, G. Riekert, and T. Just, *Study of Hydroxyl Reactions with Methanol and Ethanol by Laser-induced Fluorescence.* Berichte der Bunsengesellschaft für physikalische Chemie, 1985. **89**(3): p. 325-327.
27. Jiang, Z., P.H. Taylor, and B. Dellinger, *Laser photolysis/laser-induced fluorescence studies of the reaction of hydroxyl with 1,1-dichloroethane over an extended temperature range.* The Journal of Physical Chemistry, 1992. **96**(22): p. 8964-8966.
28. Kasner, J.H., P.H. Taylor, and B. Dellinger, *Laser photolysis/laser induced fluorescence study of hydroxyl-chloroethane rate constants from 294 to 789 K.* The Journal of Physical Chemistry, 1990. **94**(8): p. 3250-3253.
29. Taylor, P.H., Z. Jiang, and B. Dellinger, *Determination of the gas-phase reactivity of hydroxyl with chlorinated methanes at high temperature: Effects of laser/thermal photochemistry.* International Journal of Chemical Kinetics, 1993. **25**(1): p. 9-23.

30. Ishiwata, T., I. Fujiwara, Y. Naruge, K. Obi, and I. Tanaka, *Study of nitrate radical by laser-induced fluorescence.* The Journal of Physical Chemistry, 1983. **87**(8): p. 1349-1352.
31. Martinez, E., B. Cabañas, A. Aranda, P. Martin, and S. Salgado, *A temperature dependence study of the gas-phase reaction of the nitrate radical with 3-fluoropropene followed by laser induced fluorescence detection.* International Journal of Chemical Kinetics, 1997. **29**(12): p. 927-932.
32. Bogan, D.J., M. Kaufman, C.W. Hand, W.A. Sanders, and B.E. Brauer, *Laser-induced fluorescence study of methoxy radical formation from the reactions of fluorine(2P) atoms with methanol (CH3OH, CD3OH, and CH3OD).* The Journal of Physical Chemistry, 1990. **94**(21): p. 8128-8134.
33. Inoue, G., H. Akimoto, and M. Okuda, *Laser-induced fluorescence spectra of CH3O.* Chemical Physics Letters, 1979. **63**(2): p. 213-216.
34. Carter, C.C., S. Gopalakrishnan, J.R. Atwell, and T.A. Miller, *Laser Excitation Spectra of Large Alkoxy Radicals Containing 5–12 Carbon Atoms.* The Journal of Physical Chemistry A, 2001. **105**(13): p. 2925-2928.
35. Liu, J. and T.A. Miller, *Jet-Cooled Laser-Induced Fluorescence Spectroscopy of Cyclohexoxy: Rotational and Fine Structure of Molecules in Nearly Degenerate Electronic States.* The Journal of Physical Chemistry A, 2014. **118**(51): p. 11871-11890.
36. Stakhursky, V.L., L. Zu, J. Liu, and T.A. Miller, *High resolution spectra and conformational analysis of 2-butoxy radical.* The Journal of Chemical Physics, 2006. **125**(9): p. 094316.
37. Gopalakrishnan, S., C.C. Carter, L. Zu, V. Stakhursky, G. Tarczay, and T.A. Miller, *Rotationally resolved $\tilde{B}$–$\tilde{X}$ electronic spectra of both conformers of the 1-propoxy radical.* The Journal of Chemical Physics, 2003. **118**(11): p. 4954-4969.
38. Jin, J., I. Sioutis, G. Tarczay, S. Gopalakrishnan, A. Bezant, and T.A. Miller, *Dispersed fluorescence spectroscopy of primary and secondary alkoxy radicals.* The Journal of Chemical Physics, 2004. **121**(23): p. 11780-11797.
39. Heard, D.E., *ATMOSPHERIC FIELD MEASUREMENTS OF THE HYDROXYL RADICAL USING LASER-INDUCED FLUORESCENCE SPECTROSCOPY.* Annual Review of Physical Chemistry, 2006. **57**(1): p. 191-216.
40. Zellner, R., *B. Finlayson-Pitts, J. N. Pitts, Jr.: Atmospheric Chemistry: Fundamentals and Experimental Techniques, J. Wiley and Sons, New York, Chichester, Brisbane, Toronto and Singapore 1986. 1098 Seiten, Preis: £ 57.45.* Berichte der Bunsengesellschaft für physikalische Chemie, 1986. **90**(12): p. 1244-1244.
41. Sengupta, S., Y. Indulkar, A. Kumar, S. Dhanya, P.D. Naik, and P.N. Bajaj, *Kinetic study of the gas-phase reaction of hydroxyl radical with CF3CH2OCH2CF3 using the laser photolysis–laser induced fluorescence method.* International Journal of Chemical Kinetics, 2010. **42**(8): p. 519-525.
42. Tully, F.P., A.R. Ravishankara, R.L. Thompson, J.M. Nicovich, R.C. Shah, N.M. Kreutter, and P.H. Wine, *Kinetics of the reactions of hydroxyl radical with benzene and toluene.* The Journal of Physical Chemistry, 1981. **85**(15): p. 2262-2269.
43. Seta, T., M. Nakajima, and A. Miyoshi, *High-Temperature Reactions of OH Radicals with Benzene and Toluene.* The Journal of Physical Chemistry A, 2006. **110**(15): p. 5081-5090.

44. Poole, J.S., X. Shi, C.M. Hadad, and M.S. Platz, *Reaction of Hydroxyl Radical with Aromatic Hydrocarbons in Nonaqueous Solutions: A Laser Flash Photolysis Study in Acetonitrile.* The Journal of Physical Chemistry A, 2005. **109**(11): p. 2547-2551.
45. Martin, C.B., X. Shi, M.-L. Tsao, D. Karweik, J. Brooke, C.M. Hadad, and M.S. Platz, *The Photochemistry of Riboflavin Tetraacetate and Nucleosides. A Study Using Density Functional Theory, Laser Flash Photolysis, Fluorescence, UV−Vis, and Time Resolved Infrared Spectroscopy.* The Journal of Physical Chemistry B, 2002. **106**(39): p. 10263-10271.
46. DeMatteo, M.P., J.S. Poole, X. Shi, R. Sachdeva, P.G. Hatcher, C.M. Hadad, and M.S. Platz, *On the Electrophilicity of Hydroxyl Radical: A Laser Flash Photolysis and Computational Study.* Journal of the American Chemical Society, 2005. **127**(19): p. 7094-7109.
47. Gozzi, F., S.C. Oliveira, R.F. Dantas, V.O. Silva, F.H. Quina, and A. Machulek, *Kinetic studies of the reaction between pesticides and hydroxyl radical generated by laser flash photolysis.* Journal of the Science of Food and Agriculture, 2016. **96**(5): p. 1580-1584.
48. Greenstock, C.L., J.W. Hunt, and M. Ng, *Pulse radiolysis studies of uracil and its derivatives. Primary species attack.* Transactions of the Faraday Society, 1969. **65**(0): p. 3279-3287.
49. Nicolaescu, A.R., O. Wiest, and P.V. Kamat, *Mechanistic Pathways of the Hydroxyl Radical Reactions of Quinoline. 1. Identification, Distribution, and Yields of Hydroxylated Products.* The Journal of Physical Chemistry A, 2005. **109**(12): p. 2822-2828.
50. Nicolaescu, A.R., O. Wiest, and P.V. Kamat, *Mechanistic Pathways of the Hydroxyl Radical Reactions of Quinoline. 2. Computational Analysis of Hydroxyl Radical Attack at C Atoms.* The Journal of Physical Chemistry A, 2005. **109**(12): p. 2829-2835.
51. Truscott, T.G., *Pulse Radiolysis*, in *Photosensitisation: Molecular, Cellular and Medical Aspects*, G. Moreno, R.H. Pottier, and T.G. Truscott, Editors. 1988, Springer Berlin Heidelberg: Berlin, Heidelberg. p. 39-51.
52. Mezyk, S.P., D.B. Ewing, J.J. Kiddle, and K.P. Madden, *Kinetics and Mechanisms of the Reactions of Hydroxyl Radicals and Hydrated Electrons with Nitrosamines and Nitramines in Water.* The Journal of Physical Chemistry A, 2006. **110**(14): p. 4732-4737.
53. Wander, R., P. Neta, and L.M. Dorfman, *Pulse radiolysis studies. XII. Kinetics and spectra of the cyclohexadienyl radicals in aqueous benzoic acid solution.* The Journal of Physical Chemistry, 1968. **72**(8): p. 2946-2949.
54. Ma, J., U. Schmidhammer, and M. Mostafavi, *Picosecond Pulse Radiolysis of Highly Concentrated Sulfuric Acid Solutions: Evidence for the Oxidation Reactivity of Radical Cation H2O•+.* The Journal of Physical Chemistry A, 2014. **118**(23): p. 4030-4037.
55. Baseggio Conrado, A., M. D'Angelantonio, A. Torreggiani, L. Pecci, and M. Fontana, *Reactivity of hypotaurine and cysteine sulfinic acid toward carbonate radical anion and nitrogen dioxide as explored by the peroxidase activity of Cu,Zn superoxide dismutase and by pulse radiolysis.* Free Radical Research, 2014. **48**(11): p. 1300-1310.

56. Scaiano, J.C., *Nanosecond Laser Flash Photolysis: A Tool for Physical Organic Chemistry*, in *Reactive Intermediate Chemistry*. 2005, John Wiley & Sons, Inc. p. 847-871.
57. Milosavljevic, B.H. and J.A. LaVerne, *Pulse Radiolysis of Aqueous Thiocyanate Solution.* The Journal of Physical Chemistry A, 2005. **109**(1): p. 165-168.
58. Liu, A., W.A. Mulac, and C.D. Jonah, *Kinetic isotope effects in the gas-phase reaction of hydroxyl radicals with ethylene in the temperature range 343-1173 K and 1-atm pressure.* The Journal of Physical Chemistry, 1988. **92**(13): p. 3828-3833.
59. Coeur-Tourneur, C., F. Henry, M.-A. Janquin, and L. Brutier, *Gas-phase reaction of hydroxyl radicals with m-, o- and p-cresol.* International Journal of Chemical Kinetics, 2006. **38**(9): p. 553-562.
60. Wang, X., T. Liu, F. Bernard, X. Ding, S. Wen, Y. Zhang, Z. Zhang, Q. He, S. Lü, J. Chen, S. Saunders, and J. Yu, *Design and characterization of a smog chamber for studying gas-phase chemical mechanisms and aerosol formation.* Atmos. Meas. Tech., 2014. **7**(1): p. 301-313.
61. Huang, M., C. Hu, X. Guo, X. Gu, W. Zhao, Z. Wang, L. Fang, and W. Zhang, *Chemical composition of gas and particle–phase products of OH–initiated oxidation of 1,3,5–trimethylbenzene.* Atmospheric Pollution Research, 2014. **5**(1): p. 73-78.
62. Feilberg, A. and T. Nielsen, *Effect of Aerosol Chemical Composition on the Photodegradation of Nitro-polycyclic Aromatic Hydrocarbons.* Environmental Science & Technology, 2000. **34**(5): p. 789-797.
63. Platz, J., O.J. Nielsen, T.J. Wallington, J.C. Ball, M.D. Hurley, A.M. Straccia, W.F. Schneider, and J. Sehested, *Atmospheric Chemistry of the Phenoxy Radical, C6H5O(•): UV Spectrum and Kinetics of Its Reaction with NO, NO2, and O2.* The Journal of Physical Chemistry A, 1998. **102**(41): p. 7964-7974.
64. Irei, S., J. Rudolph, L. Huang, J. Auld, F. Collin, and D. Hastie, *Laboratory Studies of Carbon Kinetic Isotope Effects on the Production Mechanism of Particulate Phenolic Compounds Formed by Toluene Photooxidation: A Tool To Constrain Reaction Pathways.* The Journal of Physical Chemistry A, 2015. **119**(1): p. 5-13.
65. Wang, Q. and A.T. Lemley, *Competitive Degradation and Detoxification of Carbamate Insecticides by Membrane Anodic Fenton Treatment.* Journal of Agricultural and Food Chemistry, 2003. **51**(18): p. 5382-5390.
66. Wang, Q. and A.T. Lemley, *Oxidation of diazinon by anodic Fenton treatment.* Water Research, 2002. **36**(13): p. 3237-3244.
67. Friedman, C.L., A.T. Lemley, and A. Hay, *Degradation of Chloroacetanilide Herbicides by Anodic Fenton Treatment.* Journal of Agricultural and Food Chemistry, 2006. **54**(7): p. 2640-2651.
68. Garcia Einschlag, F.S., J.I. Felice, and J.M. Triszcz, *Kinetics of nitrobenzene and 4-nitrophenol degradation by UV irradiation in the presence of nitrate and nitrite ions.* Photochemical & Photobiological Sciences, 2009. **8**(7): p. 953-960.
69. Tezuka, T., N. Narita, W. Ando, and S. Oae, *Isomer distribution ratios of phenols in aromatic hydroxylation with the hydroxyl radical generated from .alpha.-azohydroperoxide in anhydrous organic media. Comparison with Fenton's reagent.* Journal of the American Chemical Society, 1981. **103**(11): p. 3045-3049.

70. Smith, D.F., C.D. McIver, and T.E. Kleindienst, *Primary Product Distribution from the Reaction of Hydroxyl Radicals with Toluene at ppb NOX Mixing Ratios.* Journal of Atmospheric Chemistry. **30**(2): p. 209-228.
71. Kovács, K., V. Mile, T. Csay, E. Takács, and L. Wojnárovits, *Hydroxyl radical-induced degradation of fenuron in pulse and gamma radiolysis: kinetics and product analysis.* Environmental Science and Pollution Research, 2014. **21**(22): p. 12693-12700.
72. Raghavan, N.V. and S. Steenken, *Electrophilic reaction of the hydroxyl radical with phenol. Determination of the distribution of isomeric dihydroxycyclohexadienyl radicals.* Journal of the American Chemical Society, 1980. **102**(10): p. 3495-3499.
73. Gramatica, P., P. Pilutti, and E. Papa, *Validated QSAR Prediction of OH Tropospheric Degradation of VOCs: Splitting into Training−Test Sets and Consensus Modeling.* Journal of Chemical Information and Computer Sciences, 2004. **44**(5): p. 1794-1802.
74. Tratnyek, P.G. and J. Hoigne, *Oxidation of substituted phenols in the environment: a QSAR analysis of rate constants for reaction with singlet oxygen.* Environmental Science & Technology, 1991. **25**(9): p. 1596-1604.
75. Cherkasov, A., E.N. Muratov, D. Fourches, A. Varnek, I.I. Baskin, M. Cronin, J. Dearden, P. Gramatica, Y.C. Martin, R. Todeschini, V. Consonni, V.E. Kuz'min, R. Cramer, R. Benigni, C. Yang, J. Rathman, L. Terfloth, J. Gasteiger, A. Richard, and A. Tropsha, *QSAR Modeling: Where Have You Been? Where Are You Going To?* Journal of Medicinal Chemistry, 2014. **57**(12): p. 4977-5010.
76. Oliferenko, A.A., P.V. Oliferenko, J.G. Huddleston, R.D. Rogers, V.A. Palyulin, N.S. Zefirov, and A.R. Katritzky, *Theoretical Scales of Hydrogen Bond Acidity and Basicity for Application in QSAR/QSPR Studies and Drug Design. Partitioning of Aliphatic Compounds.* Journal of Chemical Information and Computer Sciences, 2004. **44**(3): p. 1042-1055.
77. Liang, Y., D.T.F. Kuo, H.E. Allen, and D.M. Di Toro, *Experimental determination of solvent-water partition coefficients and Abraham parameters for munition constituents.* Chemosphere, 2016. **161**: p. 429-437.
78. Raies, A.B. and V.B. Bajic, *In silico toxicology: computational methods for the prediction of chemical toxicity.* Wiley Interdisciplinary Reviews: Computational Molecular Science, 2016. **6**(2): p. 147-172.
79. Vorpagel, E.R., A. Streitwieser, and S.D. Alexandratos, *Ab initio modeling of substituent effects in Hammett correlations.* Journal of the American Chemical Society, 1981. **103**(13): p. 3777-3781.
80. Hammett, L.P., *The Effect of Structure upon the Reactions of Organic Compounds. Benzene Derivatives.* Journal of the American Chemical Society, 1937. **59**(1): p. 96-103.
81. Anbar, M., D. Meyerstein, and P. Neta, *The Reactivity of Aromatic Compounds toward Hydroxyl Radicals.* The Journal of Physical Chemistry, 1966. **70**(8): p. 2660-2662.
82. O'Shea, K.E. and C. Cardona, *Hammett Study on the TiO2-Catalyzed Photooxidation of Para-Substituted Phenols. A Kinetic and Mechanistic Analysis.* The Journal of Organic Chemistry, 1994. **59**(17): p. 5005-5009.
83. Hansch, C., A. Leo, and R.W. Taft, *A survey of Hammett substituent constants and resonance and field parameters.* Chemical Reviews, 1991. **91**(2): p. 165-195.

84. Zhu, X., S. Shi, J. Wei, F. Lv, H. Zhao, J. Kong, Q. He, and J. Ni, *Electrochemical Oxidation Characteristics of p-Substituted Phenols Using a Boron-Doped Diamond Electrode.* Environmental Science & Technology, 2007. **41**(18): p. 6541-6546.
85. Keenan, S.L., K.P. Peterson, K. Peterson, and K. Jacobson, *Determination of Hammett Equation Rho Constant for the Hydrolysis of p-Nitrophenyl Benzoate Esters.* Journal of Chemical Education, 2008. **85**(4): p. 558.
86. Kirsch, J.F. and A. Kline, *Acyl substituent effects in the general base catalyzed ammonolysis reactions of esters.* Journal of the American Chemical Society, 1969. **91**(7): p. 1841-1847.
87. Bentley, T.W. and H.C. Harris, *Solvolyses of Benzoyl Chlorides in Weakly Nucleophilic Media.* International Journal of Molecular Sciences, 2011. **12**(8): p. 4805-4818.
88. Wurst, J.M., G. Liu, and D.S. Tan, *Hydrogen-Bonding Catalysis and Inhibition by Simple Solvents in the Stereoselective Kinetic Epoxide-Opening Spirocyclization of Glycal Epoxides to Form Spiroketals.* Journal of the American Chemical Society, 2011. **133**(20): p. 7916-7925.
89. Atkinson, R., *Kinetics and mechanisms of the gas-phase reactions of the hydroxyl radical with organic compounds under atmospheric conditions.* Chemical Reviews, 1986. **86**(1): p. 69-201.
90. Bonin, J., I. Janik, D. Janik, and D.M. Bartels, *Reaction of the Hydroxyl Radical with Phenol in Water Up to Supercritical Conditions.* The Journal of Physical Chemistry A, 2007. **111**(10): p. 1869-1878.
91. Wong, M.W. and L. Radom, *Radical Addition to Alkenes: Further Assessment of Theoretical Procedures.* The Journal of Physical Chemistry A, 1998. **102**(12): p. 2237-2245.
92. Degirmenci, I. and M.L. Coote, *Comparison of Thiyl, Alkoxyl, and Alkyl Radical Addition to Double Bonds: The Unusual Contrasting Behavior of Sulfur and Oxygen Radical Chemistry.* The Journal of Physical Chemistry A, 2016. **120**(10): p. 1750-1755.
93. Peirone, S., J.D. Nieto, P.M. Cometto, T. da Silva Barbosa, G.F. Bauerfeldt, G. Arbilla, and S.I. Lane, *Comparative Kinetics of the 3-Buten-1-ol and 1-Butene Reactions with OH Radicals: A Density Functional Theory/RRKM Investigation.* The Journal of Physical Chemistry A, 2015. **119**(13): p. 3171-3180.
94. Cho, J., M. Roueintan, and Z. Li, *Kinetic and Dynamic Investigations of OH Reaction with Styrene.* The Journal of Physical Chemistry A, 2014. **118**(40): p. 9460-9470.
95. Farmer, E.H. and C.G. Moore, *31. Radical mechanisms in saturated and olefinic systems. Part III. The reaction of hydroxyl radicals with olefins.* Journal of the Chemical Society (Resumed), 1951(0): p. 149-153.
96. Uc, V.H., J.R. Alvarez-Idaboy, A. Galano, I. García-Cruz, and A. Vivier-Bunge, *Theoretical Determination of the Rate Constant for OH Hydrogen Abstraction from Toluene.* The Journal of Physical Chemistry A, 2006. **110**(33): p. 10155-10162.
97. Uc, V.H., I. García-Cruz, A. Grand, and A. Vivier-Bunge, *Theoretical Prediction of EPR Coupling Constants for the Determination of the Selectivity in the OH Addition to Toluene.* The Journal of Physical Chemistry A, 2001. **105**(25): p. 6226-6231.
98. Shiroudi, A. and M.S. Deleuze, *Theoretical Study of the Oxidation Mechanisms of Naphthalene Initiated by Hydroxyl Radicals: The H Abstraction Pathway.* The Journal of Physical Chemistry A, 2014. **118**(20): p. 3625-3636.

99. Fan, J. and R. Zhang, *Atmospheric Oxidation Mechanism of p-Xylene: A Density Functional Theory Study.* The Journal of Physical Chemistry A, 2006. **110**(24): p. 7728-7737.
100. Uc, V.H., I. García-Cruz, and A. Vivier-Bunge, *A Theoretical Study of the OH Radical Addition to the Xylenes*, in *Quantum Systems in Chemistry and Physics Volume 2: Advanced Problems and Complex Systems Granada, Spain, 1998*, A. Hernández-Laguna, et al., Editors. 2000, Springer Netherlands: Dordrecht. p. 241-259.
101. Kovacevic, G. and A. Sabljic, *Theoretical study on the mechanism and kinetics of addition of hydroxyl radicals to fluorobenzene.* Journal of Computational Chemistry, 2013. **34**(8): p. 646-655.
102. Bryukov, M.G., V.D. Knyazev, W.M. Gehling, and B. Dellinger, *Kinetics of the Gas-Phase Reaction of OH with Chlorobenzene.* The Journal of Physical Chemistry A, 2009. **113**(39): p. 10452-10459.
103. Milhøj, B.O. and S.P.A. Sauer, *Kinetics and Thermodynamics of the Reaction between the •OH Radical and Adenine: A Theoretical Investigation.* The Journal of Physical Chemistry A, 2015. **119**(24): p. 6516-6527.
104. Chan, B., A. Karton, C.J. Easton, and L. Radom, *α-Hydrogen Abstraction by •OH and •SH Radicals from Amino Acids and Their Peptide Derivatives.* Journal of Chemical Theory and Computation, 2016. **12**(4): p. 1606-1613.
105. Prosdocimi, T., L. De Gioia, G. Zampella, and L. Bertini, *On the generation of OH· radical species from H2O2 by Cu(I) amyloid beta peptide model complexes: a DFT investigation.* JBIC Journal of Biological Inorganic Chemistry, 2016. **21**(2): p. 197-212.
106. Khosravian, N., B. Kamaraj, E.C. Neyts, and A. Bogaerts, *Structural modification of P-glycoprotein induced by OH radicals: Insights from atomistic simulations.* Scientific Reports, 2016. **6**: p. 19466.
107. Aliagas, I. and S. Gronert, *Accuracy of G2 Calculations for the Reactions of Hydroxyl Radicals with Alkanes.* The Journal of Physical Chemistry A, 1998. **102**(15): p. 2609-2612.
108. Jeong, K.M. and F. Kaufman, *Kinetics of the reaction of hydroxyl radical with methane and with nine chlorine- and fluorine-substituted methanes. 2. Calculation of rate parameters as a test of transition-state theory.* The Journal of Physical Chemistry, 1982. **86**(10): p. 1816-1821.
109. Korchowiec, J., S.-i. Kawahara, K. Matsumura, T. Uchimaru, and M. Sugie, *Hydrogen Abstraction from Methane and Hydrofluoromethanes by •OH Radical: Modified GAUSSIAN-2 Study.* The Journal of Physical Chemistry A, 1999. **103**(18): p. 3548-3553.
110. Zheng, J., G.A. Oyedepo, and D.G. Truhlar, *Kinetics of the Hydrogen Abstraction Reaction From 2-Butanol by OH Radical.* The Journal of Physical Chemistry A, 2015. **119**(50): p. 12182-12192.
111. Hollman, D.S., A.C. Simmonett, and H.F. Schaefer, *The benzene+OH potential energy surface: intermediates and transition states.* Physical Chemistry Chemical Physics, 2011. **13**(6): p. 2214-2221.
112. Tokmakov, I.V. and M.C. Lin, *Kinetics and Mechanism of the OH + C6H6 Reaction: A Detailed Analysis with First-Principles Calculations.* The Journal of Physical Chemistry A, 2002. **106**(46): p. 11309-11326.

113. Foresman, J.B. and A. Frisch, *Exploring chemistry with electronic structure methods*. Vol. 2nd. 1996, Pittsburgh, PA: Gaussian, Inc.
114. Young, D.C., *Computational chemistry: a practical guide for applying techniques to real-world problems*. 2001, New York: Wiley-Interscience.
115. Berger, R., *Computational Chemistry. Introduction to the Theory and Applications of Molecular and Quantum Mechanics. By Errol G. Lewars.* Angewandte Chemie International Edition, 2004. **43**(38): p. 4979-4980.
116. Atkins, P.W., *Physical chemistry*. Vol. 5th. 1994, New York: W.H. Freeman.
117. Lewars, E., *Computational chemistry: introduction to the theory and applications of molecular and quantum mechanics*. 2003, Boston: Kluwer Academic.
118. Hiscock, H.G. and A.J.W. Thom, *Holomorphic Hartree–Fock Theory and Configuration Interaction.* Journal of Chemical Theory and Computation, 2014. **10**(11): p. 4795-4800.
119. Kohn, W. and L.J. Sham, *Self-Consistent Equations Including Exchange and Correlation Effects.* Physical Review, 1965. **140**(4A): p. A1133-A1138.
120. Parr, R.G., *Density Functional Theory of Atoms and Molecules*, in *Horizons of Quantum Chemistry: Proceedings of the Third International Congress of Quantum Chemistry Held at Kyoto, Japan, October 29 - November 3, 1979*, K. Fukui and B. Pullman, Editors. 1980, Springer Netherlands: Dordrecht. p. 5-15.
121. Kohn, W., *Nobel Lecture: Electronic structure of matter\char22{}wave functions and density functionals.* Reviews of Modern Physics, 1999. **71**(5): p. 1253-1266.
122. Jones, R.O. and O. Gunnarsson, *The density functional formalism, its applications and prospects.* Reviews of Modern Physics, 1989. **61**(3): p. 689-746.
123. Hohenberg, P. and W. Kohn, *Inhomogeneous Electron Gas.* Physical Review, 1964. **136**(3B): p. B864-B871.
124. Becke, A.D., *Density‐functional thermochemistry. III. The role of exact exchange.* The Journal of Chemical Physics, 1993. **98**(7): p. 5648-5652.
125. Becke, A.D., *A new mixing of Hartree–Fock and local density‐functional theories.* The Journal of Chemical Physics, 1993. **98**(2): p. 1372-1377.
126. Curtiss, L.A., K. Raghavachari, P.C. Redfern, and J.A. Pople, *Assessment of Gaussian-2 and density functional theories for the computation of enthalpies of formation.* The Journal of Chemical Physics, 1997. **106**(3): p. 1063-1079.
127. Curtiss, L.A., K. Raghavachari, G.W. Trucks, and J.A. Pople, *Gaussian‐2 theory for molecular energies of first‐ and second‐row compounds.* The Journal of Chemical Physics, 1991. **94**(11): p. 7221-7230.
128. Curtiss, L.A., P.C. Redfern, K. Raghavachari, and J.A. Pople, *Assessment of Gaussian-2 and density functional theories for the computation of ionization potentials and electron affinities.* The Journal of Chemical Physics, 1998. **109**(1): p. 42-55.
129. Ochterski, J.W., G.A. Petersson, and J.A. Montgomery, *A complete basis set model chemistry. V. Extensions to six or more heavy atoms.* The Journal of Chemical Physics, 1996. **104**(7): p. 2598-2619.
130. Ochterski, J.W., G.A. Petersson, and K.B. Wiberg, *A Comparison of Model Chemistries.* Journal of the American Chemical Society, 1995. **117**(45): p. 11299-11308.
131. Frisch, M.J., G.W. Trucks, H.B. Schlegel, P.M. Gill, B.G. Johnson, M.A. Robb, J.R. Cheeseman, T. Keith, G.A. Petersson, J.A. Montgomery, K. Raghavachari, M.A. Al-

Laham, V.G. Zakrzewski, J.V. Ortiz, J.B. Foresman, C.Y. Peng, P.Y. Ayala, W. Chen, M.W. Wong, J.L. Andres, E.S. Replogle, R. Gomperts, R.L. Martin, D.J. Fox, J.S. Binkley, D.J. Defrees, J. Baker, J.P. Stewart, M. Head-Gordon, C. Gonzalez, and J.A. Pople, *Gaussian 94*. 1995.

132. Ditchfield, R., W.J. Hehre, and J.A. Pople, *Self‐Consistent Molecular‐Orbital Methods. IX. An Extended Gaussian‐Type Basis for Molecular‐Orbital Studies of Organic Molecules.* The Journal of Chemical Physics, 1971. **54**(2): p. 724-728.
133. Clark, T., J. Chandrasekhar, G.W. Spitznagel, and P.V.R. Schleyer, *Efficient diffuse function-augmented basis sets for anion calculations. III. The 3-21+G basis set for first-row elements, Li–F.* Journal of Computational Chemistry, 1983. **4**(3): p. 294-301.
134. Wiberg, K.B., *Ab Initio Molecular Orbital Theory by W. J. Hehre, L. Radom, P. v. R. Schleyer, and J. A. Pople, John Wiley, New York, 548pp. Price: $79.95 (1986).* Journal of Computational Chemistry, 1986. **7**(3): p. 379-379.
135. Merrick, J.P., D. Moran, and L. Radom, *An Evaluation of Harmonic Vibrational Frequency Scale Factors.* The Journal of Physical Chemistry A, 2007. **111**(45): p. 11683-11700.
136. Scott, A.P. and L. Radom, *Harmonic Vibrational Frequencies: An Evaluation of Hartree−Fock, Møller−Plesset, Quadratic Configuration Interaction, Density Functional Theory, and Semiempirical Scale Factors.* The Journal of Physical Chemistry, 1996. **100**(41): p. 16502-16513.
137. Pople, J.A., A.P. Scott, M.W. Wong, and L. Radom, *Scaling Factors for Obtaining Fundamental Vibrational Frequencies and Zero-Point Energies from HF/6–31G* and MP2/6–31G* Harmonic Frequencies.* Israel Journal of Chemistry, 1993. **33**(3): p. 345-350.
138. Wong, M.W., *Vibrational frequency prediction using density functional theory.* Chemical Physics Letters, 1996. **256**(4–5): p. 391-399.
139. Petersson, G.A., K.K. Irikura, and D.J. Frurip, *Computational Thermochemistry: Prediction and Estimation of Molecular Thermodynamics*. Vol. 677. 1998. 237.
140. Casasnovas, R., J. Frau, J. Ortega-Castro, A. Salvà, J. Donoso, and F. Muñoz, *Simplification of the CBS-QB3 method for predicting gas-phase deprotonation free energies.* International Journal of Quantum Chemistry, 2010. **110**(2): p. 323-330.
141. Pickard, F.C., E.K. Pokon, M.D. Liptak, and G.C. Shields, *Comparison of CBS-QB3, CBS-APNO, G2, and G3 thermochemical predictions with experiment for formation of ionic clusters of hydronium and hydroxide ions complexed with water.* The Journal of Chemical Physics, 2005. **122**(2): p. 024302.
142. Somers, K.P. and J.M. Simmie, *Benchmarking Compound Methods (CBS-QB3, CBS-APNO, G3, G4, W1BD) against the Active Thermochemical Tables: Formation Enthalpies of Radicals.* The Journal of Physical Chemistry A, 2015. **119**(33): p. 8922-8933.
143. Lin, C.Y., E.I. Izgorodina, and M.L. Coote, *How Accurate Are Approximate Methods for Evaluating Partition Functions for Hindered Internal Rotations?* The Journal of Physical Chemistry A, 2008. **112**(9): p. 1956-1964.
144. Modglin, J.D., J.C. Dunham, C.W. Gibson, C.Y. Lin, M.L. Coote, and J.S. Poole, *Computational Study of the Chemistry of 3-Phenylpropyl Radicals.* The Journal of Physical Chemistry A, 2011. **115**(11): p. 2431-2441.

145. Monard, G. and J.-L. Rivail, *Solvent Effects in Quantum Chemistry*, in *Handbook of Computational Chemistry*, J. Leszczynski, Editor. 2012, Springer Netherlands: Dordrecht. p. 561-571.
146. Miertuš, S. and J. Tomasi, *Approximate evaluations of the electrostatic free energy and internal energy changes in solution processes.* Chemical Physics, 1982. **65**(2): p. 239-245.
147. Miertuš, S., E. Scrocco, and J. Tomasi, *Electrostatic interaction of a solute with a continuum. A direct utilizaion of AB initio molecular potentials for the prevision of solvent effects.* Chemical Physics, 1981. **55**(1): p. 117-129.
148. Marenich, A.V., C.J. Cramer, and D.G. Truhlar, *Universal Solvation Model Based on Solute Electron Density and on a Continuum Model of the Solvent Defined by the Bulk Dielectric Constant and Atomic Surface Tensions.* The Journal of Physical Chemistry B, 2009. **113**(18): p. 6378-6396.
149. Frisch, M.J., G.W. Trucks, H.B. Schlegel, G.E. Scuseria, M.A. Robb, J.R. Cheeseman, G. Scalmani, V. Barone, B. Mennucci, G.A. Petersson, H. Nakatsuji, M. Caricato, X. Li, H.P. Hratchian, A.F. Izmaylov, J. Bloino, G. Zheng, J.L. Sonnenberg, M. Hada, M. Ehara, K. Toyota, R. Fukuda, J. Hasegawa, M. Ishida, T. Nakajima, Y. Honda, O. Kitao, H. Nakai, T. Vreven, J.A. Montgomery Jr., J.E. Peralta, F. Ogliaro, M.J. Bearpark, J. Heyd, E.N. Brothers, K.N. Kudin, V.N. Staroverov, R. Kobayashi, J. Normand, K. Raghavachari, A.P. Rendell, J.C. Burant, S.S. Iyengar, J. Tomasi, M. Cossi, N. Rega, N.J. Millam, M. Klene, J.E. Knox, J.B. Cross, V. Bakken, C. Adamo, J. Jaramillo, R. Gomperts, R.E. Stratmann, O. Yazyev, A.J. Austin, R. Cammi, C. Pomelli, J.W. Ochterski, R.L. Martin, K. Morokuma, V.G. Zakrzewski, G.A. Voth, P. Salvador, J.J. Dannenberg, S. Dapprich, A.D. Daniels, Ö. Farkas, J.B. Foresman, J.V. Ortiz, J. Cioslowski, and D.J. Fox, *Gaussian 09*. 2009, Gaussian, Inc.: Wallingford, CT, USA.
150. Hammond, G.S., *A Correlation of Reaction Rates.* Journal of the American Chemical Society, 1955. **77**(2): p. 334-338.
151. Evans, M.G. and M. Polanyi, *Inertia and driving force of chemical reactions.* Transactions of the Faraday Society, 1938. **34**(0): p. 11-24.
152. Bell, R.P., *The Theory of Reactions Involving Proton Transfers.* Proceedings of the Royal Society of London. Series A - Mathematical and Physical Sciences, 1936. **154**(882): p. 414-429.
153. Evans, M.G. and M. Polanyi, *Further considerations on the thermodynamics of chemical equilibria and reaction rates.* Transactions of the Faraday Society, 1936. **32**(0): p. 1333-1360.
154. Liu, Z.-P. and P. Hu, *General trends in CO dissociation on transition metal surfaces.* The Journal of Chemical Physics, 2001. **114**(19): p. 8244-8247.
155. Ponomarev, D.A. and V.V. Takhistov, *What are Isodesmic Reactions?* Journal of Chemical Education, 1997. **74**(2): p. 201.
156. Henry, D.J., C.J. Parkinson, P.M. Mayer, and L. Radom, *Bond Dissociation Energies and Radical Stabilization Energies Associated with Substituted Methyl Radicals.* The Journal of Physical Chemistry A, 2001. **105**(27): p. 6750-6756.
157. Giese, B., J. He, and W. Mehl, *Polar effects in radical addition reactions: Borderline cases.* Chemische Berichte, 1988. **121**(11): p. 2063-2066.

158. Huang, X.L., J.J. Dannenberg, M. Duran, and J. Bertran, *Polarized .pi.-frontier molecular orbitals. A method for predicting diastereofacial selectivities.* Journal of the American Chemical Society, 1993. **115**(10): p. 4024-4030.
159. Carey, F.A. and R.J. Sundberg, *Structural Effects on Stability and Reactivity*, in *Advanced Organic Chemistry: Part A: Structure and Mechanisms*. 2007, Springer US: Boston, MA. p. 253-388.
160. Koopmans, T., *Über die Zuordnung von Wellenfunktionen und Eigenwerten zu den Einzelnen Elektronen Eines Atoms.* Physica, 1934. **1**(1): p. 104-113.
161. Linstrom, P.J. and W.G. Mallard, *NIST Chemistry WebBook*. 2011.
162. Davis, W.H., J.H. Gleaton, and W.A. Pryor, *Polar effects in radical reactions. 6. The separation of substituent effects on transition states from substituent effects on bond dissociation energies. Abstraction of iodine from substituted iodobenzenes by p-nitrophenyl radicals.* The Journal of Organic Chemistry, 1977. **42**(1): p. 7-12.
163. Viskolcz, B. and L. Seres, *Ab initio study on alkyl radical decomposition and alkyl radical addition to olefins.* Reaction Kinetics and Catalysis Letters, 2009. **96**(2): p. 245-262.
164. Creary, X., *Super Radical Stabilizers.* Accounts of Chemical Research, 2006. **39**(10): p. 761-771.
165. Shorter, J., *The separation of polar, steric, and resonance effects in organic reactions by the use of linear free energy relationships.* Quarterly Reviews, Chemical Society, 1970. **24**(3): p. 433-453.
166. Wang, B.-Y., Z.-R. Li, N.-X. Tan, Q. Yao, and X.-Y. Li, *Interpretation and Application of Reaction Class Transition State Theory for Accurate Calculation of Thermokinetic Parameters Using Isodesmic Reaction Method.* The Journal of Physical Chemistry A, 2013. **117**(16): p. 3279-3291.
167. Huynh, L.K., A. Ratkiewicz, and T.N. Truong, *Kinetics of the Hydrogen Abstraction OH + Alkane →H2O + Alkyl Reaction Class: An Application of the Reaction Class Transition State Theory.* The Journal of Physical Chemistry A, 2006. **110**(2): p. 473-484.
168. Muszyńska, M., A. Ratkiewicz, L.K. Huynh, and T.N. Truong, *Kinetics of the Hydrogen Abstraction C2H3 · + Alkane →C2H4 + Alkyl Radical Reaction Class.* The Journal of Physical Chemistry A, 2009. **113**(29): p. 8327-8336.
169. Bankiewicz, B., L.K. Huynh, A. Ratkiewicz, and T.N. Truong, *Kinetics of 1,4-Hydrogen Migration in the Alkyl Radical Reaction Class.* The Journal of Physical Chemistry A, 2009. **113**(8): p. 1564-1573.
170. Zhang, S. and T.N. Truong, *Kinetics of Hydrogen Abstraction Reaction Class H + H−C(sp3): First-Principles Predictions Using the Reaction Class Transition State Theory.* The Journal of Physical Chemistry A, 2003. **107**(8): p. 1138-1147.
171. Kungwan, N. and T.N. Truong, *Kinetics of the Hydrogen Abstraction •CH3 + Alkane → CH4 + Alkyl Reaction Class: An Application of the Reaction Class Transition State Theory.* The Journal of Physical Chemistry A, 2005. **109**(34): p. 7742-7750.
172. Szori, M., C. Fittschen, I.G. Csizmadia, and B. Viskolcz, *Allylic H-Abstraction Mechanism: The Potential Energy Surface of the Reaction of Propene with OH Radical.* Journal of Chemical Theory and Computation, 2006. **2**(6): p. 1575-1586.

173. Truong, T.N., *A direct ab initio dynamics approach for calculating thermal rate constants using variational transition state theory and multidimensional semiclassical tunneling methods. An application to the CH4+H↔CH3+H2 reaction.* The Journal of Chemical Physics, 1994. **100**(11): p. 8014-8025.
174. Lynch, B.J., P.L. Fast, M. Harris, and D.G. Truhlar, *Adiabatic Connection for Kinetics.* The Journal of Physical Chemistry A, 2000. **104**(21): p. 4811-4815.
175. Zhang, Q., R. Bell, and T.N. Truong, *Ab Initio and Density Functional Theory Studies of Proton Transfer Reactions in Multiple Hydrogen Bond Systems.* The Journal of Physical Chemistry, 1995. **99**(2): p. 592-599.